Homing endonuclease-based model systems for the study of DNA double strand break induced cell signaling and repair

Inaugural-Dissertation

zur

Erlangung des Doktorgrades

Dr. rer. nat.

der Fakultät für Biologie

an der

Universität Duisburg-Essen

Standort Essen

vorgelegt von

Agnes Schipler

aus

Neumarkt

Juni, 2013

Die der vorliegenden Arbeit zugrunde liegenden Experimente wurden am Institut für Medizinische Strahlenbiologie an der Universität Duisburg-Essen, Standort Essen, durchgeführt.

1. Gutachter: Prof. Dr. Georg Iliakis

2. Gutachter: Prof. Dr. Shirley Knauer

Vorsitzender des Prüfungsausschusses: Prof. Dr. Andrea Musacchio

Tag der mündlichen Prüfung: 09. Oktober 2013

„Die Wirklichkeit von der wir sprechen können, ist nie die Wirklichkeit an sich, sondern eine von uns gestaltete Wirklichkeit.“

Werner Heisenberg (1901-1976)

Table of contents

Acknowledgements

First I would like to thank my supervisor Prof. Dr. George Iliakis for encouraging and supporting me constantly. I would like to particularly thank him for always giving me a second chance, especially in difficult phases of my thesis. I am very grateful that he shared his unique way of scientific thinking with me during intensive discussions. It helped me a lot in learning how to tackle scientific challenges and see things from different perspectives. It has been a pleasure to be part of your team.

I would like to thank Prof. Dr. Wolfgang-Ulrich Müller for being always helpful and Mrs Müller for her fast administrative assistance.

I would like to also thank JP for teaching me various techniques and sharing his profound knowledge and enthusiasm towards science with me.

My thanks go to Vladimir for the very efficient help in life cell experiments, the proofreading of my thesis and his scientific and great mental support.

I would like to thank Maria, Katja, Theresa and Swetlana for not only being great colleagues but also friends who contributed to have a pleasant time with a great atmosphere at this institute. Of course I would also like to thank all other lab members for always being very friendly and helpful.

My special thanks go to Max, Laura, Agnes and Melanie for going with me through nice and difficult phases, giving me strength and making me enjoy my life. Max I would like to also thank for correcting my thesis.

I am deeply grateful to my parents, who always believe in me and without whose motivation and support this thesis would not have been possible. Thank you for being such a strong foundation in my life.

Finally I would like to gratefully acknowledge the financial support by a grant (03NUK005C) from the BMBF awarded as part of the initiative for the preservation of radiation biology expertise in Germany (KVSF).

List of abbreviations

%	percent
°C	Degree Celsius
4HT	Hydroxytamoxifen
53BP1	p53 binding protein
Ab	Antibody
ADP	Adenosinediphosphate
Approx.	Approximately
ATM	Ataxia-telangiectasia-mutated
ATR	Ataxia-telangiectasia and rad3 related
BER	Base excision repair
B-NHEJ	Backup pathway of nonhomologous end-joining
bp	Base pair
Bq	Bequerel
BRCA1	Breast cancer susceptibility protein 1
BRCA2	Breast cancer susceptibility protein 2
BRCT	Breast cancer C-terminal
BSA	Bovine serum albumin
CE	Cytoplasmic extract
CHO	Chinese hamster ovary
Cpm	Counts per minute
CSR	Class switch recombination
CtIP	C-terminal binding protein interacting protein
DAPI	4',6-diamidino-2-phenylindole
dd	Double distilled
DDR	DNA damage response
DIC	Differential interference contrast
D-MEM	Dulbecco’s modified eagle’s medium
DMSO	Dimethyl sulfoxide
DNA	Deoxyribonucleic acid

DNA-PK	DNA dependent protein kinase
DNA-PKcs	Catalytic subunit of the protein DNA-PK
D-NHEJ	DNA-PK-dependent non-homologous end joining
ds	Double stranded
DSB	DNA double strand break
e.g.	exempli gratia
ECL	Enhanced chemiluminescence
EDTA	Ethylene diamine tetraacetic acid
EGFP	Enhanced green fluorescent protein
et al.	et alii (and others)
EtBr	Ethidium bromide
eV	Electron volt
Exo1	Exonuclease 1
FACS	Fluorescence activated cell sorting
FBS	Fetal bovine serum
FHA	Fork head-associated
FITC	Fluorescein isothiocyanate
FPLC	Fast protein liquid chromatography
G1	Cell cycle phase gap 1
G2	Cell cycle phase gap 2
Gy	Gray
H	Histidine
h	Hour
HE	Homing endonuclease
HEPES	4-(2-Hydroxyl)-1-piperazineethanesulfonic acid
HR	Homologous recombination repair
HST	Histogram
IR	Ionizing radiation
IR/DR	Inverted/directed repeat
IRIF	Ionizing radiation induced foci
K	Lysine

kDa	Kilodalton
keV	Kilo electron volt
KO	Kusabira orange
LET	Linear energy transfer
LIF	Leica image format
Lig	Ligase
LMDS	Locally multipy damaged site
LSB	Low salt buffer
m	Mouse
Mab	Monoclonal antibody
MDC1	Mediator of the mammalian DNA damage checkpoint 1
MEM	Minimal essential medium
MI	Mitotic index
Min	Minute
MMEJ	Microhomology-mediated end joining
MMR	DNA mismatch repair
M-phase	Cell cycle phase mitosis
MQ	Milli-Q
MRE11	Meiotic recombination 11
MRN complex	Mre11-Rad50-Nbs1 complex
MW	Molecular weight
NBS1	Nijmegen breakage syndrome1
NE	Nuclear extract
ng	Nanogram
NHEJ	Non-homologous end joining
NLS	Nuclear localization signal
Pab	Polyclonal antibody
PAGE	Polyacrylamide gel electrophoresis
PARP	Poly (ADP-ribose) polymerase
PBS	Phosphate buffer saline

PBST	PBS with Tween 20
PCC	Premature chromosome condensation
PFGE	Pulsed field gel electrophoresis
PI	Propidium iodide
PIKK	Phosphoinositide-3-kinase-related protein kinase
PMSF	Phenylmethylsulfonylfluoride
PMT	Photomultipliers
r	Rabbit
RAP80	Receptor-associated protein 80
RBE	Relative biological effectiveness
RE	Restriction endonuclease
RNAse	Ribonuclease
RNF8/168	Ring finger protein 8/168
ROS	Reactive oxygen species
RPA	Replication protein factor A
rpm	Revolution per minute
RS	Recombination signal
RT	Room temperature
SB	Sleeping beauty
SDS	Sodium dodecyl sulfate
SDSA	Synthesis dependent strand annealing
Sec	Second
Ser	Serine
SMC	Structural maintenance of chromosome
S-Phase	Cell cycle synthesis phase
ss	Single stranded
SSA	Single strand annealing
SSB	Single strand break
SUMO	Small ubiquitin-like modifier
TEMED	*N*'-Tetramethylethylenediamine
Thr	Threonine

Tris	Tris-(hydroxymethyl)-aminomethane
Tyr	Tyrosine
Ub	Ubiquitylation
UIM	Ubiquitin interacting motive
UV	Ultraviolet light
V(D)J	Variable (diversity) joining
WCE	Whole cell extract
wt	Wild type
XRCC	X-ray cross complementation group
γ-H2AX	Phosphorylated form of histone H2AX at Ser-139

Abstract

In cells exposed to ionizing radiation (IR) energy deposition events in the form of ionization clusters induce clustered damages in the DNA. The processing of clustered DNA damage is likely to be different from that of the constituent lesions when induced in isolation, and possibly error-prone. The prevalent view in the field is that base lesions and breaks clustered within one or two DNA helical turns impair processing, not only of the secondarily induced DSBs, but also of themselves causing mutations or cell death.

A special form of clustered DNA damage, which received attention in the past but is presently only rarely studied, is two DSBs induced in close proximity on the DNA molecule. Such clustering of DSBs at distances between a few hundred to a few thousand base pairs is likely to generate unstable chromatin fragments highly prone to loss, which may locally destabilize the genome and initiate adverse biological consequences. Although IR is known to generate this potentially highly-dangerous form of DNA damage, study of its biological relevance is hampered by difficulties to induce it in a controlled manner. This leaves theoretical modeling as the only approach for estimating its induction, but still without offering means for analyzing its effects. In an attempt to close this gap we used advanced biological approaches to model DSB clustering and test its biological consequences.

Therefore cell lines in which simple DSBs and DSB-clusters can be induced in the genome by restriction of I-*Sce*I sites engineered at defined distances in the DNA were developed. For this purpose, constructs carrying one, two or four I-*Sce*I sites, placed at precisely defined distances to model increased clustering of DSBs, were randomly integrated in the genome using the Sleeping Beauty transposon technology. This thesis presents results obtained with clonal cell lines generated from wild type CHO cells, as well as from CHO mutants which are deficient in HR (irs1SF) or NHEJ (Xrs6, XR-C1-3). Before use for experiments, each clone is characterized for the number of construct integrations by Southern blotting, which provides the maximum number of complex DSBs that can be induced upon transfection with I-*Sce*I.

Performing cell survival experiments by colony formation, we could show that CHO clones with high number of integrations undergo extensive killing after induction of DSBs by I-*Sce*I that is proportional to lesion complexity. In accordance with the strong killing observed in survival experiments the probability for misrepair measured by G2-PCC is clearly elevated for DSB clusters, showing that clustered DSBs have a high risk for the formation of chromosomal aberrations. Furthermore life cell imaging of 53BP1 foci revealed differences in signaling characteristics for different levels of DSB complexity unraveling unexpected activation characteristics of the DNA damage response that require further investigations.

1. Introduction

1.1. Cellular mechanisms for signaling and repair of DNA double strand breaks (DSBs)

1.1.1. DSBs - a threat for genomic stability

Maintaining genomic integrity is crucial for cell growth and survival. One of the most dangerous DNA lesions leading to adverse biological consequences are DSBs. They interrupt the continuity of the DNA molecule as both strands of the DNA duplex are severed by a break in the phosphodiester backbone at opposite sites within 10 bps. Unrepaired DSBs may lead to the loss of genomic stability by triggering the formation of translocations, deletions, mutations and by destabilizing chromatin. These repair failures can constitute key driving forces for the development of various human syndromes, neurological disorders, immunodeficiency and cancer (Jackson and Bartek 2009; Bohgaki, Bohgaki *et al*. 2010).

There are different ways how DNA-DSBs can arise, either by exogenous DNA-damaging agents like ionizing radiation (IR) and chemical compounds (radiomimetic drugs, topoisomerase inhibitors) or by endogenous cellular processes, such as generation of reactive oxygen species (ROS), V(D)J recombination and class switch recombination (CSR) during maturation of B- and T-lymphocytes, as well as during DNA replication. A highly regulated signaling network activated upon DSB induction is crucial for cells to orchestrate the DNA repair pathways and maintain genomic integrity. Two main DSB repair pathways have evolved: Homologous recombination (HR) and non-homologous end joining (NHEJ). HR mainly operates in the G2 phase of the cell cycle using a sister chromatid or a homologous chromosome as a template, faithfully restoring the sequence. NHEJ is an error prone pathway that operates in all phases of the cell cycle and promotes direct ligation of the DSB ends thus restoring the DNA structure. In addition, when NHEJ is impeded an alternative end joining pathway termed Backup NHEJ (B-NHEJ) operates (Mladenov and Iliakis 2011).

This work focuses on investigating the possible sources of repair failures of these highly effective repair machineries. We want to test the hypothesis that clustered DSBs are much more prone to repair accidents compared to simple DSBs. The following sections describe cellular responses to DSBs and give examples for various genotoxic agents and endogenous intracellular processes that lead to the formation of DSBs with different levels of complexity.

1.1.2. DNA damage response (DDR)

The signaling process known as DNA damage response is activated after DSB induction to counteract adverse consequences for the cell like translocations and chromosomal aberrations. It triggers a coordinate series of events that regulate cell cycle progression and repair of DNA lesions.

1.1.2.1. Activation of cell cycle checkpoints or apoptosis

In response to DNA damage DDR activates cell cycle checkpoints and pauses cell cycle progression, thus granting time for damaged cells to repair in order to prevent duplication and segregation of the damaged DNA. The DDR is organized into an elaborate network of interacting pathways that have a well-defined hierarchy of their components comprising sensors, transducers, mediators and effectors (Fig. 1). Three members of the phosphatidylinositol-3 kinase-related kinases (PIKK) family namely ATM, ATR and DNA-PKcs play important roles in the signaling network of DDR proteins. These effector proteins consist of serine/threonine protein kinases and have the ability to phosphorylate a number of mediators leading to the propagation of DSB signaling (Shiloh 2003).

Active PIKK kinases phosphorylate the effector kinases CHK1 and CHK2 that can activate different cell cycle checkpoints. Activated ATM, ATR and CHK2 phosphorylate p53 that transactivates p21 leading to the inhibition of cyclin-dependent-kinases and a G1 arrest to stop the cell before replication. In the case that DNA damage is too extensive and cannot be repaired, p53 activates its transcriptional targets including Bax, Puma and Noxa to promote apoptosis.

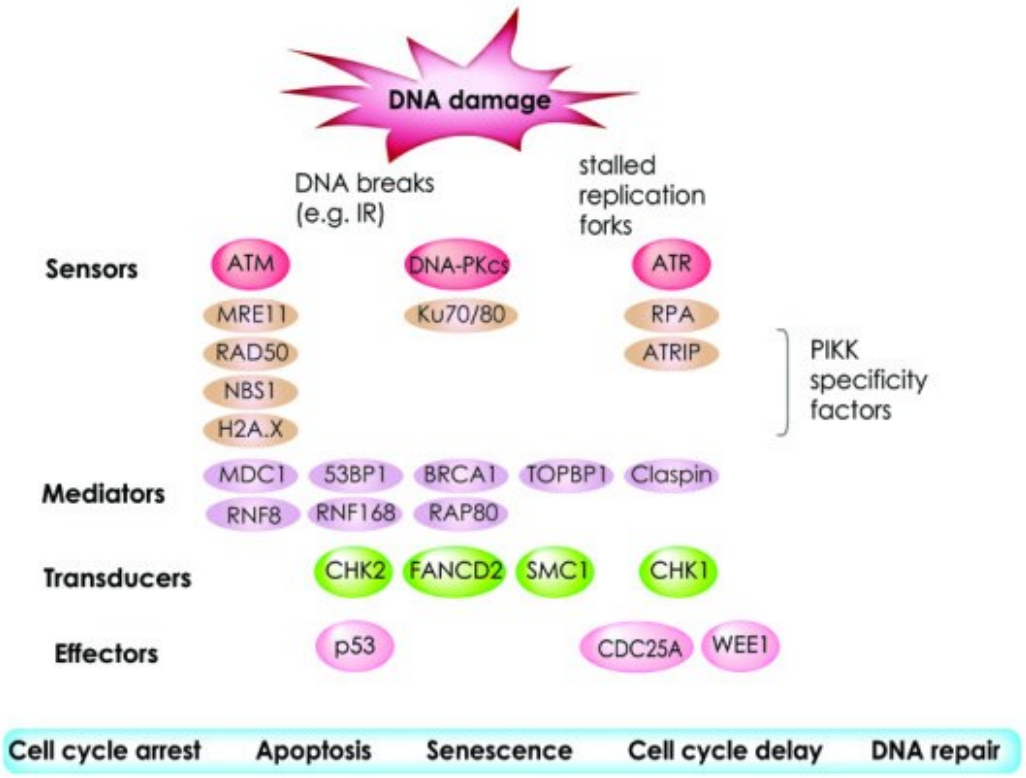

Fig. 1: Schematic representation of DNA damage-signaling and the proteins involved in the different steps (Bohgaki, Bohgaki et al. 2010). DNA lesions are recognized by sensor proteins. Mediators serve to amplify the signaling of DNA damage. Next, proteins including CHK1 and CHK2 serve to transduce the generated DNA damage signals to effector molecules. Finally, the effectors trigger the appropriate, DNA damage-associated cellular responses including apoptosis, senescence, cell-cycle arrest or delay that give time to cells to repair their damaged DNA.

CHK1 mediates intra S and G2 checkpoint activation to prevent cell division. It inactivates CDC25C and activates WEE1 through their phosphorylation resulting in inhibition of CDC2/cyclinB activity, and thus in a G2/M arrest. The CHK1 phosphorylation of CDC25A leads to CDK2 inactivation and a delayed intra S-Phase checkpoint (Sanchez, Wong *et al.* 1997).

1.1.2.2. Multistep signaling of DSBs

The highly ordered assembly of proteins at the DSB-flanking chromatin is mainly mediated by post translational modifications like phosphorylation, ubiquitylation, methylation, SUMOylation and acetylation that regulate protein-protein interactions. While most of the DDR proteins are always synthesized in the cell, activation of the DDR triggers a dramatic increase in their availability, activity and intracellular distribution. The increased local concentration of DDR proteins at DSB sites in distinct nuclear compartments forms the so called Ionizing Radiation Induced Foci (IRIF), a highly regulated and at the same time dynamic process with a tight spatiotemporal coordination of assembly and disassembly of protein complexes (Bekker-Jensen and Mailand 2010).

Immediately after DSB induction the DSB ends are sensed by the MRN (Carson, Schwartz et al. 2003) and the Ku70/80 complexes. The Ku heterodimer has a toroidal structure with a hole through which it loads onto DSB ends (Ciccia and Elledge 2010) within seconds. PARP1/2 also sense DSBs and catalyzes the rapid formation of poly (ADP-ribose) (PAR) chains. PARP1 competes with Ku and promotes B-NHEJ (Wang, Wu et al. 2006). The MRN complex that is also involved in DSB end processing comprises the components Mre11, Rad50 and NBS1. Mre11 has a single strand endonuclease activity and a 3`- 5` DNA exonuclease activity. Rad50 belongs to the structural maintenance of chromosome (SMC) protein family. The third component of the MRN complex, NBS1 (Nijmegen breakage syndrome 1) upregulates the endonuclease activity of Mre11 whereas Rad50 upregulates its endo- and exonuclease activity. MRN mediates the recruitment of ATM whereas Ku70/80 recruits DNA-PKcs to DSB ends. MRN interacts with the N-terminal domain of ATM and is also required for ATM activation. In its inactive state ATM forms dimers or multimers, whereas upon activation, ATM is autophosphorylated on Ser 1981 and dissociates into active monomers. ATM mediates H2AX phosphorylation on Ser 139 to form γ-H2AX which serves as a key regulator of checkpoint signaling and repair (Rogakou, Pilch *et al.* 1998; Fernandez-Capetillo, Chen *et al.* 2002; Chapman, Taylor *et al.* 2012).

MDC1 recognizes and binds to γ-H2AX via its tandem BRCA1-C-terminal (BRCT) domains (Stucki, Clapperton *et al.* 2005). MDC1 serves as a key recruitment factor for downstream IRIF associated proteins and protects γ-H2AX from de-phosphorylation.

The MDC1 recruitment to γ-H2AX promotes further accumulation and retention of active ATM and MRN complexes (Lukas, Melander *et al.* 2004) and a subsequent extension of H2AX phosphorylation to flanking nucleosomes (Fig. 2). During this step a positive feedback loop can be created that extends the γ-H2AX domain up to a 2 Mbp region of chromatin (Kinner, Wu et al. 2008). MDC1 and ATM recruit additional DDR factors on γ-H2AX marked chromatin, like RNF8, RNF168, BRCA1 and 53BP1.

DDR dependent MDC1 phosphorylation and recruitment to γ-H2AX initiates an ubiquitilation cascade at DSB sites. RNF8 belongs to the U3 ubiquitin ligases containing an FHA domain at its N-terminus that recognizes distinct phosphorylation sites in the N-terminal half of MDC1. It signals accumulation of DDR factors downstream of the γ-H2AX-MDC1 interaction (Mailand, Bekker-Jensen et al. 2007). RNF168 regulates RNF8-mediated ubiquitylation of histones and maintains this modification at DSBs causing chromatin remodeling. RNF168 contains a RING finger domain and two motifs that interact with ubiquitin (UIM). It ubiquitylates H2A and H2AX generating ubiquitin chains on H2A that are required for the recruitment of 53BP1 and BRCA1 (van Attikum and Gasser 2009). To distinguish the ubiquitylated H2A in IRIF from the ubiquitylated H2A throughout the whole nucleus, RNF8 and RNF168 together with an E2 ubiquitin ligase, UBC13 generate K63-linked non proteolytic ubiquitin chains on histones.

In addition to ubiquitylation and phosphorylation SUMOylation is also required for DSB signaling. The SUMO E3 ligases PIAS1 and PIAS4 are recruited to DSBs and mediate DSB induced ubiquitylation of RNF8 and RNF168. Furthermore, PIAS4 mediates SUMO1 modification of 53BP1 and BRCA1, while SUMO2/3 modification of BRCA1 is also mediated by PIAS4.

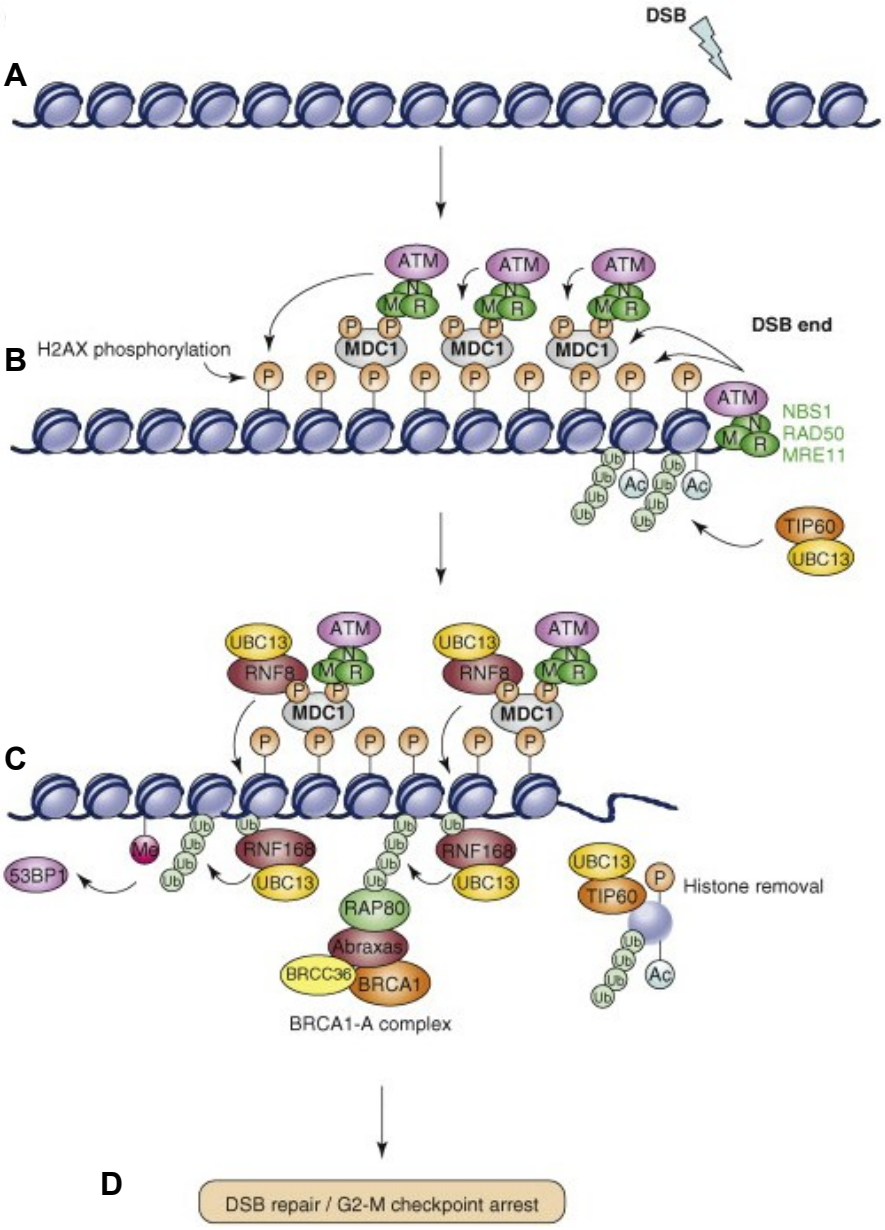

Fig. 2: Model for the function of γ-H2AX at DSB in mammals (van Attikum and Gasser 2009) A: A DSB is induced by IR. **B:** The MRN complex binds to the ends of the DSB and recruits ATM, which phosphorylates H2AX. MDC1 is recruited and binds to γ-H2AX. Phosphorylation of MDC1 recruits more MRN-ATM that phosphorylates more H2AX. TIP60 acetylates (Ac) γ-H2AX. Subsequently it associates with the E2 ubiquitin-conjugating enzyme UBC13 to regulate polyubiquitylation (Ub) of acetylated γ-H2AX. **C:** Polyubiquitylated and acetylated γ-H2AX is removed from chromatin. ATM phosphorylates MDC1 to recruit an RNF8–UBC13 complex that regulates ubiquitylation of histone H2AX and H2A. RNF168 binds to these ubiquitylated histones and promotes the formation of ubiquitin conjugates. Polyubiquitylated histones recruit the BRCA1-A complex and 53BP1. The BRCA1-A complex directly binds Ub-histones through the RAP80 subunit. 53BP1 binds to methylated (Me) histones after RNF8–RNF168–UBC13-mediated polyubiquitylation. **D:** Finally, these events facilitate DSB checkpoint arrest and repair.

The recruitment kinetics of MRN, γ-H2AX, MDC1 and RNF8 foci following DSB induction is rapid, reaching maximum accumulation within a few minutes. After 1-2 min a second wave of protein accumulation follows including 53BP1 and BRCA1.

RNF8 facilitates this accumulation of the two checkpoint mediator proteins 53BP1 and BRCA1 to the damaged chromatin through the phospho-dependent FHA domain-mediated binding of RNF8 to MDC1, as well as through its role in ubiquitylating H2AX (Huen, Grant et al. 2007).

The BRCA1-A complex bridges the interaction between BRCA1 and ubiquitylated histones. The ubiquitin BRCA1 response is controlled by chromatin remodeling events mediated by p400 ATPase together with TIP60 acetyltransferase that are recruited by MDC1 to destabilize nucleosomes for efficient ubiquitylation (Luijsterburg and van Attikum 2012). RAP80, which is the central component of the BRCA1-A complex, contains two ubiquitin interaction motifs (UIM) that bind ubiquitylated histones. Together with Abraxas, BRCC36, BRE and NBA1, RAP80 forms the so called MERIT40 complex. Abraxas is a coiled coil domain protein that forms the structural core for protein assembly and binds to the tandem BRCT domains of BRCA1.

The RNF8/RNF168 pathway regulates the efficient association of 53BP1 with H4K20 (histone 4 methylated at Lys 20) by recruiting the ubiquitin selective ATPase VCP (p97) and its cofactor NPL4 to chromatin. VCP mediates the extraction of the polycomb protein L3MBTL1 from chromatin unmasking 53BP1 binding sites. In addition the MMSET methyltransferase promotes 53BP1 recruitment by mediating di-methylation of H4K20 after recruited to the DSB by MDC1 (Luijsterburg and van Attikum 2012).

1.1.3. Repair pathways

The highly efficient DSB repair pathways that function as a part of the DDR are described in the following section.

1.1.3.1. HR

Homologous recombination is an error free process that can be divided into the following three main stages: presynapsis, synapsis and postsynapsis. (Heyer, Ehmsen *et al.* 2010). In the presynaptic stage the DNA DSB is sensed by MRN (Fig. 3A). Subsequently the DNA ends are resected to form extended regions of single stranded DNA (ssDNA) with 3`overhangs. The nucleases Exo1, Dna2 and CtIP are involved in this process together with MRN and the BLM helicase. The ssDNA is coated by RPA (replication protein A) to eliminate secondary structures and stabilize the ssDNA for the formation of the Rad51 nucleoprotein filament. The Rad51 filament formation requires different classes of mediator proteins like the group of Rad51 paralogs (Rad51B, Rad51C, Rad51D, XRCC2, and XRCC3) and BRCA2.

During synapsis the nucleoprotein filament searches for homology and performs strand invasion to form a Holliday junction. Rad54 promotes DNA synthesis associated with branch migration by dissociating Rad51 from the heteroduplex DNA.

During the postsynapsis, predominantly synthesis-dependent strand annealing (SDSA) occurs, where the extended Holliday junction is resolved enabling the annealing of the newly synthesized strand with the resected strand of the second end. Finally after subsequent DNA synthesis and ligation the DNA sequence is restored. In a scenario where the second DNA end is absent, which can occur at telomeres or replication forks, BIR (break induced replication) takes place that restores the integrity of the chromosome but can lead to loss of heterozygosity (San Filippo, Sung *et al.* 2008). Another possibility is the formation of double Holliday Junctions that migrate towards each other, while priming DNA synthesis. In this case the final resolution of the Holliday junctions may lead to the formation of crossover or non-crossover events (Bzymek, Thayer *et al.* 2010). If strand invasion does not occur, a further pathway called single

strand annealing SSA can be utilized by the cell. SSA proceeds by annealing of longer than 30 nt homologous sequences after resection resulting in large deletions.

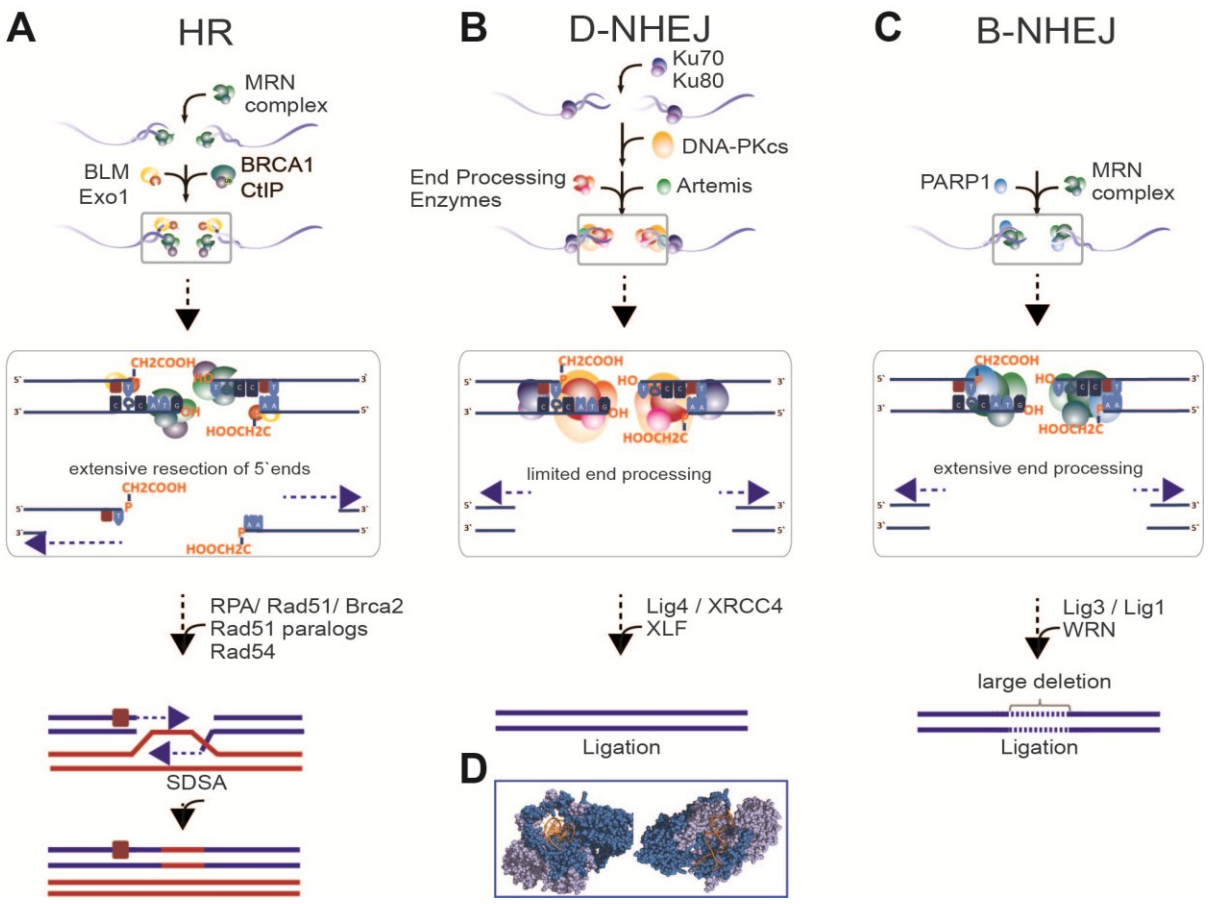

Fig. 3: Schematic representation of the three DSB repair pathways HR, D-NHEJ and B-NHEJ. (Schipler and Iliakis 2013). A: During HR, extensive processing of the 5`-ends takes place that can remove lesions in the vicinity of DSB ends. **B:** For D-NHEJ, limited end processing takes place at both DNA strands. **C:** For B-NHEJ extensive end processing takes place. B-NHEJ often results in large deletions and translocations. **D:** The ring shaped Ku proteins binds to 15 bp DNA at the DSB ends

1.1.3.2. D-NHEJ

D-NHEJ is considered as the prevalent DSB repair pathway in higher eukaryotes that essentially mediates the fast (direct) ligation of broken DNA ends to maintain chromosome integrity. (Iliakis, Wang *et al.* 2004). It is initiated by the binding of the Ku70/Ku80 heterodimer to DSB termini generating a scaffold that can associate with all other NHEJ factors (Fig. 3B). The Ku heterodimer has a ring-shaped structure allowing the protein to slide over the ends of the DNA molecule (Walker, Corpina *et al.* 2001). After forming the Ku-DNA complex, Ku recruits (Chappell, Hanakahi *et al.* 2002) and activates the DNA-dependent protein kinase catalytic subunit (DNA-PKcs) that protects the DNA termini against degradation and premature ligation. Furthermore DNA-PKcs tethers the DNA ends and forms a synaptic complex that juxtaposes the broken DNA ends for processing upon a conformational change induced by DNA-PKcs autophosphorylation (Weterings and Chen 2007).

End processing of the DNA termini is required for almost all DSB types except blunt ended DSBs that can be simply religated without further processing. NHEJ enzymes tolerate wide spectra of structural DNA end substrate configurations like variations in the overhang length, DNA end sequence and/or chemistry (Weterings and Chen 2008). Non-compatible single stranded DNA overhangs can be either removed by resection or a new complementary strand is synthesized using the nucleotide sequence overhang as template. In the second case DNA synthesis is performed by proteins like the DNA polymerases λ, μ, and Artemis (that can have a DNA-PKcs-independent exonuclease activity or a DNA-PKCS-dependent endonuclease activity). These end processing steps can lead to different repair outcomes like deletions, insertions or sequence alterations, some of the reasons why NHEJ is considered to be an error prone pathway. End processing can also require the addition of a 5`phosphate group mediated by the mammalian polynucleotide kinase (PNK) in an XRCC4-and DNA-PKcs-dependent manner (Chappell, Hanakahi *et al.* 2002), or the removal of a 3`phosphoglycolate by different enzymes like the tyrosyl-DNA phosphodiesteraseTDP1, the polynucleotide kinase PNK and Artemis (Lieber 2010).

In the final step the processed DNA ends are ligated by the Ligase4/XRCC4 protein complex that is attracted to the synaptic repair complex by the Ku-DNA scaffold after releasing DNA-PKcs. Alternatively the XLF/Cernunnos interacts with the XRCC4/Ligase4 complex by stimulating ligation of non-compatible single strand ends followed by synthesis of the complementary strand to prevent nucleotide loss during end resection (Tsai, Kim *et al.* 2007).

1.1.3.3. B-NHEJ

An alternative end-joining pathway termed B-NHEJ (Backup Pathway) or alternative end-joining (alt-NHEJ) operates particularly when classical NHEJ and possibly also HR are impeded (Fig. 3C). This pathway utilizes proteins like PARP-1 and DNA Ligase 3/XRCC1 (Wang, Rosidi *et al.* 2005) that are also known to be involved in the repair of single strand breaks (SSB). Competition for DNA end binding between PARP and Ku is considered as a possible scenario for the initial step after DSB formation, whereas Ku has a significantly increased affinity for binding, underlining the backup character of B-NHEJ (Wang, Wu et al. 2006). DNA end processing by Mre11 is implicated as a further step in B-NHEJ, as inhibition of Mre11 in NHEJ compromised CHO cells suppresses end joining (Rass, Grabarz et al. 2009). Furthermore the linker Histone H1 has been identified to be involved in the backup pathway probably aligning DNA ends prior to ligation (Rosidi, Wang et al. 2008). The finding of abundant regions of microhomology at B-NHEJ mediated repair junctions leads to the assumption that stabilization of the DNA prior to ligation may be promoted by microhomologies. During the final step of the pathway, Ligase 3 functions in a complex with XRCC1 to ligate the DNA ends, a process that is regulated by PARP1 (Audebert, Salles et al. 2004). Recent evidence suggests other proteins like the Werner Syndrome Proteins (WRN) and BCR/Abl to be involved in this pathway, whereas WRN forms a complex with Lig3 prior to ligation (Sallmyr, Tomkinson *et al.* 2008).

The activity of B-NHEJ shows strong cell cycle fluctuations. It increases in G2 and is reduced in G1 and is significantly abrogated in resting cells.

This change in activity levels hints to a backup role of B-NHEJ not only for classical NHEJ (D-NHEJ) but also for aberrant HRR, an observation that requires further investigation (Wu, Wang *et al.* 2008).

Although B-NHEJ is facilitated by fortuitously present micro-homologies exposed after resection at the DNA ends (therefore also termed microhomology-mediated end-joining, MMEJ (McVey and Lee 2008), this is not a requirement for its function. DSB processing pathways with absolute requirement for extensive homology, like homologous recombination (HR) and single strand annealing (SSA) operate after DNA replication when a sister chromatid becomes available; they include gene conversion and deletion.

1.2. Possible sources of DSB induction

1.2.1. Ionizing Radiation (IR)

Ionizing radiation (IR) is unique in the broad spectrum of various DNA damage types it can induce as a result of the special characteristics of the initial local energy deposition events (Goodhead, Thacker *et al.* 1993).

IR deposits its energy along the radiation track it traverses producing ionization clusters and is therefore up to 1000 times more effective at cell killing compared to other types of DNA damaging agents that give rise to randomly distributed radicals. The dose of radiation to biological material is defined in terms of the amount of energy absorbed per unit mass. 1 Gy is equivalent to 1 J/kg. DNA damage by IR is formed either as direct action by the local properties of radiation tracks within the DNA, or as an indirect action in the surrounding cellular environment within a radical diffusion distance of around 4 nm. Indirect action is mainly mediated by the radiolysis of water.

The biological effects of IR are the end product of the initial physical events comprising ionizations and excitations of atoms and molecules along the tracks of the ionizing particles. Therefore the interaction of IR with matter can be described by the following consecutive processes: Physicochemical reactions, chemical reactions and finally the biological effect.

1.2.1.1. Physical and chemical aspects of IR interaction with matter

IR is classified as electromagnetic or particulate, whereas the electromagnetic radiation, comprising X-rays and γ-rays is indirectly ionizing as it deposits the majority of its energy through the production of secondary electrons. Particulate radiation including electrons, protons, α-particles, neutrons and heavy charged particles is directly ionizing as its charged particles have sufficient kinetic energy to disrupt the atomic structure of the absorber through which they pass directly producing chemical and biological changes (Hall and Giaccia 2006).

Various computational approaches, named Monte Carlo track structure codes, have been developed to simulate the stochastic effect of ionizing radiation of different

qualities. Monte Carlo computer simulations of radiation tracks include each ionization or excitation of the primary charged particles and all their secondary particles until they come to rest (Paretzke 1987).

The features for the highly structured radiation tracks clearly vary between densely ionizing high linear energy transfer (LET) radiation like neutrons and alpha particles and sparsely ionizing, low LET X-rays or γ-rays (Fig. 4). LET is defined as the average energy that an ionizing particle deposits per unit length of track (KeV/µm) as it traverses matter. In case of low LET radiation most of the energy is deposited as single isolated sparse ionizations whereas localized ionization clusters are formed by low energy secondary electrons at the end of the track comprising 30-50% of the local energy deposition of low LET radiation (Goodhead and Nikjoo 1989). High LET radiation deposits most of its energy within a small volume in the target. Compared to low LET, high LET radiation has a higher number of primary radicals close together in the radiation track therefore, the yield of molecular products from pairs of radicals increases, whereas the single radical products decrease.

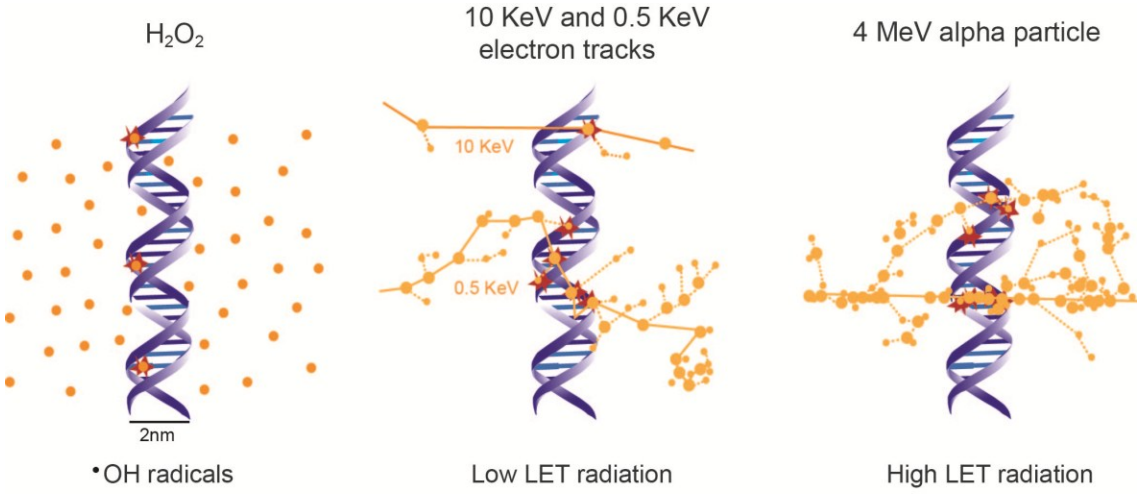

Fig. 4: Random DNA damage induction by H_2O_2 compared to DNA damage induction by low and high LET radiation tracks. ·OH radicals are evenly distributed in space and induce DNA damage randomly. In the case of IR, ionization events localize along the radiation tracks and therefore induce clustered damage. With increasing LET the damage clustering increases. Large dots represent ionizations and small dots represent excitations along the radiation track. The Monte Carlo simulated tracks are drawn on the same scale as the DNA (Goodhead 1995; Schipler and Iliakis 2013)

1.2.1.2. Biological consequences of clustered DNA damage induced by IR

It is assumed that the clustering of DNA damage induced by ionization clusters within single tracks determines the effectiveness of radiation.

Furthermore, differences have been observed in DSB repair efficiency, as well as in the yield of DSBs causing lethal events - by densely or sparsely ionizing radiation. Isolated DNA damages including SSBs as well as DSBs correlate poorly with biological effectiveness for cellular effects. Only slight LET dependence is observed in the general yield of DSBs for different radiation qualities due to the balance between the number of particles and the increased local ionization density. In contrast, the formation of clustered complex DSBs shows a strong LET dependence. Whereas for low energy electrons around 30% of DSBs contain more than two strand breaks, clustering is observed for 70% of DSBs induced by alpha-particles by alpha-particles (Durante and Loeffler 2010; Georgakilas, O'Neill et al. 2012).

All types of IR can induce severe, clustered DNA damage due to its unique characteristics of depositing energy along the tracks of the constituent ionizing particles. Monte Carlo simulations for mammalian cells for low and high LET radiation revealed an increase in cluster complexity with increasing LET, and an associated increase in the ratio of DSBs to SSBs (Nikjoo, O'Neill et al. 1999). Per unit absorbed dose approx. the same number of DNA lesions are created for low and high LET radiation; they comprise around 1000 SSBs and base damages and 20-40 DSBs per Gy of radiation (Ward 1990). But the distribution of the lesions with high LET radiation occurs within smaller regions of the target, causing an increase in cluster complexity. The increased ionization clustering along the tracks of densely ionizing forms of IR generates DNA damage that is more complex, in the sense that it comprises more lesions within the same DNA segment (one or two helical turns), than that induced by low LET radiations. Yet, per unit absorbed dose approx. the same number of DNA lesions are created for low and high LET radiation (Ward 1990). Since high LET forms of IR have greater relative biological effectiveness (RBE) per unit dose than those exposed to low LET radiation, it can be concluded that not the total number of ionizations alone, but also their spatial distribution determine the gravity of the resulting biological effect.

(Goodhead 1994). The RBE of a radiation is defined as the dose of reference radiation divided by the dose of the test radiation to give the same biological effect. The reference radiation has historically been 250 kV X-rays.

1.2.1.3. VDJ/CSR

V(D)J recombination is an essential process in generating a high diversity of B-cell and T-cell receptors during the maturation of B- and T-lymphocytes in order to recognize a wide range of pathogen epitopes. Both processes involve a highly regulated induction of DSB clusters and the loss of intervening sequences.

V(D)J recombination is a specialized somatic DNA rearrangement mechanism that randomly combines variable (V), diversity (D) and joining (J) encoding gene segments of the immunoglobulin heavy chains (IgH) and VJ segments of the immunoglobulin light chains (IgL). The process is initiated by the lymphoid specific factors of the V(D)J recombinases, RAG1 and RAG2 (recombination activating genes), that recognize recombination signal sequences (RSS) flanking each V, D and J gene segment and induce blunt ended DSBs adjacent to them (Dudley, Chaudhuri *et al.* 2005). RSS are composed of conserved heptamer and nonamer sequences and an intervening spacer sequence of 12 or 23 bp. For DSB induction RAG1 and RAG2 form a protein complex and align two RSS to induce two SSBs at the 5`end of each RSS. The resulting 3`OH groups attack the phosphodiester bond on the other strand and produce a 5' phosphorylated double-stranded break at the RSS and a covalently closed hairpin at the coding end that has to be processed prior to rejoining. The induced DSBs are resolved by the DSB repair pathway NHEJ forming signal end joints (SJs) and coding end joints (CJs) finally resulting in recombination of V, D, and J gene segments.

CSR (class switch recombination) occurs exclusively in immunoglobulin genes of mature B-cells. This process allows the expression of an antibody with the same antigen-binding specificity but with an altered effector function, thus enabling the production of different isotypes. During CSR the constant region of the IgH is changed by rejoining the variable domain exon of the heavy chain locus (C_μ) with a downstream constant domain exon (C_H) after deleting the intervening sequence. For this recombination process DSBs are generated by the AID enzymes (activation induced

cytidine deaminases) at conserved nucleotide motifs called switch regions (S) located upstream of all C_H genes except C_{δ}.

In contrast to V(D)J recombination where DSBs are induced at short conserved signal sequences (RS), the S DSB target regions for CSR comprise 1-12 kbp repetitive DNA sequences. AID deaminates cytosine residues at S regions to generate uracil, which is processed by base excision repair (BER) and/or mismatch repair (MMR) pathways into DSBs (Di Noia and Neuberger 2007). Rejoining of DSBs in the last step of CSR is mediated either by NHEJ or by B-NHEJ.

1.2.1.4. Endonucleases

Restriction endonucleases (RE) are prokaryotic enzymes that have the role to protect host cells from invasion of foreign DNA i.e. bacteriophage infection. RE disrupt the phosphodiester bonds on both strands of the DNA molecule to generate either blunt or staggered DSB-ends while retaining the 5' phosphate and 3' OH groups at each strand. Depending on the enzymatic properties, different types of RE are distinguished. The most frequently applied RE in molecular biology are type II RE that are homodimers which recognize a 4-8 bp palindromic DNA sequence. Cleavage of these sites is symmetric about the dyad axis of the restriction site and may result in blunt ends, 5′ overhanging fragments, or 3′ overhanging fragments, depending on the particular enzyme (Gruen, Chang et al. 2002).Homing endonucleases (HEs) are double stranded DNases that have large, asymmetric recognition sites and coding sequences that are usually embedded in either introns or inteins (Belfort and Roberts 1997). Homing is the lateral transfer of an intervening sequence, either the intron or the intein to a homologous allele that lacks the sequence. The homing endonuclease is encoded by an ORF within the mobile intervening sequence and has evolved to catalyze highly specific DSBs in cognate alleles. In contrast to REs they tolerate some minor sequence degeneracy and bind long DNA target sites (14-40 bp) despite their small size (<40 kDa). The large recognition sequence ensures high specificity and low toxicity associated with excessive cleavage of a host genome (Chevalier and Stoddard 2001). HE recognition sites are extremely rare, with an 18 bp recognition sequence occurring once in every $7x10^{10}$ bp of a random sequence (Jasin 1996).

1.2.1.5. I-*Sce*I as a tool to study DSB repair

The homing endonuclease I-*Sce*I originates from the mitochondria of *Saccharomyces cerevisiae* with an 18 bp non-palindromic recognition sequence (Fig. 5). I-*Sce*I is a monomer composed of two pseudosymmetric subdomains that recognize asymmetric substrates. It is widely used to study DSB repair pathways in mammalian cell lines as the 18bp recognition sequence is not inherent in mammalian cells (Honma, Sakuraba *et al.* 2007). Therefore cutting of intrachromosomally inserted I-*Sce*I recognition sites result in double-strand DNA cleavage exclusively at the inserted site.

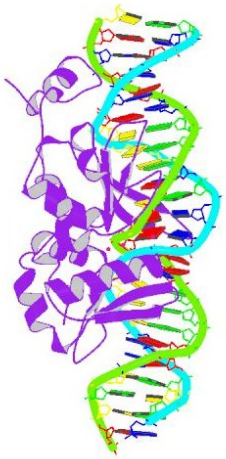

Fig. 5: I-SceI bound to DNA (1R7M protein data bank).

Various fluorescence based assays have been developed allowing functional analysis of specific repair pathways after site specific induction of DSBs by I-*Sce*I. DSBs are either generated by transient transfection of I-*Sce*I expressing vectors, or by a controlled translocation from the cytoplasm into the nucleus of constitutively expressed I-*Sce*I. A widely used recombinational reporter system to measure HR in living cells is the direct repeat green fluorescent protein (DR-GFP) assay. In this system a chromosomally integrated construct harbors the I-*Sce*I recognition site that has been integrated into the GFP gene disrupting the ORF. A truncated GFP gene fragment with the correct ORF sequence has been placed downstream in the construct. Repair of the cleaved I-*Sce*I site by HR using the downstream fragment gives rise to a functional GFP gene, and GFP fluorescence then can be measured by flow cytometry. Using this

assay, the authors could show that error free HR repair of DSBs is decreased 25-fold in XRCC3 deficient CHO cells (Pierce, Johnson *et al.* 1999).

GFP-based chromosomal reporters have been developed to measure D-NHEJ with two I-*Sce*I sites flanking an intervening sequence that separates the promoter from the GFP coding cassette. Simultaneous cleavage of both sites leads to the loss of the intervening sequence resulting in GFP expression upon successful rejoining of the two nearby I-*Sce*I-induced DSBs. Using this assay Mansour *et al.* showed that mammalian cells require Ku for rapid NHEJ for complementary and non-complementary DSB ends. In the absence of Ku, B-NHEJ is employed that is completely dependent on PARP1 but does not need extensive microhomologies (Mansour, Rhein *et al.* 2010).

A further study showed that Mre11 promotes efficient NHEJ in both wild-type and Xrcc4-/- mouse embryonic stem cells. End resection is supressed in Xrcc4-/- cells after depletion of Mre11, revealing specific roles for Mre11 in both D- and B-NHEJ (Hartlerode, Odate et al. 2011).

Bindra et *al*. have developed an assay to measure mutagenic nonhomologous end-joining (B-NHEJ, termed here mut-NHEJ) repair combined with a homologous recombination (HR) assay enabling the simultaneous monitoring of both pathways in living cells (Bindra, Goglia et al. 2013). They could show that B-NHEJ repair is suppressed in growth-arrested and serum deprived cells. These results are in accordance with previous observations from our lab (Windhofer, Wu *et al.* 2007; Singh, Wu *et al.* 2011; Singh, Bednar *et al.* 2012) suggesting that end-joining activity in proliferating cells is more likely to be mutagenic.

1.3. Not all DSBs are created equal: Levels of DSB complexity

The cellular responses described in the previous sections (1.1) are based on the assumption that all DSBs are created equal. But depending on the type of the DSB inducing agent, different levels of DSB complexity can be generated (Fig. 6). With increasing complexity also the possibility for processing errors may increase. The following section describes various categories of DSBs, Type 1-6 (T1-6) on the basis of increasing complexity (Schipler and Iliakis 2013).

1.3.1. T1-DSB: simple DSBs with clean ends

T1-DSBs generated by RE or HE are considered as the simplest form as they retain a 5' phosphate and the 3' OH group at each strand break after disrupting the phosphodiester bond (Obe and Natarajan 1985; Bryant and Johnston 1993). Endonuclease induced DSBs have clean ends as the disruption of the continuity of the DNA molecule occurs without chemically altering any of its constituent moieties, i.e. sugar or base modifications do not occur (Fig. 6A). Although T1-DSBs can be rejoined by simple ligation, subtle differences like type, 3' or 5', or length of protruding ends will affect DSB processing. Blunt ended DSBs are, at least *in vitro*, more difficult to ligate than DSBs with overlapping ends (Pfeiffer, Feldmann et al. 2005; van Gent and van der Burg 2007).

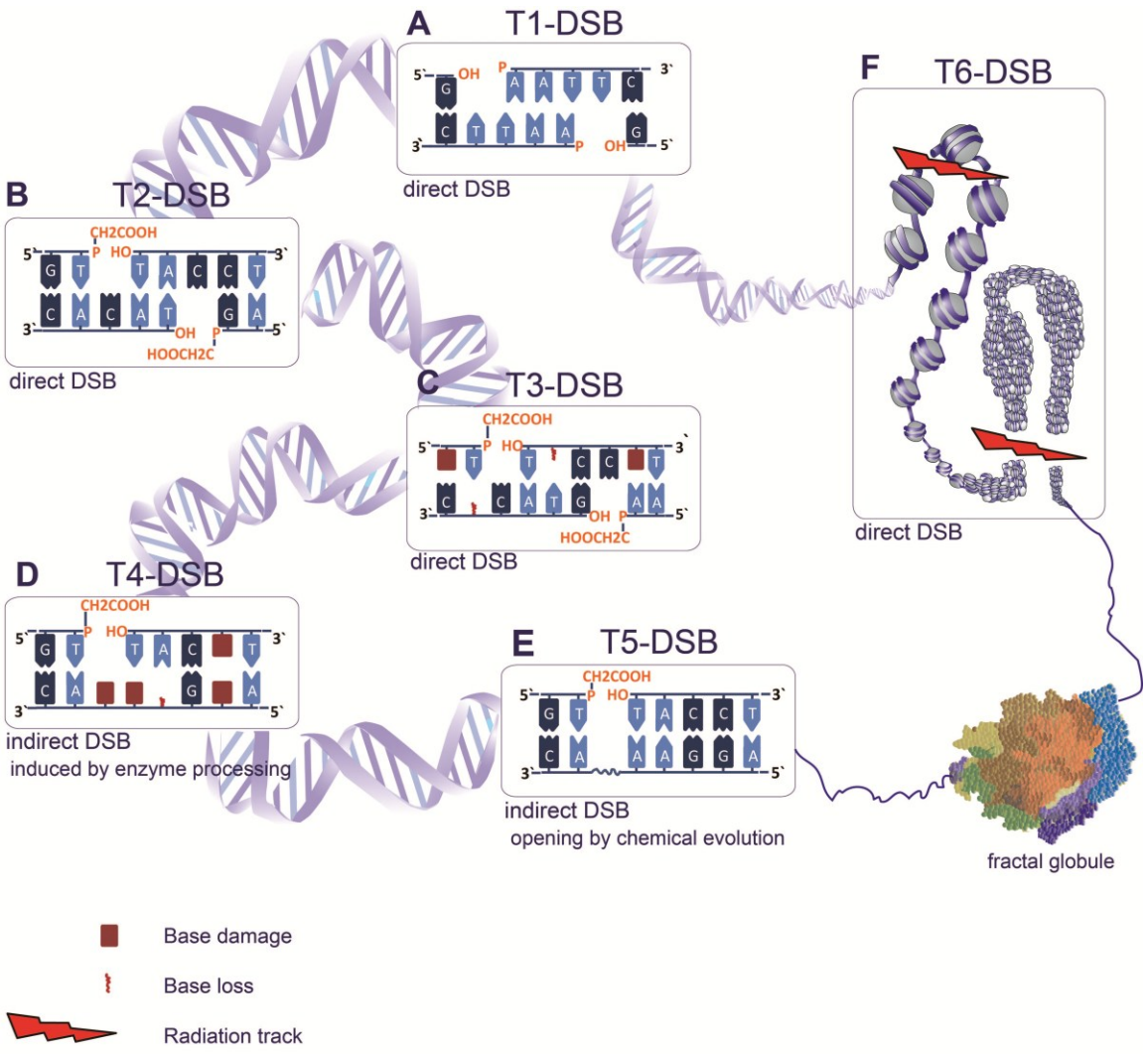

Fig.6: Schematic illustration of DSB Types 1-6. A: T1-DSBs are direct DSBs induced by RE with a 5` phosphate and a 3` OH group. **B:** T2-DSBs are induced by IR and frequently comprise a 3` phosphoglycolate and a 5'-OH. **C:** T3-DSB comprises also other types of lesions like base damages or base loss in close proximity to the DSB. **D:** T4-DSB represents a non-DSB cluster that can convert to DSBs by subsequent enzyme processing. **E:** T5-DSBs represent a non-DSB cluster that can convert to DSBs by chemical processing. **F:** T6-DSBs are composed of clustered DSBs. Two examples are shown. A single radiation track induces two DSBs in the linker regions of a nucleosome leading to nucleosomal loss, shown on the left. On the right higher order packaging of nucleosomes is illustrated forming a loop that is also hit by a single radiation track that can lead to chromatin destabilization (Schipler and Iliakis 2013). In the right lower corner the chromatin compacted as a fractal globule is illustrated (Mirny 2011; Bancaud, Lavelle et al. 2012).

1.3.2. T2-DSB: simple DSBs with modified ends

IR generated DSBs differ from those induced by RE because they frequently comprise a 3' damaged sugar in the form of phosphoglycolate and a 5' OH. Therefore the T2-DSBs are categorized as simple DSBs where the complexity derives from modified ends (Fig. 6B). This form of ends precludes direct ligation and necessitates end-processing as a step during repair. In contrast to RE and HE, IR in the form of X-rays or γ-rays, induces, a wide spectrum of lesions through the formation of free radicals resulting in oxidative damage, including sugar and base damages each of which outnumbers DSBs by approx. 20:1 (Ward 1985; Ward 1990). Certain forms of sugar damage disrupt the phosphodiester backbone of the DNA molecule and generate SSBs. Since IR-induced DSBs are generated by coincidence of two SSBs, blunt ends, or ends with protruding single strands similar to those described for RE can be generated.

1.3.3. T3-DSB: Locally multiply damaged sites

The presence of two or more DNA lesions comprising base damages or strand breakages on opposing strands within one helical turn of the DNA constitutes clustered DNA damage that potentially will have more severe biological consequences than the T2-DSBs described above. This possibility was pointed out by John Ward who proposed the term locally multiply damaged sites (LMDS-later simplified as MDS) (Ward 1985). Formations of MDS occur through multiple direct ionizations of the DNA, as well as from combinations of free radical attack and direct ionization events. A single energy deposition is able to produce 2-5 ionizations in a region of 1-4 nm (up to one helical turn) of the DNA-strand.

T3-DSB describes the simultaneous presence of base damages and DSBs within an MDS and generates the next level of complexity (Fig. 6C). The increased complexity of T3-DSB may impair cellular repair systems by simultaneous recruitment and even engagement of two or more repair pathways (DSB repair and base damage repair); thus it may impair the function of both pathways. In addition, base damages in close proximity to DSBs may inhibit enzymes involved in DSB repair. Therefore it is likely that

the probability for accidental misrepair is highly increased compared to the simpler forms of DSBs described above (Schipler and Iliakis 2013).

1.3.4. T4-DSB: Indirect DSB induced by enzymatic processing

In addition to the above described DNA damage clusters comprising DSBs that are induced immediately after radiation exposure, damage clusters can also be generated by IR that partly develop to DSBs at different times after irradiation by enzymatic processing of the initial lesions (non-DSB clusters) (Fig. 6D). DSBs forming by the simultaneous disruption of the phosphodiester bond at base damage sites in opposite strands, or with the combination of BER opposing an SSB, form yet another level of complexity that integrates the parameter time in the induction process and is termed therefore T4-DSB (Schipler and Iliakis 2013). Experimental evidence exists that this form of clustered DNA damage outnumbers T3-DSBs by nearly 4:1. Although BER and SSB repair pathways may remove individual lesions within non-DSB clusters restoring thus the DNA molecule, repair attempts may also fail.

It was shown that the reparability of non-DSB clusters is determined by the composition, spacing and polarity of the lesions comprising the cluster (Hada and Sutherland 2006). One or more lesions within a non DSB cluster can remain unrepaired due to reduced activity of glycosylase or altered nuclease activity. Furthermore a delayed formation of DSB can result as a consequence of attempted post irradiation repair of sugar and base residues (Gulston, de Lara *et al.* 2004). In the case of a bistranded cluster that contains either two AP sites or a SSB opposing an AP site most probably a DSB will be formed through the incision of the AP site during repair (Georgakilas 2008).

1.3.5. T5-DSB: Indirect DSB induced by chemical processing

Recent evidence suggests that IR also generates sugar damage within clustered damage sites that fail to directly break the DNA backbone, but do so after chemical processing within about 1 h after IR (Singh, Wang *et al.* 2011). This way of generating DSBs within a clustered damage site is termed T5-DSB (Fig. 6E).

1.3.6. T6-DSB: Clustered DSBs

Multiple DSBs at close proximity may affect nucleosomal stability and lead to processing failures like deletions and exchange-type aberrations (Fig. 6F). Notably, in this case the outcome in terms of damage probability will depend not only on the stochastic nature of the track structure, but also on the compactness of the targeted chromatin site.

Nucleosomes represent the lowest level of chromatin organization with a nucleosome core particle consisting of approx. 147 bps wrapped 1.67 left handed superhelical turns around the octameric histone core. Two strands of DNA within the nucleosome width of 3 nm are presented on the nucleosomal surface. The histone core contains a modular complex of two H2A–H2B dimers and a (H3–H4) tetramer that are connected by a 0-80 bp linker DNA. It is considered that the nucleosome filament is packed into the secondary structure of an approx. 30 nm chromatin fiber including 6-7 nucleosomes per 10 nm length of fiber. Recent results using novel chromosome conformational capture techniques question the existence of such structure (Dekker 2008; Eltsov, MacLellan et al. 2008; Fussner, Strauss et al. 2012; Nishino, Eltsov et al. 2012) and favour an alternative structural model of human chromosome with the 10-nm fiber folded in a regulated manner as a long-lived fractalGlobule (lower right corner of Fig. 6) (Lieberman-Aiden, van Berkum et al. 2009; van Berkum and Dekker 2009; Thurman, Rynes et al. 2012).

The clustering of DSBs at distances from about hundred bp to few hundred thousand bp will destabilize chromatin and may lead to fragment loss. The process of destabilization will strongly depend upon the actual chromatin structure in the region that sustained this form of DNA damage. Chromatin structure may also affect the linear distance of interacting DSBs. Thus while under some circumstances interaction distances of a few hundreds of bp are envisioned, interactions may also be possible between DSBs separated by Mbp (Fig. 7). Forms of such interactions are actually naturally occurring in a cell during the process of V(D)J and class-switch recombination.(Boboila, Alt et al. 2012). T6-DSB can also be considered as a form of highly local chromothripsis, a

phenomenon by which tens to hundreds of chromosomal rearrangements occur in a single event of cellular crisis.(Stephens, Greenman et al. 2011; Forment, Kaidi et al. 2012; Molenaar, Koster et al. 2012).

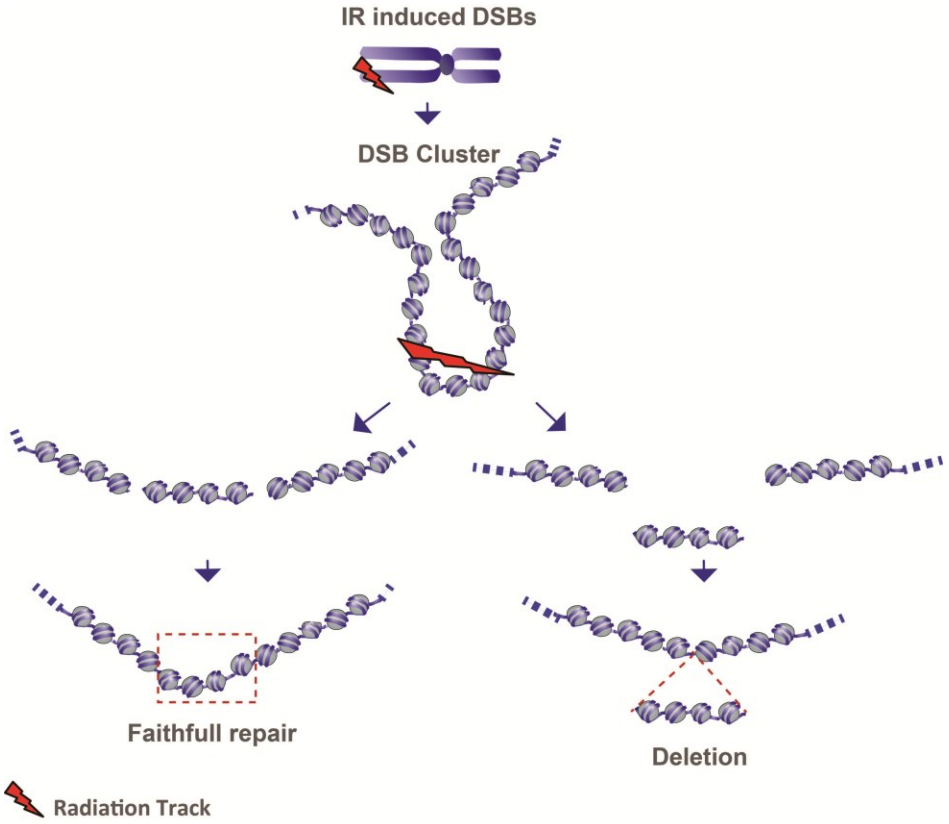

Fig.7: Nucleosomal loss induced by DSB clusters. Two scenarios of repair outcomes for clustered DSBs are shown. In the first scenario (left) the sequence is restored. In the second scenario a deletion occurs due to nucleosomal loss (right) (Schipler and Iliakis 2013).

Several investigations applying theoretical modeling by Monte Carlo Calculations, PFGE and atomic force microscopy (AFM) after high and low LET irradiation describe the potential of clustered DSBs to fragment the genome (reviewed in Schipler and Iliakis 2013). Monte Carlo simulations for DSB induction on higher order structure by radiations of different LET showed regional DSB clustering with the potential of generating DNA fragments (Friedland, Jacob et al. 1998; Friedland, Jacob et al. 2003; Friedland, Dingfelder et al. 2005; Ponomarev and Cucinotta 2006; Friedrich, Scholz et al. 2011). Fragmentation peaks were found at 85bp and multiples of 1000bp

independently of LET (Holley and Chatterjee 1996). This fragmentation pattern represents the revolution period about the nucleosome (~85 bp). In support to this theoretical modeling approach, PFGE showed the generation in human fibroblasts exposed to X-rays and iron ions of DNA fragments in the predicted size range (0.1-2 kbp) (Rydberg 1996). Results obtained using atomic force microscopy imaging (AFM) provide further support for the induction of clustered DSBs forming short DNA fragments - even when irradiating “naked” DNA devoid of any organization in form of chromatin (Pang, Winters *et al.* 2011). Thus, low LET irradiation of pUC19 plasmid DNA (2864 bp) shows that 35% of the generated fragments are 0-50 nm in size (<147 bp), and this proportion increases to 70% after exposure to high LET argon irradiation.

In conclusion, the generation of short DNA fragments by T6-DSBs point to their high risk potential to induce severe biological consequences, but to this date a biological system enabling the investigation of clustered DSBs does not exist.

2. Aim of the work

To assess whether clustered DSBs (T6-DSBs) are a relevant source for adverse biological consequences generated after the induction of DNA damage by IR, we developed an I-*Sce*I homing-endonuclease-based model system. Until now the possible consequences of DSB clustering were modeled by Monte Carlo simulations; a biological system for *in vivo* validation of the expected biological effects was missing, because the stochastic nature of DNA-lesion-induction by IR does not allow the controlled generation of appropriate forms of DNA damage.

For our model systems we constructed plasmids harboring different numbers of I-*Sce*I restriction sites, ranging from one to four, located at defined distances. The distance of two hundred bps between consecutive I-*Sce*I sites was chosen at first since it reflects the length of DNA that winds around a nucleosome plus the associated linker region. We are hypothesizing that such distances will affect nucleosomal stability, may lead to nucleosome loss and thus to repair failures causing chromosomal aberrations or large deletions. To increase the level of complexity, the I-*Sce*I restriction sites were engineered in the same and in opposite orientation, generating thus either compatible or incompatible ends after the loss of the intervening sequence. Compatible ends can be simply ligated by the repair machinery whereas incompatible ends require end processing before ligation. Constructs harboring different assemblies of I-*Sce*I restriction sites were integrated at multiple locations in the genome of wt and mutant CHO cells. This generated model systems that can mimic events caused by IR, where DSBs are induced simultaneously along the particle tracks at various locations throughout the genome.

To achieve multiple random integrations we introduced the highly efficient Sleeping Beauty transposon technology (SB). The various I-*Sce*I constructs were cloned into the transposon plasmid carrying a neomycin resistance gene for selection and co-transfected with the transposase expressing plasmid that catalyzes the cut and paste transposition event. In order to investigate the contribution of the different repair pathways for simple and clustered DSBs we utilized in addition to wt CHO cells the

following HR and D-NHEJ mutants: Irs1SF with defect in XRCC3, Xrs6 defective in Ku80, and XR-C1-3 defective in DNA-PKcs. After generating a large set of genetically modified cells we characterized them by Southern blotting for the number of integrations, which reflects the number of possible clustered DSBs that can be induced upon transfection and expression of I-*Sce*I. A schematic showing cells with integrations of constructs harboring different combinations of I-*Sce*I sites is shown in Fig. 8.

Experiments were performed using clonal cell lines generated from wt cells and the above outlined CHO mutants and harboring different numbers of the different forms of I-*Sce*I recognition site clusters. From these I-*Sce*I recognition site clusters, DSB clusters can be generated by transient expression of I-*Sce*I and the mediated responses can be investigated at different relevant biological endpoints (Fig. 8). The killing potential of clustered DSBs was examined by the clonogenic survival assay and repair failures that cause chromosome aberration were measured by premature chromosome condensation (PCC) in G2-phase cells. Furthermore, consequences of DSB clustering on cell signaling were investigated by life-cell imaging with reporter plasmid expressing fluorescently tagged (EGFP) MDC1, or 53BP1 fusion proteins.

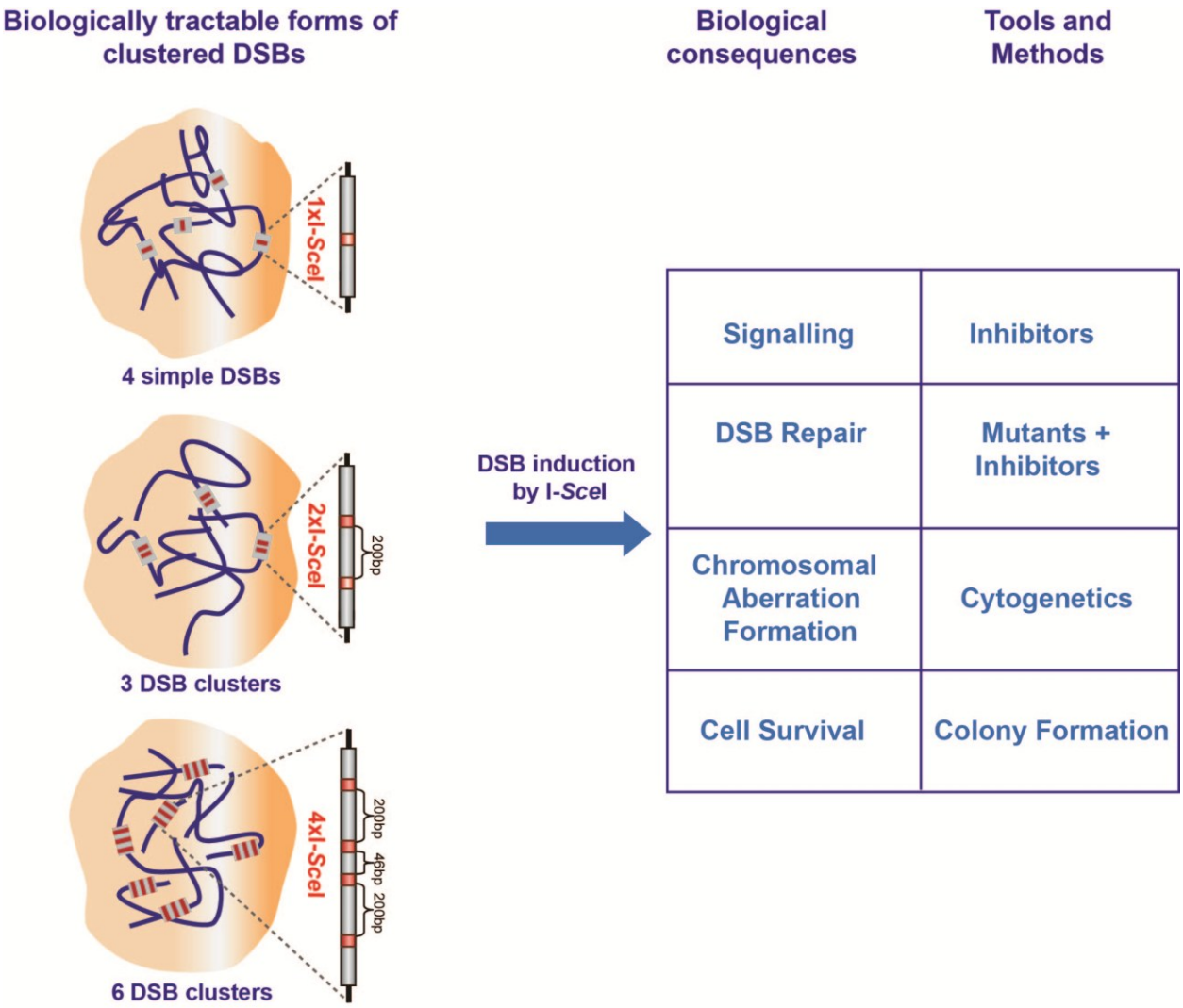

Fig. 8: Schematic illustration of the experimental design. On the left three vertebrate cells are shown with different numbers of genomic integrations. For each of the cells one integration is magnified showing the constructs with 1-, 2- and 4xI-*Sce*I recognition sites modeling potential simple and clustered DSBs, respectively. After DSB induction by I-*Sce*I several biological endpoints (indicated at the right) can be evaluated in vivo with this model system using the indicated approaches and methods.

3. Previous investigations with the I-*Sce*I model system

In the first attempt to elucidate the cellular effects of DSB clustering, experiments with the I-*Sce*I model system established in the human A549 cell line were performed in collaboration with J. Saha (Saha 2010). Survival experiments with A549 clones showed strong cell killing after I-*Sce*I induced two-DSB clusters in contrast to simple DSBs. The observed killing effect was dependent on DSB clustering, as well as on the number of I-*Sce*I construct-integrations in the genome. The conclusion was drawn that closely located DSBs are prone to DNA fragment loss and are therefore biologically more effective than simple DSBs. The PCR analysis of the repair junctions revealed that deletions occur around the break junctions in the case of clustered DSBs. Furthermore the DSB end configuration also played a role for cell survival. DSBs forming incompatible ends after the loss of the intervening sequence lead more often to cell death than DSBs with directly ligatable, compatible ends.

To investigate the effect of clustered lesions on chromosome level the formation of chromosomal aberrations was analyzed. But the results were puzzling as the low number of chromosome breaks did not correlate with the strong killing observed in the survival experiments. A possible explanation for this discrepancy was found by live cell imaging of an A549 clone bearing clustered DSBs after co-transfection with I-*Sce*I and a 53BP1-EGFP- expressing plasmid. Observations lead to the suggestion that a large fraction of the cells underwent apoptosis after transfection. The conclusion was drawn that transfected cells may activate apoptotic signals resulting in cell death. Apoptotic cells evade the analysis performed for the evaluation of chromosomal aberrations.

Taken together the results obtained with the A549 model system partially confirm the hypothesis that clustering of DSBs at distances affecting nucleosomal stability may be highly lethal for the cell, but the model system has to be refined to overcome limitations that hamper analysis. In an attempt to find a solution, we established the system in the p53 deficient cell line CHO10B4 that is less prone to apoptosis, as part of this thesis. Furthermore the cell line is advantageous as it has different mutants of the HRR and NHEJ pathway that were additionally applied for the generation of clones.

4. Materials and methods

4.1. Materials

4.1.1. Laboratory apparatus

Beckman Tabletop GS-6R centrifuge	Beckman Coulter, USA
BioFuge (Fresco)	Thermo Scientific, Germany
Cell culture “Herasafe” hood	Thermo Scientific, Germany
CO_2 Incubator	Sanyo, Japan
Confocal laser scanning microscope	Leica Microsystems, Germany
Coulter Counter	Beckman Coulter, USA
Electro-Transfer Unit	Bio-Rad, USA
Express Pipet-Aid	BD Falcon, USA
Flow Cytometer	Beckman Coulter, USA
FluorImager Typhoon 9400	Molecular Dynamics, Germany
Heating unit	Peter Oehman, Germany
Hybridizer HB-1000	UVP LLC, USA
Inverted Microscope	Olympus, Japan
Magnetic Stirrer	Heidolph, Germany
Molecular Imager VersaDoc	Bio-Rad, USA
Nanodrop	Thermo Scientific, Germany
Nucleofector	Lonza Cologne GmbH, Germany

Odyssey® infrared imaging system	LI-COR Biosciences, Germany
Overnight Culture Shaker	Infors, Germany
Pasteur pipette	BD Falcon, USA
Peristaltic pump	Ismatec, Switzerland
pH Meter	InoLab, Germany
Pipettes	Eppendorf, Germany
Rocky Shaker	Peter Oehmen, Germany
Roller drum	Bellco Biotechnology, USA
Scintillation Counter	Beckman Coulter, USA
SDS PAGE mini gels	Mini PROTEAN, Bio-Rad, USA
Temperature control system for Microscopes, environmental chamber for live cell imaging experiments, “Cube & Box”	Live Imaging Services, Switzerland
Thermo-mixer	Eppendorf
Typhoon Scanner	GE Healthcare, USA
Ultracentrifuge	Beckman Coulter, USA
UV Spectrophotometer	Shimadzu Corp., Japan
Vortexer (Vortex-Genie 2)	Scientific Industries, USA
Water Bath	GFL Instruments, Germany
Weighing Balance	Sartorius (BP110 S)
X-ray machine	GE Pantak, Germany

4.1.2. Disposable elements

0.2 µm filter	Millipore, USA
1.5 and 2 ml tubes	Eppendorf, Germany
15 & 50 ml Centrifuge Tubes	BD Falcon, USA
Cell Culture Dishes	Cell Star, USA
Dounce homogenizer	KonTes, Kimble Chase, USA
Flasks and beakers	Schott Duran, Germany
Nitrocellulose membrane	Schleicher Schuell, Germany
Nylon membrane	Roche, Germany
Parafilm	Lab Depot Inc. USA
PVDF membrane	GE Health care, USA
Rainin Pipettes	Mettler Toledo, Germany
Spinner Flask	Bellco, USA
UV Cuvettes	Hellma, Germany

4.1.3. Chemical reagents

Acrylamide-Bis-acrylamide	Roth, Germany
Albumin Bovine	Sigma-Aldrich, USA
Bromophenol Blue	Sigma-Aldrich, USA
Commassie brilliant blue G-250	Serva, USA
DMEM	Sigma-Aldrich, USA
dNTPs	Promega, USA

DTT	Roth, Germany
EDTA	Roth, Germany
Ethanol	Roth, Germany
FCS/FBS	Gibco Life Sciences, USA
Glycerol	Roth, Germany
Glycine	Roth, Germany
Isopropanol	Roth, Germany
KCl	Roth, Germany
Lactalbumin hydrolysate	Sigma-Aldrich, USA
Luria Agar	USB Corp, USA
Luria Broth	USB Corp, USA
McCoy’s 5A	Sigma-Aldrich, USA
MEM	Gibco Life Sciences, USA
Methanol	Sigma-Aldrich, USA
NaCl	Roth, Germany
Non-Fat dry milk	Roth, Germany
Nonidet P40	Roche, Germany
Phusion Hot-Start High Fidelity Polymerase	Finnzymes-NEB, USA
Poly L-Lysine	Biochrom AG, Germany
ProLong Gold Antifade solution	Invitrogen, USA.
Propidium Iodide	Sigma-Aldrich, USA

RNase	Sigma-Aldrich, USA
TEMED	Roth, Germany
TRIS Base	Roth, Germany
Tris-HCL	Sigma-Aldrich, USA
Triton X-100	Roth, Germany
Trypsin	Biochrom, Germany
Tween 20	Roth, Germany

4.1.4. Commercial kits

Calf Thymus DNA	Invitrogen
DNA cellulose resins	Sigma-Aldrich, Germany
DNA Maxi-prep Kit	Qiagen, USA
ECL Western Blotting Reagent	GE Healthcare, USA
FlexiGene DNA Kit	Qiagen, USA
Hi Load (26/60) SuperDex 200	GE Healthcare, USA
HiTrap^{TM} Heparin prepacked column	GE Healthcare, USA
Label IT CX Rhodamine Labeling kit	Mirus Bio, USA
Prime-It II Random Primer Labeling kit	Stratagene, USA.
ProbeQuant G-50 Columns	GE Healthcare, USA
QIAquick Nucleotide removal Kit	Qiagen, Germany
QuikHyb Hybridization Solution	Stratagene, USA
α-^{32} P CTP	Perkin Elmer, USA

4.1.5. Cell lines

Species	Name	Cell type	Description
Chinese hamster	CHO-10B4	Fibroblast	Repair proficient
Chinese hamster	Irs1SF	Fibroblast	mutation in XRCC3
Chinese hamster	XR-C1-3	Fibroblast	mutation in DNA-PKcs
Chinese hamster	Xrs6	Fibroblast	mutation in Ku 80
Human	U2OS-HA-ER-AsiSI	Osteosarcoma	Cell line stably transfected with the pBABE vector HA-ER-AsiSI
Human	U2OS	Osteosarcoma	-

4.1.6. Antibodies

Name	Provider
Alexa Fluor 488 (mPab, rPab)	Invitrogen, Germany
GAPDH (mMab)	Millipore, Germany
IRDye 680 (mPab, rPab)	LI-COR Biosciences, Germany
I-*Sce*I (rPab)	Santa Cruz Biotechnology, Germany
Lamin A/C (mMab)	Santa Cruz Biotechnology, Germany
Myc Tag (mMab)	Gene Tex, USA
γ-H2AX (mMab)	Abcam, UK

4.1.7. Software

Name	Provider
Adobe Creative Suite® 5.5	Adobe Systems, USA
Image Quant	Adobe Systems Inc. USA
ImarisXT® 6.0	Bitplane AG, Switzerland
Kaluza®	Beckman Coulter, USA
Las AF®	Leica Microsystems, Germany
Metafer®	MetaSystems, Germany
Quantity One®	Bio-Rad, USA
SigmaPlot® 11	Systat Software Inc. USA
Wincycle™	Phoenix Flow Systems, USA

4.1.8. Plasmids

Name	Description
pcDNA3B-puro-mycNLSERt I*Sce*-ERt	Expresses a controllable I-*Sce*I protein ((Hartlerode, Odate et al. 2011)
pCMV3xnlsI*Sce*I	I-*Sce*I expressing Plasmid (M. Jasin)
pCMVT7-SB100x	Transposase experessing plasmid (Ivics, Hackett et al. 1997)
pIRESNeo2-53BP1-EGFP	Expresses a 53BP1-EGFP fusion protein
pEGFP-C2-MDC1	Expresses a MDC1-EGFP fusion protein

pmaxGFP	GFP expressing plasmid
pPCRScript 1SB-1NS	Cloning vector with one I-*Sce*I site
pPCRScript 200A	Cloning vector with two I-*Sce*I sites in direct orientation
pPCRScript 200B	Cloning vector with two I-*Sce*I sites in reverse orientation
pT2SVNeo	Transposon (Ivics, Hackett et al. 1997)
pT2SVNeo 1SB-1NS	Transposon with one I-*Sce*I site construct
pT2SVNeo 200A	Transposon with two I-*Sce*I site constructs in direct orientation
pT2SVNeo 200B	Transposon with two I-*Sce*I site constructs in reverse orientation

4.1.9. Oligonucleotides

Name	Sequence
Double 200Isce1Agfw5`	CCCGAATTCGGGTCTAGACTCGAGG
Double 200Isce1Agrev5`	CCAGAGCTCTACCCGCGGAGATCT
Double 200Isce1Agfw3`	CCAGAGCTGGGTCTAGACTCGAGGG
Double 200Isce1Agrev5`	CCAGAGCTCGAATTCTACCCGCGC

4.2. Methods

4.2.1. Cell culture

Cells were cultivated in 100 mm tissue culture dishes with 15 ml McCoy's growth media supplemented with 10% fetal bovine (FBS) and kept in incubators (Sanyo) at 37 °C with 5% CO_2. Exponentially growing cells were passaged every two (CHO) or three (U2OS) days keeping them at a maximum confluence of less than 75%. For passaging, media was removed and cells were washed with 1 x PBS. 2 ml of 0.05% trypsin-EDTA was added and incubated for 3 min at 37 °C to detach the adhering cells. Trypsin was inactivated by adding 5 ml growth media and cells were resuspended with a Pasteur pipette to reduce cell clumping. Cells were counted with the Coulter Counter (Multisizer™, Beckman Coulter) and appropriate numbers of cells were plated for subculture. Cells were discarded after approx. 30 passages. When frozen cells were thawed, they were passed two times before performing experiments with them.

4.2.2. Cryopreservation of cells

For long term cell storage the freezing protocol of Borrelli was applied (M.J. Borrelli et *al.* 1987). $5x10^6$ cells were centrifuged after trypsinization at 4 °C, the media was removed and the pellet was dissolved in cold 500 µl freezing solution A (80% freezing stock: 5 mM KH2P04, 25 mM KOH, 30 mM NaCl, 0.5 mM $MgCl_2$, 20 mM L-lactic acid, 5 mM glucose and 0.2 M sorbitol; with 20% sterile MQ water) and kept on ice. 500 µl of freezing solution B (80% freezing stock with 20% DMSO) was added and finally the cells were frozen at -150 °C in cryo vials. One day after thawing the cells, media was changed to remove DMSO and the cells were passaged twice prior to use for experiments.

4.2.3. Drug treatments

Inhibitors were dissolved in dimethyl sulfoxide (DMSO) and added to the culture medium immediately after transfection. The DNA-PKcs inhibitor NU7441 was applied at a concentration of 5 µmol/l. PJ34 inhibits PARP and was used at a concentration of 10 µmol/l.

50 mg/ml stock of G418 was prepared in 100 mM HEPES. The solution was sterilized by filtering through a 0.22 µm filter. Different concentrations were applied for specific cell lines (ranging from 300-500 µg/ml). All stocks were stored at -20 °C.

4.2.4. Transfection by electroporation

The Amaxa Nucleofector® device was used for transfection. $1x10^6$ – $8x10^6$ exponentially growing cells were transfected with 500-1000 ng plasmid/$1x10^6$ cells. The cells were trypsinized, centrifuged at 900 rpm and dissolved in 100 µl transfection reagent. The solution was mixed with max. 10 µl of plasmid and transferred to the electroporation cuvette. According to manufacturer instructions, transfection programs U32 and X05 were used for CHO and U2OS cells, respectively. After transfection the cells were transferred to prewarmed media. Transfection efficiency, measured by FACS analysis of pmax-GFP transfected cells, varied between 90-95% for CHO cells, and was about 70% for U2OS cells.

4.2.5. Ionizing Radiation (IR) exposure

Cells were irradiated with X-rays using an X-ray machine ("Isovolt 320HS", Seifert/Pantak, General Electric-Pantak). Tube voltage and current were set to 320 kV and 10 mA respectively and 1.65 mm aluminium filter (GE-Healthcare) was used to absorb "soft" X-rays. The dose rate was estimated to 1.3 Gy/min using in-field ionization monitor, calibrated with a PTB dosimeter (Physikalisch-Technische Bundesanstalt, Braunschweig, Germany). Radiation dose was confirmed with Fricke's chemical dosimetry. An even irradiation field was ensured by rotating the radiation table. Cells were returned to the incubator immediately after IR and collected at different time points post irradiation.

4.2.6. PCR

PCR (Polymerase chain reaction) was performed to amplify DNA sequences and introduce additional restriction sites for further cloning. The PCR reaction mixture was set up in a total volume of 20 µl containing of 1-10 ng template DNA, 100 mM dNTP Mix, 1 x PCR-Buffer, 2.5 U Phusion® Polymerase, 0.2 µm of reverse and forward primer and MQ water. For primer sequences see Table 1. The amplification reactions were

performed in a Mastercycler-ep-gradient-S thermal cycler (Eppendorf) with the program illustrated in Table 1. The PCR fragment was run on an agarose gel and extracted using the Qiagen gel extraction kit.

Table 1: program set in the thermo cycler for PCR

Program	Cycles	Temperature	Time
Denaturation	1	98 °C	30 sec
Denaturation	35	98 °C	15 sec
Annealing		65-68 °C	15 sec
Elongation		72 °C	15 sec
Elongation	1	72 °C	5 min
	∞	4 °C	

4.2.7. Agarose gel electrophoresis

1% Agarose gels were prepared for plasmid DNA and 0.8% gels were prepared for genomic DNA. After mixing the agarose with 100 ml 1xTAE (40 mM Tris-Acetate, 1 mM EDTA) the solution was heated in the microwave until boiling. The warm liquid agarose was poured into a 10 x 7 cm gel tray and left to cool down for 1 h RT in order to polymerize. The gel was loaded and run in a 1 x TAE filled electrophoresis chamber (Life Technologies ^{TM}) at 1 Volt/cm for 1.5 h in case of plasmid DNA and 6 h with 0.5 Volts/cm in case of genomic DNA. In order to visualize the DNA, the gel was stained for 1 h in 50 ml 1 x TAE containing 1% ethidium bromide (EtBr) under gentle shaking.

4.2.8. Restriction enzyme digestion

The restriction reactions for cloning-fragments were carried out in a total volume of 20 µl. 3 µg vector DNA and 900 ng insert DNA, were mixed with 1 U restriction enzyme, 1 x enzyme buffer and MQ water. The reaction mixture was incubated for 30 min at 37 °C. Prior to ligation the fragments were eluted with the QIAquick Gel Extraction Kit (Qiagen).

4.2.9. Ligation

Ligation of insert and vector were carried out at a 1:4 ratio. The reaction mixture with total volume of 20 µl contained 1 x ligation buffer, 1 U T4 Ligase and MQ water. The reaction mixture was incubated at 22 °C overnight.

4.2.10. Transformation

100 µl competent *E.coli* cells were transformed with10 ng of plasmid DNA, or 7 µl of ligation reaction, respectively. The reaction was incubated for 40 min on ice before heat shock was performed at 42 °C for 50 sec in a Thermo Mixer (Eppendorf) and immediately incubated on ice for 2 min. 800 µl SOC Media was added to the bacterial culture and incubated for 1.5 h at 37 °C with orbital shaking at 220 rpm. Finally 300 µl of the culture was plated on LB-Agar plates containing the antibiotics (100 µg/mL ampicillin and K50 µg/ml kanamycin) according to the resistance gene of the transformed plasmid. LB-Agar plates were incubated at 37 °C overnight.

4.2.11. Generation of competent *E.coli*

For generation of competent *E.Coli* cells of the BL1-blue strain, 50 µl competent cells were incubated in 2 ml LB overnight at 37 °C under orbital shaking at 220 rpm (Thermo). In the next step 2 ml of the overnight culture were added to 200 ml LB media and grown at 37 °C on the shaker until they reached an OD_{600} of 0.4. The culture was chilled on ice for 5 min and centrifuged at 3300 x g at 4 °C for 10 min. The pellet was resuspended in 30 mL ice cold 0.1 M $CaCl_2$, incubated on ice for 30 min and centrifuged. The pellet was dissolved in 6 ml 0.1 M $CaCl_2$ solution supplemented with 15% glycerol. Finally, 500 µl aliquots were frozen at -80 °C.

4.2.12. Plasmid preparation

Supercoiled SB transposon (pt2SVNeo) plasmids with different integrations and SB transposase plasmids (pcMV100x) were prepared using CsCl/EtBr gradients. 1 l of plasmid transformed *E. Coli* culture was grown overnight to an OD_{600} of 1.0. The cells were centrifuged for 30 min at 1300xg at 4 °C. After re-suspending the pellet in 10 ml Sucrose/Tris/EDTA solution, 2 ml lysozyme was added, mixed by swirling and incubated for 30 min at RT. 4 ml Triton lysis mix was added and the culture incubated at 37 °C before centrifuging for 1 h in a Beckman JA 25.50 rotor at 48400 x g. The volume of the decanted supernatant was determined and 0.95 g CsCl per ml was added and dissolved. In the next step 0.1 ml of 10 mg/ml EtBr solution was added per ml supernatant and centrifuged for 20 min in a Beckman JA 25.50 rotor at 7000 rpm. For plasmid banding the solution was transferred to Beckman: 4.2 ml ultracentrifuge tube and centrifuged for 16 hours at 20 °C in an ultracentrifuge (Beckman Optima Max) in a near vertical rotor MLN80 at 240000xg.

The lower band containing the supercoiled plasmid was transferred to another 4.2 ml ultracentrifuge tube and topped with CsCl/TE solution containing 0.2 mg/ml EtBr and centrifuged under the same conditions as before. The lower plasmid band was removed and extracted with 1:1 phenol/chloroform twice. The upper phenol phase was discarded while the lower phase was transferred to a fresh tube and precipitated with final ethanol concentration of 66% overnight at –20 °C. After centrifugation (Beckman JA 25.50 at 40.000xg for 30 min) the pellet was dissolved in 0.5% SDS in TE buffer and extracted

again with phenol/chloroform saving the upper phase that was precipitated with ethanol twice. Finally the pellet was dissolved in TE and dialysed.

4.2.13. Preparation of whole cell lysate

Whole cell lysates were prepared using $2x10^6$ cells. After washing in 1 x PBS and pelleting, cells they were dissolved in 200 µl RIPA buffer. 1 x protease inhibitor cocktail (10 µl for 1 ml) was added to the reaction mixture and incubated for 30 min on ice. The mixture was centrifuged at 14000 x g for 20 min at 4 °C to finally transfer the whole cell lysate to a new tube. The colorimetric Bradford assay was applied to measure protein concentration using a calibration curve generated with different amounts of BSA.

4.2.14. Protocol for REAP nuclear/cytoplasmic fractionation

For subcellular fractionation the REAP (rapid, efficient and practical) protocol was applied (K. Suzuki et *al*. 2010). $4x10^6$ cells were washed twice with ice cold PBS, the cells were scraped with a cell scraper and collected in a 1.5 ml micro-centrifuge tube. After 1 min centrifugation (1200 rpm at 4 °C) the supernatant was decanted. The following steps were carried out on ice. The cell pellet was triturated five times with 500 µl cold 0.1% NP40-PBS (Calbiochem, San Diego, CA, USA) and spun down for 1 min. The supernatant, containing the cytoplasmic fraction was removed and centrifuged at 8000xg at 4 °C for 1 min and transferred to a new tube. The cell pellet, containing the nuclear fraction was resuspended in 500 µl cold 0.1% NP40-PBS and centrifuged for 1 min. After decanting the supernatant the pellet was re-suspended in 200 µl 0.1% NP40-PBS and sonicated on ice twice for 10 sec.

4.2.15. Clonogenic survival assay

For the clonogenic survival assay, exponentially growing cells were irradiated with 4, 8 and 12 Gy of X-rays, trypsinized immediately and plated in different dilutions according to the dose of radiation delivered. For survival with I-*Sce*I transfected cells, 100 and 200 cells were plated in 60 mm dishes immediately after transfection. Transfection with the GFP expressing plasmid max-GFP served as an additional control. Furthermore, to measure the transfection efficiency, $1x10^6$ max-GFP transfected cells were plated and FACS analysis measuring the GFP intensity was performed 24 h after transfection.

Cells plated for survival were grown for 10 days (CHO), or 14 days (U2OS) and then stained with 0.75% crystal violet dissolved in 100% methanol. Colonies were counted either manually using a microscope or with the colony counter.

4.2.16. Cell cycle analysis by FACS

Fluorescence-activated cell sorting (FACS) is a specialized type of flow cytometry that allows cell sorting by assessing fluorescence intensity. Cell cycle distribution was evaluated by measuring the propidium iodide (PI) fluorescence intensity. The stoichiometry of PI binding to DNA is sequence independent, making it a convenient means of quantification. Cells were washed with 1 x PBS, trypsinized at 37 °C for 5 min and resuspended in growth media. $1x10^6$ untreated or irradiated cells and $2x10^6$ transfected cells were collected and centrifuged with 100 x g at 4 °C for 5 min. The media was removed, the cell pellets dissolved in cold 70% ethanol and stored at -20 °C overnight. In the next step the cells were centrifuged (100 x g, 5 min), the supernatant was removed and the cells were dissolved in 800 µl PI staining solution (40 µg/ml PI, 62 µg/ml RNaseA dissolved in PBS) per $1x10^6$ cells for 20 min. at 37 °C. The samples were measured in a flow cytometer (Coulter Epics XL, or Gallios™, Beckman Coulter) according to pre-established protocols that were optimized for each cell line. To obtain standard histograms 15000 events were counted, and gated. LMD data files were analysed using the Kaluza® flow cytometry analysis software. Cell cycle distribution calculations were made by WinCycle® software using the generated HST files.

4.2.17. G2-premature chromosome condensation (G2-PCCs)

For G2-PCC preparation $6x10^6$ I-*Sce*I transfected and $2x10^6$ untreated or irradiated cells were plated for the 8 h time point and $4x10^6$ or $1x10^6$ cells for the 24 h time point, respectively. At the indicated times 100 nM Calyculin A was added for 25 min. Due to Calyculin A treatment the cells round up and detach, therefore the cells could be “shaken off” by slightly tapping the dish. The cells were collected and centrifuged at 1300 rpm for 7 min. The media was removed leaving 1 ml behind to dissolve the pellet. 10 ml of hypotonic solution (75 mM of KCl) was added drop wise while slightly tapping the tube and incubated for 5 min at RT. After 5 min. centrifugation the supernatant was removed, cells were dissolved and fixed in 10 ml Fixative (3:1 methanol: glacial acetic

acid) and kept at 4 °C overnight. After washing the cells twice in fixative, metaphase spreads were prepared and stained in 3% Giemsa stain, dissolved in 1 x Sörensen`s buffer for 15 min and washed with tap water. The slides were air dried at RT overnight and finally mounted with coverslips using Entellan® (Merck). An automated imaging system (MetaSystems) was used to obtain high quality images of metaphase chromosomes.

For searching metaphases the M-Search module of the Metafer software (MetaSystems) was employed, using the 10x objective of the Zeiss microscope. A classifier was used for M-Search that was specifically trained for the selected cell line. After performing M-Search, metaphases with good spreading were selected and captured at a higher magnification (63x oil immersion objective) using the AutoCapt setting of the Metafer software.

Images were analysed using the Ikaros Software. For analysis 100 G2-PCC spreads were scored for each time point in three independent repeats. G2-PCC fragments and inter-chromosomal exchanges were counted separately. The data shows the average of G2-PCC breaks or exchanges of three experiments with the error bars representing the standard deviation; significance values were calculated by the t-test for dependent samples.

4.2.18. Southern blotting

Southern blotting is applied to detect specific sequences of plasmid, bacteriophage or genomic DNA by a radioactive probe. The methodology for Southern blotting is divided into several steps. After digestion of the genomic DNA and separation of the digested fragments by agarose gel electrophoresis the DNA fragments are transferred via upward capillary transfer onto a nylon membrane resulting in immobilization of the DNA fragments and preservation of the same DNA banding pattern that was present on the gel. During the next step the membrane is used as a substrate for hybridization with radioactively labelled DNA probes that recognize a specific DNA sequence.

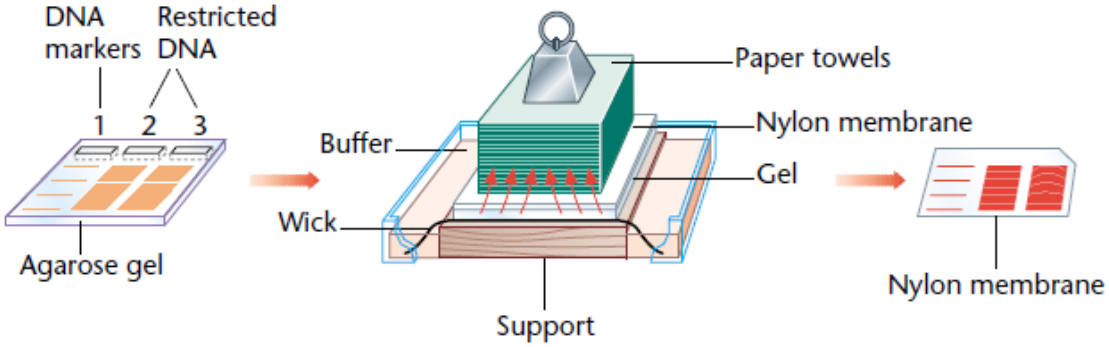

Fig. 9: Schematic representation of Southern blotting (T. A. Brown 2001).

4.2.18.1. Preparation and digestion of genomic DNA

For genomic DNA preparation from CHO cells the DNeasy Blood & Tissue Kit from Qiagen was used with the following modification of the protocol provided by the manufacturer: $12x10^6$ CHO cells were spun at 1500 rpm after trypsinization and washing with 1 x PBS. The supernatant was removed and cells were dissolved in 2 ml FG1 solution in a 15 ml falcon tube. In the next step 2 ml FG2 solution mixed with 100 µl Proteinase K from a 10 ug/ml stock solution was added. The reaction mixture was incubated at 54 °C for 6 h while shaking (400 rpm) in a Thermo-mixer (Eppendorf). After incubation the reaction mixture was transferred to a 50 ml Beckman centrifuge tube,

5 ml isopropanol were added and the tube was shaken until the DNA precipitate was visible. The tubes were centrifuged for 20 min at 4 °C in the Beckman centrifuge. The pellet was washed with 2 ml 70% EtOH and centrifuged again for 15 min. In the last step the pellet was dried at 37 °C and dissolved in 1 ml FG3 while shaking at 64 °C in a water bath. In order to prepare genomic DNA for Southern blotting, 18 µg of genomic DNA were digested with 0.3 Fast Digest Unit (FDU)/µg DNA. After adding the enzyme the reaction was incubated for 12 h at 37 °C and shaken every 15 min at 400 rpm for 15 min in the Thermo-mixer. After digestion the DNA was EtOH precipitated.

Table2: Reaction Mixture for gDNA digestion

DNA	x µL (15 µg)
FD Restriction enzyme buffer (10x)	20 µL
Milli-Q water	x µL
FD XbaI	6 µL (6 x 1 FDU)
Total volume	200 µl

4.2.18.2. Ethanol precipitation of digested DNA

0.1 Vol. of 5 M NaCl and 2.5 Vol. of 100% ethanol were added to 200 µl DNA restriction reaction and incubated at –80 C overnight. The reaction mixture was centrifuged for 30 min at 1300 rpm at 4 °C. After removing the supernatant 200 µl of 70% ethanol was added to the DNA pellet and centrifuged. The pellet was dried for 15 min at 37 °C and dissolved in 25 µl TE buffer. To remove residual ethanol, the dissolved DNA was incubated at 65 °C for 10 min with opened lid of the micro-centrifuge tubes.

4.2.18.3. Depurination and denaturation

Since fragments larger than 15 kb are difficult to transfer to a blotting membrane, the agarose gel was treated with depurination solution (0.2 M HCl) for 7 min on a platform shaker to cleave the DNA strands. During depurination the β-N-glycosidic bond is hydrolytically cleaved leading to the formation of apurinic sites in the DNA. After

depurination the gel was rinsed twice in MQ water and subsequently treated twice for 15 min with denaturation solution (1.5 M NaCl and 0.5 M NaOH) while shaking. This step is required to denature the double stranded DNA to single stranded DNA so that it can be efficiently transferred to the nylon membrane and hybridized to a labelled probe. Furthermore in combination with depurination, denaturation results in the hydrolysis of the phosphodiester backbone at apurinic sites. The gel is again rinsed twice in MQ water and incubated twice on the shaker for 15 min in neutralization solution (1 M Tris (pH 7.4) and 1.5 M NaCl).

4.2.18.4. Transfer to a nylon membrane

A transfer apparatus was built to perform the transfer of the DNA fragments from the agarose gel to the nylon membrane (Fig. 9). After equilibrating the agarose gel for 20 min in 20 x SSPE (3 M NaCl, 0.2 M $NaH_2PO_4 \cdot H_2O$ and 0.02 M EDTA) it was placed on Whatman paper soaked in 20 x SSPE. The Whatman paper is placed on a glass plate on the top of a plastic support and forms a connection between the gel and the container with the reservoir of 20 x SSPE. The wet nylon membrane was placed on the top of the gel and fixed with Para film at the sites before four pieces of 20 x SSPE soaked Whatman paper and a tower of paper towels were placed on the membrane. Additionally four pieces of plastic wrap were fixed on the sides of the nylon membrane and stretched over the sides of the plastic container. This avoids contact between the paper towels and the Whatman paper that would hinder capillary transfer. To stabilize the construct and increase capillary transfer, a 500 g weight was placed on the top of the paper towels. After 24 h of transfer, the transfer apparatus was disassembled and the nylon membrane was rinsed in MQ water and equilibrated in 6 x SSPE for 10 min. In order to crosslink the DNA to the membrane, it was baked at 110 °C for 50 min.

4.2.18.5. Generating radioactive probes for hybridization reactions

A 1.7 kb sequence of the integrated transposon construct served as the probe binding site. 3 µg of the pt2SVNeo transposon plasmid was digested with 1 unit HindIII. The digested plasmid DNA was separated on a 1% agarose gel run at 2 Volts/cm and the DNA fragment needed as a probe was purified with the Qiagen gel purification kit. In

order to prepare and radioactively label the hybridization probe the Prime-It II Random Prime Labeling Kit from Agilent Technologies was used. The procedure is based on the synthesis of complementary DNA strands facilitated by random hexa-nucleotides that serve as primers. The Klenow fragment of DNA polymerase I incorporates nucleotides at the free 3´ OH group of the primer. Radioactive nucleotides ([α−32P]-dCTP at 3000 Ci/mmol) are incorporated into the newly synthesized strand. In the first step of the protocol 25 ng probe-DNA dissolved in MQ water and 10 µl of random oligonucleotide primers were prepared in a total volume of 34 µl in a 1.5 ml micro centrifuge tube and incubated for 5 min in a boiling water bath. After brief centrifugation 10 µl of dCTP primer buffer, 5 µl of [α-32P]-dCTP and 1 µl of Klenow enzyme were added and incubated at 37 °C for 30 min. In the last step 2 µl of stop mix were added. Finally the activity of the probe was determined by scintillation counting.

Table 3: Reaction Mixture to generate radioactively labeled probe

Components	Volume
25 ng DNA template	x µL
sterile double-distilled H_20	x µL
5X random primers solution	10 µL
Total Volume	**34 µL**
5X dCTP buffer	10 µL
α-^{32}P dCTP	5 µL
Exo (-) Klenow Enzyme	1 µL
Stop Mix	2 µL

4.2.18.6. Hybridization

For hybridization the QuikHyb Hybridization Solution from Agilent Technologies was used. First, for pre-hybridization, the nylon membrane was soaked in MQ water and incubated while rolling in a roller bottle for 1.5 h in 10 ml prewarmed pre-hybridization solution (for 10 cm^2 membrane) at 58 °C. The pre-hybridization solution contains 1% calf thymus DNA that was heated prior to use to 96 °C for 5 min and immediately chilled on ice before mixing with the QuikHyb solution.

In the next step 22 µl ($2x10^7$ cpm) of the radioactive probe were mixed with 100 µl (10 mg/ml) of calf thymus DNA, incubated 5 min at 96 °C and immediately chilled on ice. 1 ml of the pre-hybridization solution was removed, mixed with the probe and placed back in the roller bottle for hybridization at 58 °C overnight.

The hybridized membrane was washed four times to remove excess radioactivity. The first two washes were performed at RT for 5 min in 200 ml 2 x SSPE with 0.5% SDS and 15 min in 250 ml 2 x SSPE with 0.1% SDS. For the third wash 250 ml of 0.1 x x SSPE with 0.1% SDS were prewarmed and incubated with the membrane for 1-3 h, until counts of 200-300 Bq were measured with a Geiger-Müller counter. At last the membrane was washed in 200 ml 0.1 x SSPE briefly at RT, wrapped in saran wrap, exposed on a storage phosphor screen (GE Healthcare) and placed in a cassette for two days. The film was scanned with the Typhoon™ Variable Mode Imager (GE Healthcare). Before and after scanning the storage phosphor screen was exposed for 15 min to a white light source (ImageEraser) to erase latent images and prepare it for re-use.

4.2.19. SDS Page

Cell lysates were resolved on 10% polyacrylamide gels. For loading 30 µg cell extract were mixed in a 1:1 ratio with 2x Laemmli Buffer, denatured for 5 min at 96 °C and centrifuged briefly at 13000 x g. SDS-PAGE mini gels were prepared using casting stand (Bio-Rad) according to the manufacturer's instructions. For electrophoresis a constant voltage of 130 V was set for 1.5 h.

Table 4: SDS-PAGE

	5 ml Stacking Gel (5%)	5 ml Resolving gel (10%)
Mon. Sol.	840 µl	1.7 ml
4 x SGB (0.125 M)	1.25 ml	-
4 x RGB (0.37 M)	-	1.25 ml
Milli-Q water	2.8 ml	1.9 ml
10% SDS	50 µl	50 µl
10% APS	50 µl	50 µl
TEMED	10 µl	5 µl

4.2.20. Immunoblotting

During Western blotting the proteins are transferred from the SDS-polyacrylamid gel onto a nitrocellulose membrane. Therefore blotting paper (GB004 Whatman), transfer sponge and nitrocellulose membrane of the desired size were prepared and equilibrated in cold 1 x transfer buffer (consisting of 25% 4 x electrode buffer at pH 8.3 (0.1 M Tris-HCl, 0.7 M glycine) and 20% methanol). All components were assembled together with the gel into the electro-transfer unit according to the instructions of the manufacturer (Biorad) and run at 100 V for 60 min. After transfer the membrane was incubated for 2 h in 5% non-fat dry milk in 1 x TBS-T (0.05% Tween20 in 1 x PBS). For immunodetection the membranes were incubated overnight at 4 °C with the primary antibody. After washing three times for 10 min in PBS-T the secondary antibody was incubated for 1.5 h and the membrane was again washed three times in PBS-T prior to detection. The

antibodies were diluted in 5% blocking solution with different dilutions depending on the manufacturer's protocol for the specific antibody. The Odyssey® Infrared Imaging System from LI-COR Biosciences was used for detection and analysis.

4.2.21. Immunofluorescence staining

For γ–H2AX immunofluorescence staining, $0.2x10^6$ transfected cells were plated in 35 mm dishes with 2 ml growth medium. 12 h after transfection the growth media was removed, cells were washed with PBS and fixed in 2 ml 2% paraformaldehyde PFA for 15 min. Cells were washed again 3 x for 5 min in PBS and permeabilized in 2 ml P solution (100 mM Tris, (pH 7.4), 50 mM EDTA, 0.5% Triton X-100) for 10 min. After washing, cells were blocked in PBG (0.2% gelatin, 0.5% BSA in PBS) at 4 °C overnight. The primary antibody was diluted 1:400 in PBG and 90 µl droplets were pipetted on a Parafilm. The cover slips were placed on the antibody solution and incubated for 2 h at RT. After returning the cover slips into the dishes they were washed with PBST (PBS + 0.05% Tween 20) 3 x 10 min at RT. In the next step the cells were incubated for 1.5 h at RT with the secondary antibody diluted 1:400 and finally washed 3 x in PBST. The cells were mounted with 15 µl ProLong® Gold antifade mounting media (P-7481, Invitrogen) mixed with 1/3 DAPI givng a final DAPI concentration of 50 ng/ml. Before scanning, slides were kept for 24 h at RT and finally stored at 4 °C. Scanning of the slides was carried out on a Confocal Laser Scanning Microscope (CLSM) from Leica Microsystems (DMI 6000 B).

4.2.22. Live cell imaging

Live Cell Imaging was applied to monitor cellular dynamic events, motility and proliferation over a time period of 24 h. The observation of living cells over time was carried out with the Leica TCS SP5 confocal microscope that enables the recording of z-series of optical sections together with time-series (t-dimension). In addition to laser scanning also differential interference contrast (DIC) was applied to observe cell viability and morphology together with foci kinetics. DIC and fluorescence were captured simultaneously in a single image frame.

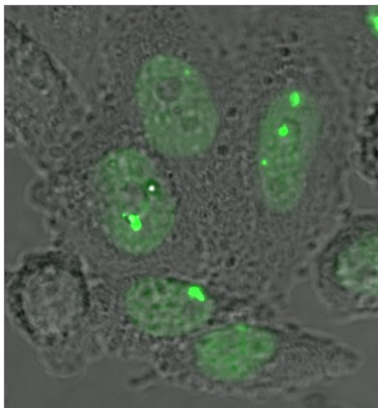

Fig.10: Representative image of cells expressing 53BP1-EGFP visualized by CLSM and merged with the corresponding DIC image.

During live cell imaging optimal environmental conditions have to be provided to the cells to keep them alive and proliferating. In order to substitute for the 5% CO_2 requirement, the cells were cultured in L-15 Leibovitz`s Medium containing HEPES. This Medium was specifically designed to grow cells in a CO_2 free atmosphere. Furthermore a temperature controlled system with the microscope inside an environmental chamber, including a stage warmer and an objective heater provides optimum temperature of 37 °C for the cells.

Experiments were carried out with transiently transfected cells that express a EGFP or RFP tagged repair protein that forms foci upon DSB induction. For optimal transfection efficiencies and signal intensities $0.2x10^6$ cells were plated three days prior to transfection. After transfection $0.5x10^6$ transfected cells were plated in an eight well or $1x10^6$ cells were plated in a four well live cell imaging chamber (PAA), respectively. 5 h after plating cells were washed twice with prewarmed PBS and growth media was changed to prewarmed L-15 Leibovitz. Prior to scanning, the chamber was placed in a specifically designed and constructed “chamber holder”, as without the special holder optimal focusing at the left and right borders of the chamber was not possible due to a space problem between the objective and the chamber. To avoid disruption of the immersion film due to aberrant focusing that happens with oil objectives during long term experiments at 37 °C, a 63x Leica water objective connected to a Water Immersion Micro Dispenser (Leica) was used for 24 h experiments. The Water Immersion Micro

Dispenser adds MQ water automatically during the whole experiment. The μ-pump mp6 (Bartels mikrotechnik) was set with a pump amplitude of 75 V pumping 279 µl water every 25 min for 10 sec. EGFP was measured with the 488 nm argon laser and RFP with the 561 nm DPSS (Diode-pumped solid state) laser. The laser power was set to 30% to reduce photo bleaching. Scanning was performed using the following parameters: PMT gain was set at 830 V for the argon laser and 530 V for the DIC detector with the pinhole set at 95 µm. In total 16 fields were tracked at time intervals of 15 min – 1 h for 24 h.

4.2.23. Foci analysis by Imaris

The analysis of the LIF files (three dimensional data sets) that were generated after scanning was performed using the Imaris® software (Imaris 6.0; Bitplane). Movie files were generated with the "Easy 3-D" tool to analyse foci kinetics in a spatio-temporal resolution. For foci scoring, images of 2 h timeframes, starting from 6 h to 24 h were loaded and foci of 100 cells were counted for each time point. Foci were defined as spots of higher intensity than the defined threshold (set at 30-35, varying between different experiments, but constant throughout each experiment) and with minimum size of 0.5 µm. The data was analysed with Microsoft Excel 2007® and graphs were plotted with SigmaPlot® 11.0.

5. Results

5.1. Model Systems for clustered DSBs

This section describes the design and the characterization of the model systems developed for the experiments and defines the clones used to evaluate the effect of DSB clustering on various biological endpoints.

5.1.1. Design of DSB clusters of varying complexities

To model simple and complex DSBs, sequences with varying numbers of I-*Sce*I sites at different orientations were designed. We are hypothesizing that the cell will process a single DSB generated at a single I-*Sce*I recognition site as a simple DSB. Complex DSBs are defined in this context as clustered I-*Sce*I recognition sites that model clustered DSBs (T6-DSBs, see Fig. 6) upon their digestion by I-*Sce*I.

Nine different sequences modeling nine forms of lesion complexity were designed (Fig.11). One sequence contained a single I-*Sce*I site to model the simplest form of RE-induced DSB (T1-DSBs, Fig. 11A). Six further sequences were generated with a pair of I-*Sce*I sites located 200 bp, 500 bp or 1000 bp apart (Fig. 11B). For all of these sequences the I-*Sce*I sites were engineered in two different ways, either in the same or in inverted orientation, designated as direct (D) or reversed () orientation. The constructs harboring I-*Sce*I sites in the direct orientation generate upon loss of the intervening DNA segment a DSB with compatible ends, similar to those of the single-site construct (Fig. 11A). The constructs engineered with I-*Sce*I sites in inverted orientation generate upon digestion and intervening fragment loss a DSB with incompatible ends (Fig. 11C).

Furthermore, two sequences were generated harboring clusters of four I-*Sce*I sites with the relative distances in bps as indicated in Fig. 11C. Here again the I-*Sce*I sites were engineered in the direct (D) or in reversed (R) orientation to generate upon loss of all intervening fragments a DSB with either compatible or incompatible ends. The underlying working hypothesis regarding the function of this construct is that the

intervening two DSBs will destabilize DNA and will increase the probability of fragment loss and thus also of the generation of a relatively large deletion.

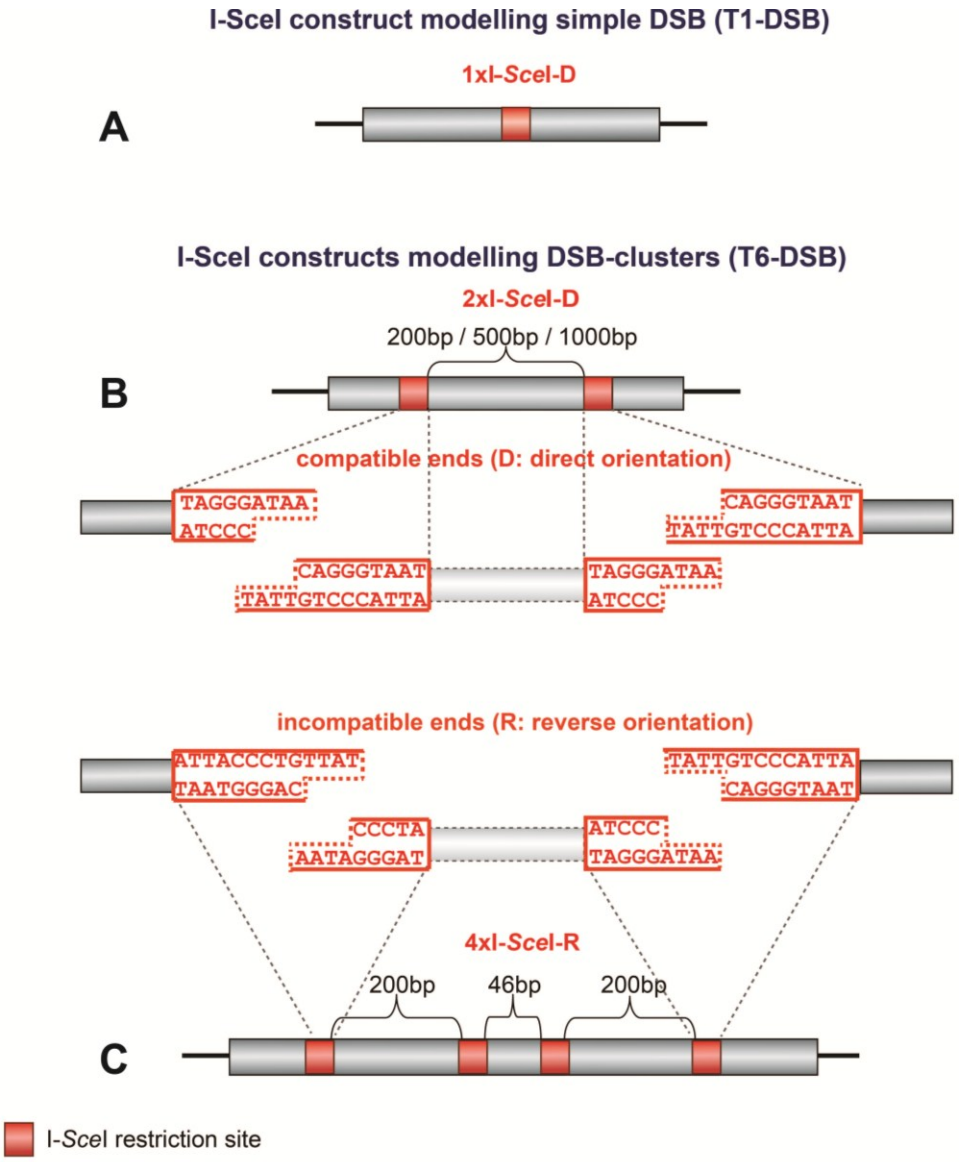

Fig. 11: Models of simple and complex lesions. Constructs carrying different numbers of I-*Sce*I sites engineered at different distances were generated to model different degrees of DSB complexity. The sequences of the I-*Sce*I restriction sites were designed in the direct (D) or reverse (R) orientation in order to generate compatible or incompatible DNA ends after the loss of the intervening sequence. R and D will be used for nomenclature.

The 1xI-*Sce*I and 2xI-*Sce*I site sequences were designed by J. Saha (Saha 2010), commercially procured from Cloning Biotech and delivered in the pPCRScript plasmid, whereas the 4xI-*Sce*I sequences were cloned using the two site sequence as a template as part of the present work. The cloning scheme employed is shown graphically in Fig. 12 and described in detail in the legend of the same figure.

These constructs provide a unique model for testing whether different levels of DSB clustering affect detection and processing by DDR, or whether they destabilize chromatin. The contribution of DSB clustering to DSB detection and signaling can be analyzed by performing live cell imaging. Co-transfection with the I-*Sce*I expression plasmid, or plasmids expressing different fluorescently tagged DDR proteins allow real time detection of DSB processing in the form of protein foci formation and decay. Destabilization of chromatin can be analyzed by performing G2-PCC experiments to analyze chromosome fragmentation and repair.

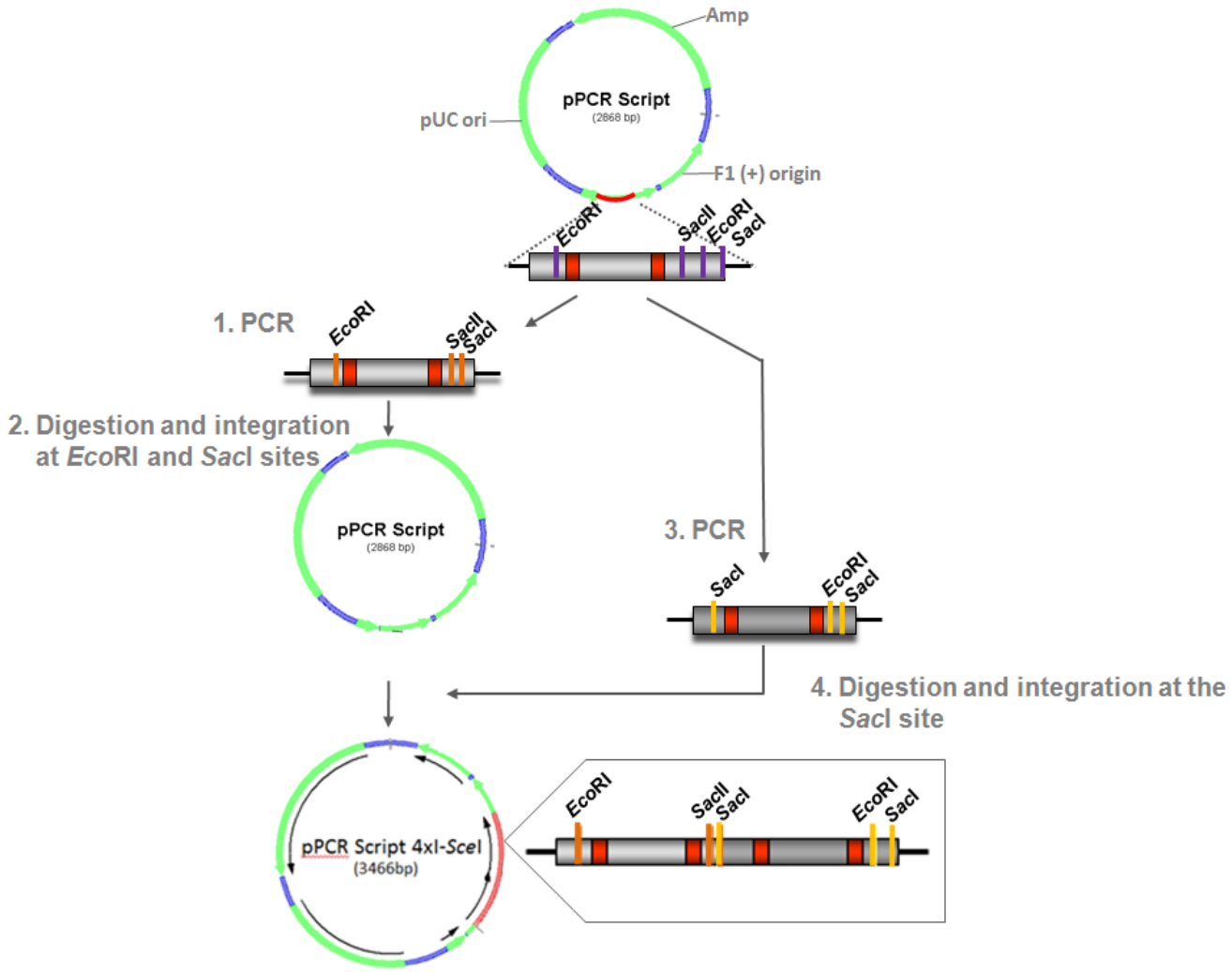

Fig. 12: Cloning strategy of the 4xI-*Sce*I site construct. Four different primers were designed flanking the two site construct with additional RE sites for further cloning (see 4.1.9). In the first step (1.PCR) the 2xI-*Sce*I sequence was amplified and digested at *Eco*RI and *Sac*I before ligation into the pPCR script vector in the corresponding sites in the second step (2.). In the third step (3.) the two-site construct was amplified again to generate sequences with a different combination of restriction sites for further cloning (*Sac*I at the 5`end and *Eco*RI and *Sac*I at the 3`end). The PCR product was digested with *Sac*I and cloned in the fourth step (4.) into the vector generated in the second step, already containing the PCR product of the first step. The *Sac*II RE site in the final vector (pPCR-4xI-*Sce*I) can be used for further cloning to increase the distance between the second and third I-*Sce*I site or for other types of insertions and further construction strategies. This cloning was performed for I-*Sce*I sites in direct as well as for inverted orientation. The *Eco*RI sites are used for further cloning into the transposon vector pt2SVNeo.

5.1.2. Transposition as a tool for achieving multiple random integrations of I-*Sce*I constructs in the mammalian genome

To achieve high numbers of I-*Sce*I construct integrations we applied the transposon technology. Transposable elements are characteristic segments of DNA which show the distinctive ability to move and replicate within genomes (Izsvak and Ivics 2004). The transposition of DNA transposons is characterized by a "cut and paste mechanism" whereby the transposon is excised from the donor locus and is reinserted randomly somewhere else in the genome. This process is catalyzed by the element-encoded transposase.

Transposons occupy about 45% of the human genome. Despite the fact that they make up such a significant fraction of the genome, there is no indication for DNA-transposon activity in the human genome for the past 50 million years possibly due to their inactivation by mutations.

The "cut and paste" transposition process involves the excision of the DNA Element from its DNA context and its reintegration into a different locus. It can be divided into four major steps.

In the first step the transposase binds as a homodimer to the inverted direct repeats (IR/DRs) of the transposon (Ivics and Izsvak 2004). In the second step the synaptic formation takes place, where the two ends of the transposon element are paired and held together by the transposase. This step serves as a checkpoint for the transposition, controlling whether all molecular requirements are fulfilled. During synaptic complex formation the two IR/DRs with the four transposase binding sites mediate the formation transposase tetramers. The third step, transposon excision, takes place when the synaptic complex formation is completed. The DDE (conserved triad of amino acids) catalytic subdomain of the transposase catalyzes the cleavage at the ends of the SB element and generates overhangs of three nucleotides, GTC, at both ends of the transposon. In the fourth step, reintegration of the transposon takes place, catalyzed by the DDE subunit of the transposase.

Transposable elements generate DSBs due to their mobility. Although HR and NHEJ are involved in the repair of transposon mediated breaks, SB transposition in HR and D-NHEJ deficient cells induces only moderate cell death (Izsvak, Stüwe et al. 2004).

For the goals of this project, we selected the Sleeping Beauty (SB) DNA transposon system developed by Z. Ivics to achieve multiple integrations for the different I-*Sce*I constructs into the chromosomes of cultured cell lines. SB is a highly efficient transposon system that clearly enhances integration events in comparison to the spontaneous integration measured after plasmid transfection (Fig. 13). The SB transposon originates from the TC1/*mariner*-type transposon found in fish genomes and was reconstructed by eliminating different inactivating mutations from the transposase gene. SB shows a random pattern of integration in the human genome (Vigdal, Kaufman et al. 2002). It prefers TA dinucleotides as integration sites, which are found approx. every 20 bp in vertebrate genomes. Palindromic AT-repeats: ATATATAT were found to often surround the integration site. The 3' ends of the excised transposon invade the target DNA molecule after the transposase cleaved the TA dinucleotide target integration site. The TA target site is duplicated upon insertion.

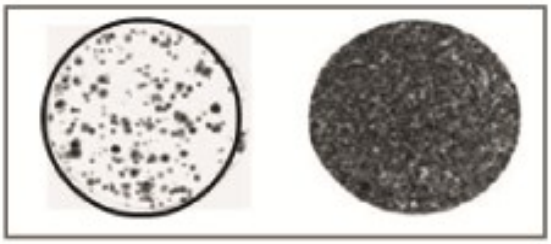

Fig.13: Comparison of spontaneous and SB Transposon mediated integration (Ivics, Hackett et al. 1997). Dishes with colonies of HeLa cells plated after transfection with a plasmid containing a neo resistance gene are shown. Cells are grown under antibiotic selection. Only cells that express the antibiotic resistance gene due to chromosomal integration survive. HeLa cell colonies are obtained in the absence (left dish) or in the presence (right dish) of transposase.

In the implementation used in the present work, SB transposition is mediated by a two component assay, where two non-autonomous transposon elements, the donor plasmid containing a *neo* selectable marker gene flanked by IRs and the helper plasmid expressing the transposase are co-transfected. The number of cell clones resistant to

the neomycin-analog G-418 serves as the indicator for the integration and expression of the *neo* transgene.

5.1.3. Cloning of I-*Sce*I constructs into the Sleeping Beauty (SB) transposon vector

All nine I-*Sce*I constructs were cloned into the SB transposon donor plasmid pT2SVNeo (Fig. 14). The SB transposon consists of the transposon sequence, which is flanked by the inverted/directed repeats (IR/DRs) containing binding sites for the transposase.

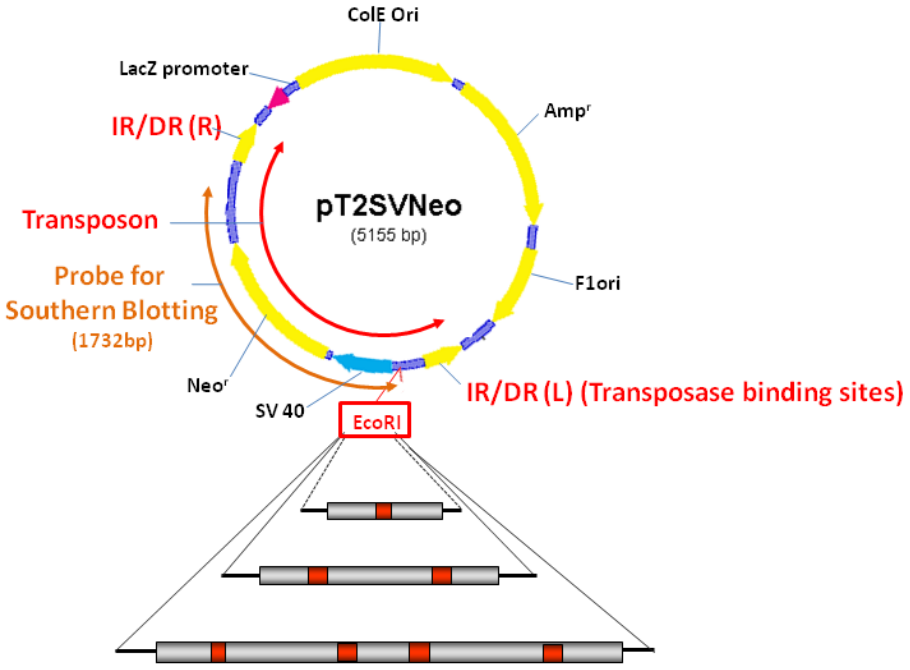

Fig. 14: Cloning of I-*Sce*I constructs into the transposon vector pt2SVNeo. The different I-*Sce*I constructs were cloned into the Sleeping Beauty (SB) transposon vector at the MCS and cotransfected with the SB transposase. Using this type of vectors a high number of random integration events can be achieved in different cell lines.

The SB transposon is non-autonomous and not able to transpose without an appropriate transposase encoding sequence. The transposase binding sites of the SB element show a specific structure. Two binding sites are located at the ends of the 200-250 bp long inverted repeats (IR) and contain short 15-20 bp direct repeats (DRs). Due to this special organization, the entire region is termed IR/DR. Fig. 15 summarizes the function of the two component SB transposition system used here for the selected components.

In pT2SVNeo, the multiple cloning site (MCS) along with the SV40 promoter and the neomycin resistance gene are located between the IR/DR-sequences. The *Eco*RI restriction site at the MCS was selected for non-directional cloning of the I-*Sce*I constructs. Prior to cloning into the pt2SVneo plasmid the I-*Sce*I constructs were excised from the pPCRScript vector by *Eco*RI digestion.

All nine I-*Sce*I constructs described in 2.1 are cloned between the IR/DRs of the pt2SVNeo plasmids and are thus ready for transfection and genomic integration. The following five pt2SVNeo plasmids were used for further experiments: pt2SVNeo-1xI-*Sce*I-D, pt2SVNeo-2xI-*Sce*I-D, pt2SVNeo-2xI-*Sce*I-R, pt2SVNeo-4xI-*Sce*I-D and pt2SVNeo-4xI-*Sce*I-R.

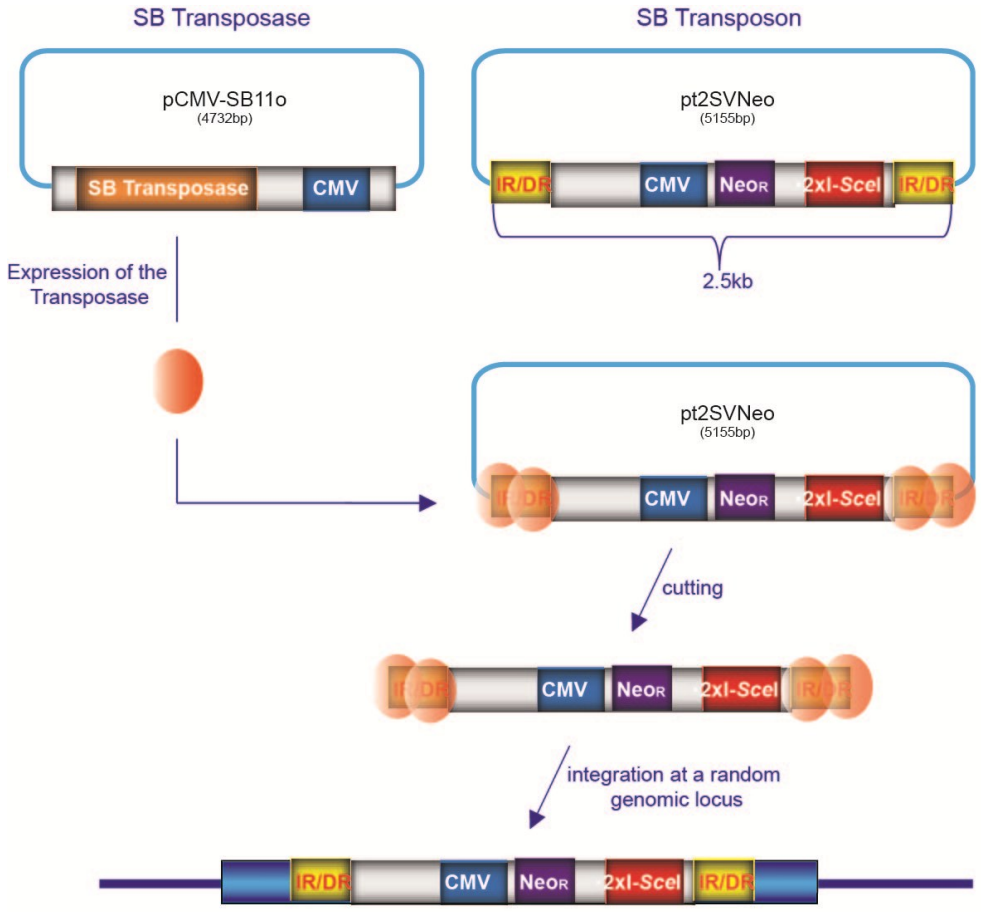

Fig. 15: The Sleeping Beauty Transposon Mechanism. The pCMV-SB11 transposase plasmid is co-transfected with pt2SVNeo at a ratio 1:10. Transposase binds to the IR/DRs of the transposon vector, forms a synaptic complex and excises the sequence from pT2SVNeo. Finally the transposase carries the excised construct to a random genomic locus by binding to a TA site that is duplicated during the integration.

5.1.4. Selected cell lines for transposition

The Chinese hamster ovary (CHO10B4) cells were selected for experiments on the basis of their excellent growth characteristics, good transfection efficiencies, but most importantly due to the availability of derivative mutants with defects in specific pathways of DSB repair. An additional advantage of these cells is their relatively low chromosome number (2n=22) that facilitates analysis of the consequences of DSBs using cytogenetic methods. Furthermore, CHO cells are lacking p53 function as a result of a mutation in codon 211 of exon 6. This was perceived as advantage because it was expected to reduce p53-mediated apoptosis. Indeed, we had indications that in the p53 wt human A549 cells, apoptosis compromised analysis of the consequences of lesion complexity using the same model system.

To investigate the contribution of homologous recombination repair (HRR) and of DNA-PK dependent non-homologous end-joining (D-NHEJ) to the processing of complex DSBs, we also selected appropriate CHO mutants for stable integration of I-*Sce*I constructs. Nine complementation groups, with mutations in genes that are involved in DSB repair, have been isolated from radiosensitive rodent cell lines and have been studied for DSB repair defects (Jones, Cox et al. 1988). The *xrs-6* mutant belongs to the X-ray radiation complementation group 5 and carries a mutation in the *XRCC5* gene, encoding the Ku80 subunit of the heterodimeric Ku protein - a component of DNA-PK. Xrs6 cells completely lack DNA end binding and kinase activities associated with DNA-PK (Finnie, Gottlieb et al. 1995). An additional NHEJ mutant cell line, XR-C1-3, has been assigned to the X-ray radiation complementation group 7 and has a mutation in the *XRCC7* gene encoding the catalytic subunit of DNA-PK (DNA-PKcs); this mutant also lacks DNA-PK catalytic activity. As a result of the corresponding mutations, both cell lines are severely impaired in DSB repair, specifically by D-NHEJ.

The third mutant selected for the present work, irs1SF, is defective in HRR as a result of a mutation in the *XRCC3* gene. The XRCC3 protein is one of the Rad51 paralogs and interacts with Rad51, thus promoting HRR.

5.1.5. SB-transposition-based integration of I-*Sce*I constructs in multiple copies in wt CHO cells and DSB repair deficient mutants

The SB transposon containing donor plasmid vector pT2SVNeo, carrying one of the five I-*Sce*I constructs, is co-transfected with the hyperactive SB transposase expressing helper plasmid pCMV(CAT)SB100x at a 10:1 ratio. Transfections are carried out using the nucleofection technology of Amaxa (see 4.2.4).

Two days post transfection cells were plated in various dilutions and grown in selective media containing the neomycin analog G418. Before inception of these experiments, a G418-toxicity curve was generated to determine the required concentration for tight selection. These experiments revealed that 500µg/ml G418 were required for CHO10B4 and 300µg/ml for Xrs6, XR-C1-3 and irs1SF. Cell clones resistant to G418, due to chromosomal integration and expression of the *neo* transgene, were selected eight days later. Clones were grown in 24 well plates for eight more days, passaged twice and frozen (-150 °C). For a detailed list of generated clones see Tables 5-8.

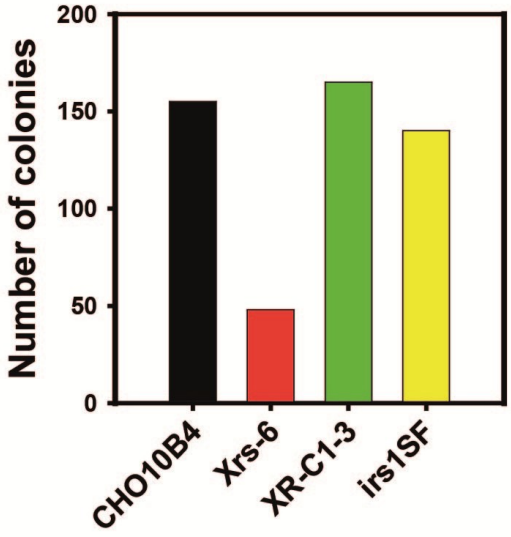

Fig. 16: I-*Sce*I construct integration in CHO wt and Xrs6, XR-C1-3 and irs1SFcells. Two million cells of each of the indicated cell lines were cotransfected with the SB transposon vector carrying 2xI-*Sce*I and the SB transposase. Two days after transfection 1000 cells were plated in G418 selective media. Mutant cell lines were transfected with a four-fold higher plasmid concentration (4 µg pt2SVNeo and 400 ng pcMV SB11 per 10^6 cells) to enhance the number of integrations (see below) and to compensate for reduced transposition activity that is sometimes associated with the repair defects.

To assess the transposition efficiencies in repair deficient mutants, the number of G418-resistant colonies obtained after the above described transfections were compared between wt cells and mutants. A reduction of approx. 70% in the number of colonies obtained in Xrs6 cells as compared to wt cells can be observed (Fig. 16) underlining that NHEJ has an important but not absolute role for transposition (Izsvak, Stüwe *et al.* 2004).

5.1.6. Nomenclature

The large number of clonal cell lines generated as part of the present work necessitates a rational, informative and clear nomenclature. In this section we describe the basis of the chosen nomenclature. The name of each cell line has four parts. The first part indicates the cell line on the genetic background of which the clones were generated. The second part indicates the construct used for integration. It is this part of the name that informs about the complexity of induced DSB. The third part of the name indicates the number of integrations achieved. The fourth part of the name identifies the specific clone. It should be pointed out, that as a results of the random integration taking place during transposition, two clones obtained after transfection with the same construct and which exhibit the same number of integrations, may show different results as result of differences in the integration sites.

To illustrate, a cell line derived from CHO cells using an I-*Sce*I construct containing two I-*Sce*I sites in reverse orientation to generate incompatible ends (see above) and which was found by Southern blotting to have 7 integrations of the construct will have as clone 4 the name:

CHO-2xI*Sce*I-R7.C4

Again, the first letters, illustrated in green, indicate the name of the cell line. Then the description of the I-*Sce*I constructs follows, shown in red, whereas the number 2x stands for the number of I-*Sce*I sites in the integrated construct. After the description of the construct, the integration site number and the reverse (R) or direct (D) orientation of the I-*Sce*I sites (shown in blue) is indicated. The clone number completes the name.

5.1.7. Characterization of the derived clones in the different genetic backgrounds

We used Southern blotting to determine the number of I-*Sce*I construct integrations in the selected clones. In general, a 1.72 kb probe, comprising the neomycin resistance gene, the CMV promoter and 121 bp of the I-*Sce*I construct (Fig. 14), was generated by random priming and used for Southern hybridization. For this purpose, genomic DNA was extracted and digested with XbaI after optimization of the incubation conditions. The Southern Blot in Fig. 17A shows that the addition of XbaI once for twelve hours, is sufficient for complete digestion. Therefore, this condition of genomic DNA digestion was used throughout this clone characterization phase.

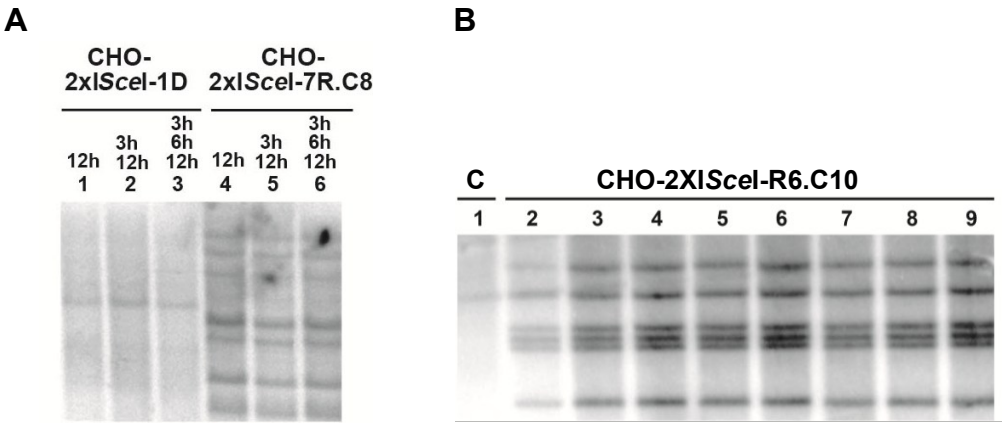

Fig. 17: Southern Blots of CHO-2x.I.*Sce*I-D.1, CHO-1x.I.*Sce*I-R.7 and CHO-2x.I.*Sce*I-R6. A: Test for complete digestion of genomic DNA: Genomic DNA (18 µg) from CHO-2xI*Sce*I-D.1 and CHO-1xI*Sce*I-R.7 cells were digested with XbaI (20.000 units per mL) for different time periods. In lanes 1 and 4, the genomic DNA was digested for 12 hours. In lanes 2 and 5, after 12 h an equal amount of enzyme was added for 3h. In lanes 3 and 6 after 12 h an equal amount of enzyme was added for 6 h and then again for 3 h. It is evident that incubation for 12 h is sufficient to complete digestion. **B:** Testing for long term stability of the genomically integrated transposon constructs: Eight clones (lane 2-9) of CHO-2xI*Sce*I-R6.C10 were passaged approx. 20 times before re-analyzing by Southern blotting. It is evident that integrations remain stable during the tested time interval. C: Control: nontransfected cells.

In the first set of CHO cell transfections we used 1 µg / 10^6 cells of pT2SVNeo-2x-I-*Sce*I and 100 ng / 10^6 cells transposase expressing plasmid. Under these conditions, clones with a maximum of six integrations were obtained. In an effort to increase the number of integrations, we increased fourfold the plasmid concentration in a second set of transfections. With the higher plasmid concentration, clones with up to thirteen integrations could be obtained. Based on this result the higher plasmid concentration

was used from the outset for the generation of clones in the mutant cell lines – also to compensate for possible reductions in transposition efficiency as a result of the repair defects (see above). Fig. 17B also shows that growing one of the selected clones for a few months has no effect on the stability of the integrations.

This form of characterization led to the selection from CHO cells of nine clones harboring 1xI-*Sce*I sites with 2-7 integrations (Fig. 18A). Fig. 17C shows similar results for 18 clones harboring the indicated (2-12) integrations of constructs with 2xI-*Sce*I sites in reverse orientation; twelve clones were also obtained with the construct harboring 2xI-*Sce*I sites in direct orientation (Fig. 18B). Eight CHO10B4 clones bearing 4xI-*Sce*I-site constructs in reverse orientation show 5-11 integrations (Fig. 18D).

Fig. 19 shows a Southern blot for the irs1SF mutant. This HR mutant shows in general a lower number of I-*Sce*I-construct integrations, ranging from 1-7. For the Xrs6 mutant, three types of clones were established and characterized (Fig. 20). Four clones with a 1xI-*Sce*I (Fig. 20A), thirteen clones with 2xI-*Sce*I (Fig. 20B and C) (7-9 integrations for direct orientation and nine clones with 3-11 integrations for reverse orientation); we also generated two clones with 4 integrations harboring 4xI-*Sce*I sites in reverse orientation (Fig. 20D). XR-C1-3 has integrations ranging from 4-9, for direct, and 5-12 for reverse orientation (Fig. 21A).

An overview of all characterized clones for the different cell lines, including nomenclature, type and number of integrated constructs, as well as number of colonies available is given in the Tables 5-8. A total pool of 270 clones was characterized and frozen and is available for use on an “as-needed” basis for the experiments of the present project.

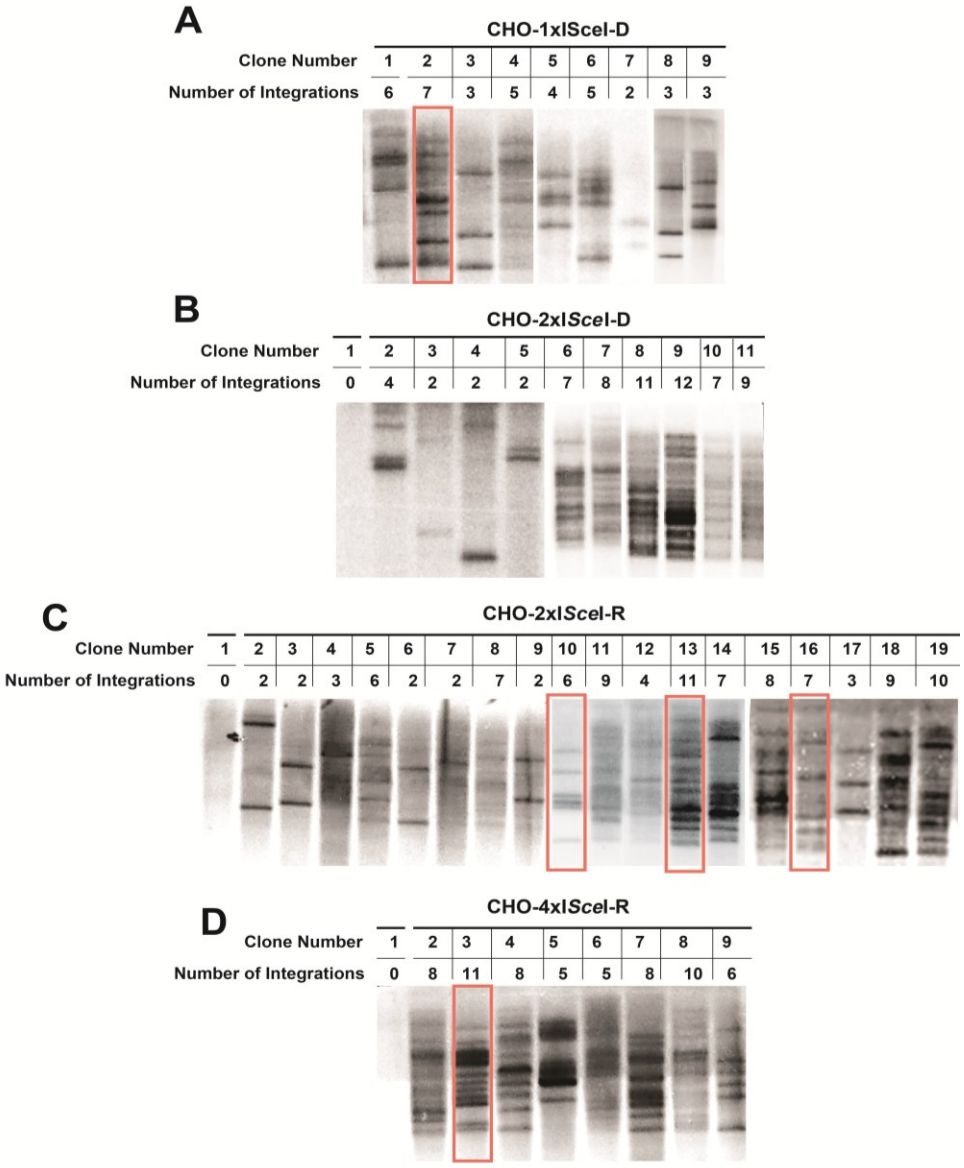

Fig.18: Characterization of CHO clones by Southern blotting harboring the following constructs: A, 1xI-*Sce*I (CHO-1xI*Sce*I-D); **B,** 2xI-*Sce*I-D (CHO-2xI*Sce*I-D) **C,** 2xI*Sce*I-R (CHO-2xI*Sce*I-R) and **D,** 4xI-*Sce*I-R (CHO-4xI*Sce*I-R). Genomic DNA of CHO wt cells without integrations serves as control (Lane 1). Lanes 2-5 in Figure B and lanes 2-9 in Figure C represent clones of cells transfected with 1 µg/10^6 transposon and 100ng/10^6 transposase plasmids ($7.2x10^{11}$ molecules Transposon / $2x10^6$ cells and $7.8x10^{10}$ molecules Transposase / $2x10^6$ cells). All other lanes represent clones obtained after transfection with 4 µg/10^6 cells transposon and 400 ng/10^6 cells transposase plasmids ($1.8x10^{11}$ molecules transposon / $2x10^6$ cells and $2x10^{10}$ molecules Transposase / $2x10^6$cells). The numbers of integrations range from 2-11. See Table 5 for a detailed list of CHO clones with the different constructs and number of integrations. Clones chosen for further experiments are indicated in red.

Table 5: List of characterized clones with I-*Sce*I construct integrations in CHO10B4 cells

CHO10B4															
Number of I-SceI sites in the construct	Orientation of I-SceI, D: direct, R:reverse	Nomenclature	Number of clones frozen	Number of clones characterized	Number of integrations per cell											
					1	2	3	4	5	6	7	8	9	10	11	12
1	D	CHO-1xI*Sce*I-D	15	9	-	1	3	1	2	1	1	-	-	-	-	-
		Clone Number			-	7	3, 8, 9	5	4, 6	1	2	-	-	-	-	-
2	D	CHO-2xI*Sce*I-D	30	10	-	3	-	1	-	-	2	1	1	-	1	1
		Clone Number			-	3, 4, 5	-	2	-	-	6, 10	7	11	-	8	9
2	R	CHO-2xI*Sce*I-R	30	17	-	5	2	1	-	2	3	1	2	-	1	-
		Clone Number			-	2, 3, 6, 7, 9	4, 17	12	-	5, 10	8, 14 16	15	11 18	19	13	-
4	R	CHO-4xI*Sce*I-R	15	8	-	-	-	-	2	1	-	3	-	1	1	-
		Clone Number			-	-	-	-	5, 6	9	-	2, 4, 7	-	8	3	-

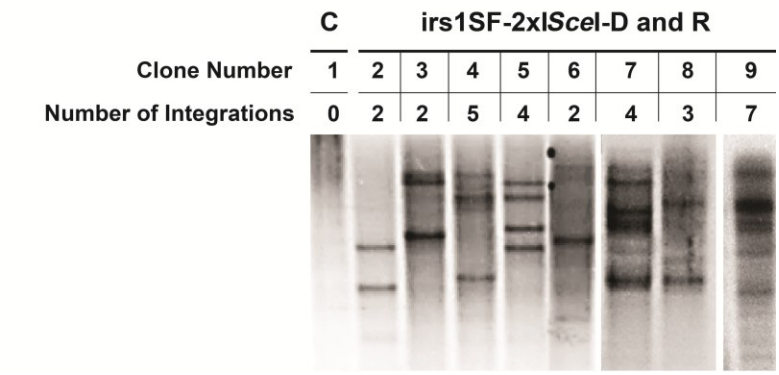

Fig. 19: Characterization of clones obtained from irs1SF cells. Clones of irs1SF cells with integration of constructs harboring 2xI-*Sce*I sites in reverse orientation (irs1SF-2xI*Sce*I-R). C: Control with genomic DNA of nontransfected irs1SF cells.

Table 6: List of characterized clones with I-*Sce*I construct integrations in irs1SF cells

irs1SF (defect in XRCC3)														
Number of I-SceI sites in the construct	Orientation of I-SceI, D: direct, R:reverse	Nomenclature	Number of clones frozen	Number of clones characterized	Number of integrations per cell											
					1	2	3	4	5	6	7	8	9	10	11	12
1	D	irs1SF-1xI*Sce*I-D	20	-	-	-	-	-	-	-	-	-	-	-	-	-
2	D	irs1SF-2xI*Sce*I-D	15	2	-	-	-	1	1	-	-	-	-	-	-	-
Clone Number								5	4							
2	R	irs1SF-2xI*Sce*I-R	15	6	-	3	1	2	-	-	1	-	-	-	-	-
Clone Number					-	2, 3, 6	8	7	-	-	9	-	-	-	-	-
4	R	irs1SF-4xI*Sce*I-R	20	-	-	-	-	-	-	-	-	-	-	-	-	-

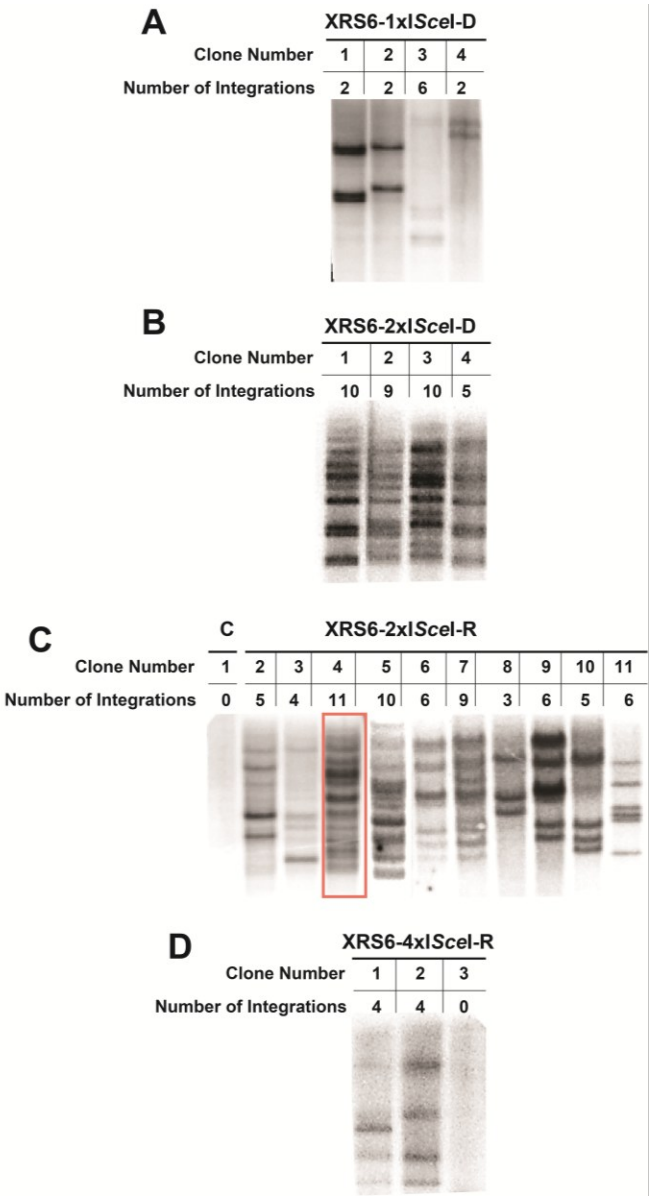

Fig. 20: Characterization of clones obtained from Xrs6 cells. Clones of Xrs6 cells with integrations of the following constructs: **A,** 1xI-*Sce*I-D (XRS6-1xI*Sce*I-D); B, 2xI-SceI-D (XRS6-2xI*Sce*I-D); **C,** 2xI-*Sce*I-R (XRS6-2xI*Sce*I-R); and D, 4xI-*Sce*I-R (XRS6-4xI*Sce*I-R); C: Control with genomic DNA of nontransfected Xrs6 cells.

Table 7: List of characterized clones with I-*Sce*I construct integrations in Xrs6 cells

Xrs6 (defect in Ku80)															
Number of I-*Sce*I sites	Orientation of I-SceI, D: direct, R:reverse	Nomenclature	Number of clones frozen	Number of clones characterized	Number of integrations per cell											
					1	2	3	4	5	6	7	8	9	10	11	12
1	D	XRS6-1xI*Sce*I	15	4	-	3	-	-	-	1	-	-	-	-	-	-
Clone Number					-	1, 2, 4	-	-	-	3	-	-	-	-	-	-
2	D	XRS6-2xI*Sce*I-D	25	4	-	-	-	-	1	-	-	-	1	2	-	-
Clone Number					-	-	-	-	4	-	-	-	2	1, 3	-	-
2	R	XRS6-2xI*Sce*I-R	25	8	-	-	1	1	2	3	-	-	1	1	1	-
Clone Number					-	-	8	3	2, 10	6, 9, 11	-	-	7	5	4	-
4	R	XRS6-4xI*Sce*I-R	15	2	-	-	-	2	-	-	-	-	-	-	-	-
Clone Number					-	-	-	1, 2	-	-	-	-	-	-	-	-

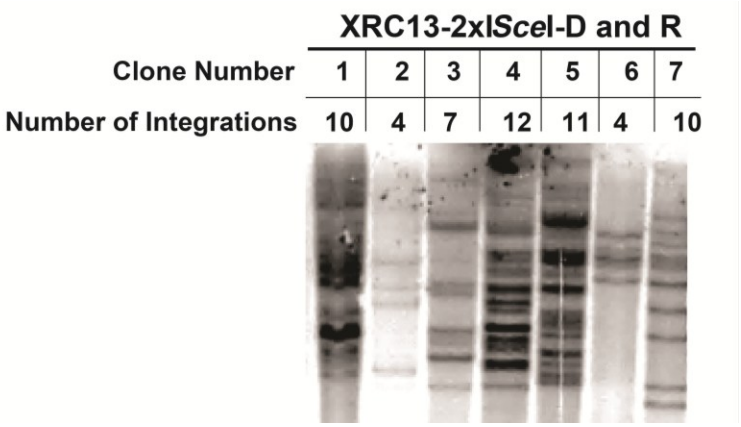

Fig. 21: Characterization of clones obtained from XR-C1-3 cells. Clones of XR-C1-3 cells with integration of constructs harboring 2xI-*Sce*I sites in reverse orientation and direct orientation (XRC13-2xI*Sce*I-R and D).

Table 8: List of characterized clones with I-*Sce*I construct integrations in XR-C1-3 cells

XR-C1-3 (defect in DNA-PKcs)														
Number of I-SceI sites	Orientation of I-SceI, D: direct, R:reverse	Nomenclature	Number of clones frozen	Number of clones characterized	Number of integrations per cell											
					1	2	3	4	5	6	7	8	9	10	11	12
1	D	XRC13-1xI*Sce*I	15	-	-	-	-	-	-	-	-	-	-	-	-	-
2	D	XRC13-2xI*Sce*I-D	10	2	-	-	-	1	-	-	-	-	-	1	-	-
Clone Number					-	-	-	2	-	-	-	-	-	7	-	-
2	R	XRC13-2xI*Sce*I-R	10	6	-	-	-	-	-	1	1	-	-	2	1	1
Clone Number					-	-	-	-	-	4	3	-	-	1, 7	5	4
4	R	XRC13-4xI*Sce*I-R	15	-	-	-	-	-	-	-	-	-	-	-	-	-

The selected clones that are used for further experiments described in the following sections are marked with red in the Southern blot figures. In this initial stage of the work, the clones were selected on the basis of their high number of integrations.

The next sections describe experiments that were performed with selected clones harboring various integrations of 1xI-*Sce*I, 2xI-*Sce*I and 4xI-*Sce*I constructs to assess the biological consequences of simple compared to clustered DSBs. A high integration number served as the most important criterion for selection at this stage of the project. The following clones were chosen from the CHO wt- (Table 5, indicated in red) cell line: CHO-1xI*Sce*I-7D.C2, CHO-2xI*Sce*I-R11.C13, CHO-4xI*Sce*I-R11.C3, CHO-2xI*Sce*I-R6.C10 and CHO-2xI*Sce*I-R7.16. In addition the D-NHEJ deficient clones XRC13-2xI*Sce*I-R11.C5 (Table 7) and Xrs6-2xI*Sce*I-R11.C4 (Table 8) were tested.

5.2. Which kind of lesion dominates the strong killing effect of IR?

Ionizing radiation has a high killing potential. The dose-response curve for cell survival is widely used to describe the loss of reproductive integrity in proliferating cells as a function of radiation dose (Hall and Giaccia 2006). Survival curves for CHO-2xI*Sce*I-6R.C10 and U2OS cell lines that have been exposed to different doses of X-rays are shown in Fig. 22. Approx. 80% of U2OS and 50% of CHO cells are killed by a radiation dose of 4 Gy.

The relationship between the initial DNA damage, attempted repair and ultimate cell killing by IR are not fully understood (Olive 1998). As described in the Introduction, the biological effects of IR are stochastic in nature. DSBs are considered as the critical lesion for cell killing although the correlation of the initial DSB number, or their repair, to radiosensitivity is still incompletely characterized. Furthermore the increase in DSB yield does not show a strong dependence on radiation quality (Goodhead, Thacker et al. 1993).

Therefore it is likely that the increase in RBE for high LET radiation compared to low LET radiation is not caused by an increase in the number, but by the changed

distribution of the induced DSBs, which in the case of high LET radiation are more frequently generated as clusters (due to the track structure).

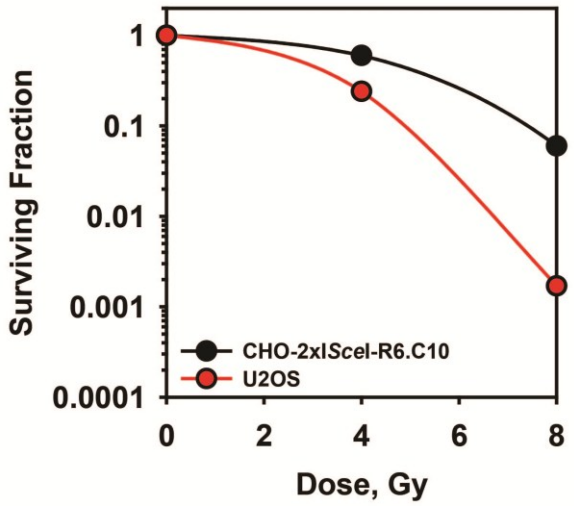

Fig. 22: Survival after irradiation with 4 and 8 Gy X-rays of CHO-2xI*Sce*I-R6.C10 and U2OS cells. After IR cells were plated in different dilutions and grown for 10 (CHO) or 14 (U2OS) days to allow colony development.

To test the hypothesis that clustered DSBs have higher probability for adverse biological consequences than simple DSBs, we performed survival experiments with I-*Sce*I-induced simple and clustered DSBs. The I-*Sce*I model system is unique in the sense that it enables the exclusive analysis of the effect of DSBs on cell survival, ruling out potential effects of other types of DNA damage like SSBs or base damages that accompany DSBs in cells exposed to IR.

5.2.1. Clustered DSBs have a markedly stronger killing capacity than simple DSBs

The clonogenic survival assay was performed to assess biological effectiveness of simple compared to clustered DSBs in the I-*Sce*I model system. Immediately after I-*Sce*I transfection of the clones CHO-1xI*Sce*I-7D.C2, CHO-2xI*Sce*I-11R.C13 and CHO-4xI.*Sce*I-11R.C3 ($2x10^6$ cells were transfected with 2µg plasmid) cells were plated in different numbers (100, 200 and 500 cells), grown for eight days and stained.

The cells were carefully stored in an incubator avoiding shaking and intensive air current fluctuation as accidentally detached cells form satellite colonies that generate analysis artefacts. Transfection of CHO cells without I-*Sce*I integrations with pmax-GFP served as a control. The transfection efficiency was measured 24h after pmax-GFP transfection by FACS analysis and ranged between 90-98%.

The results (Fig. 23) clearly show that clustered DSBs lead to increased cell killing compared to simple breaks. Whereas the simple DSBs did not show a measurable killing effect, the clustered DSBs showed 35% killing for CHO-2xI*Sce*I-11R.C13 and with increased clustering killing increased to approx. 50% - in the clone CHO-4xI.*Sce*I-11R.C3.

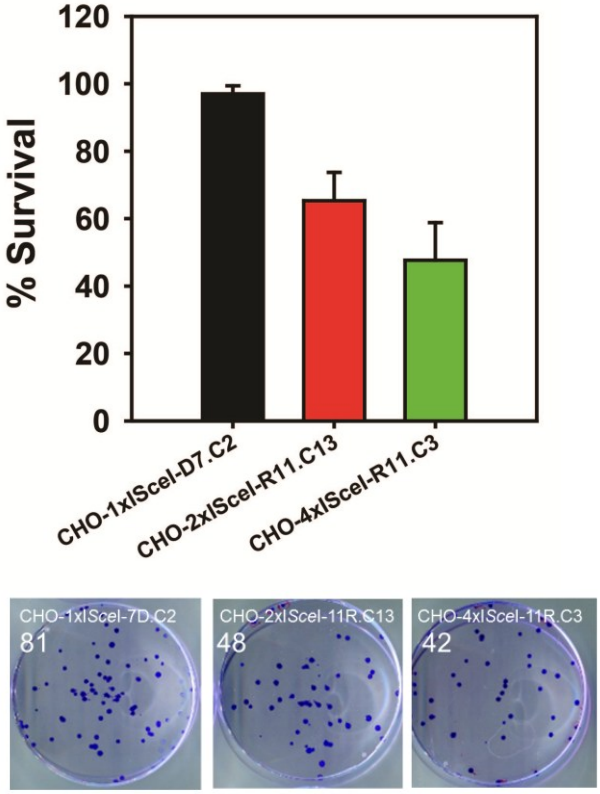

Fig. 23: Survival of cells harboring simple or clustered DSBs in the form of I-*Sce*I recognition sites after transfection with an I-*Sce*I expressing vector. 2x10^6 cells of the cell lines CHO-1xI*Sce*I-D7.C2, CHO-2xI*Sce*I-R11.C13 and CHO-4xI*Sce*I-R11.C3 were transfected with 2 µg of pCMV3xnlsI-*Sce*I. 200 cells were plated immediately after transfection and grown for 10 days. The data presented is normalized to CHO10B4 wt cells transfected with pCMV3xnlsI-*Sce*I. The plating efficiency was 78%. Representative dishes with stained colonies are shown.

As an additional control for cellular effects of simple DSBs, survival was measured with the human *Asi*SI-ER-U2OS cells. This cell line is the basis for an experimental system developed by G. Legube in U2OS cells that allows the enzymatic induction of DSBs in cells through the regulated expression of the *Asi*SI-ER RE (Iacovoni, Caron et al. 2010). *Asi*SI recognizes an 8bp sequence (Fig. 24A) that is present in multiple copies in the human genome and therefore generates multiple DSBs at average distances larger than 1 Mbp.

The *Asi*SI-ER-U2OS cells stably express a form of *Asi*SI fused to a modified ligand binding domain of the estrogen receptor. Upon binding of 4HT to this estrogen receptor domain, *Asi*SI translocates to the nucleus and generates sequence specific DSBs. The authors reason that due to CpG methylation only 25% of the approx. 1750 *Asi*SI sites (in G1) are digested.

To follow growth characteristics, growth curves were performed with the parental U2OS cell line and *Asi*SI-ER-U2OS (Fig. 24B). With the exception of the initial slower growth of the *Asi*SI-ER-U2OS cells after the first day, no clear differences in doubling times between the two cell lines could be observed. The slower initial growth may be caused by the leakiness of the system that allows some *Asi*SI molecules to pass the nuclear membrane in the absence of 4HT.

Cell survival was measured with 4HT treated *Asi*SI-ER-U2OS cells (Fig. 24C). The cells were treated for different times (0h, 2h, 4h, and 8h) with 4HT before plating. After treatment 200 cells were plated per dish and were allowed to form colonies in the absence of 4HT. The results show 40% killing after 2 h of treatment that increases to 50% after 8h treatment.

Compared to clustered DSBs where approx. 50% killing is induced for 11 clustered breaks, approx. 150 times more simple-DSBs (according to the *Asi*SI model system) are required to achieve a similar amount of killing. These results clearly imply an increase in adverse biological consequences of clustered compared to simple DSBs.

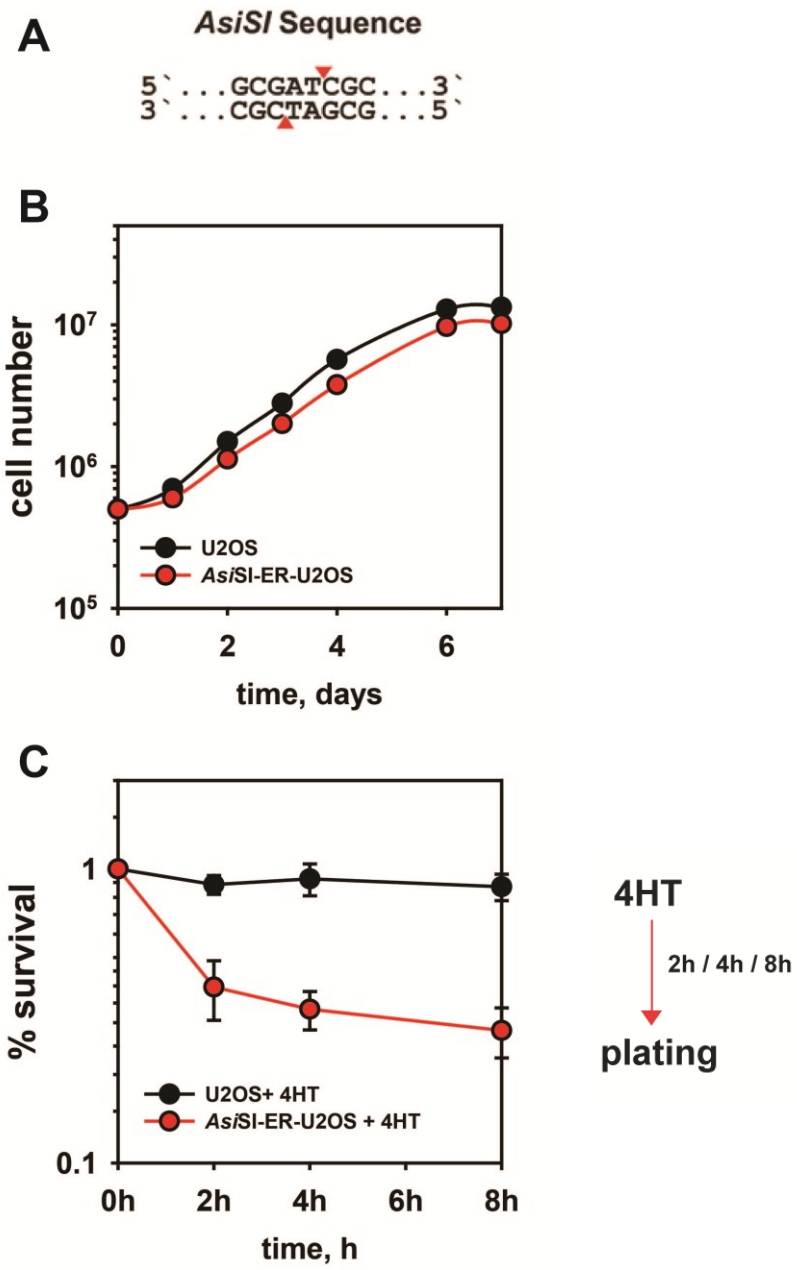

Fig. 24: A: Recognition sequence of the *Asi*SI HE. B: Growth curves of *Asi*SI-ER-U2OS and U2OS cells. 0.5x10^6 cells were plated and counted after 1-7 days. **C: Survival curves of *AsiSI*-ER-U2OS cells and the parental U2OS cells after treatment with 4HT for different times.** X-axis shows the time cells were treated with 4HT. Plating efficiency was 70%.

5.2.2. Clustered DSBs induce lethal Chromosomal Aberrations

It is widely accepted that unrepaired or misrepaired DNA double strand breaks (DSBs) lead to the formation of chromosome aberrations (Iliakis, Wang *et al.* 2004). To address the question whether clustered DSBs lead with higher probability to chromosome damage than simple DSBs the formation of chromosome aberrations was analyzed. Metaphase spreads were prepared from clones bearing simple DSBs (CHO-1xI*Sce*I-7D.C2) and clustered DSBs (CHO-2xI*Sce*I-11R.C13 and CHO-4xI*Sce*I-11R.C3) 24 h after transfection with I-*Sce*I. Cells were treated with colcemid for 2 h to arrest at mitosis before processing for cytogenetic analysis.

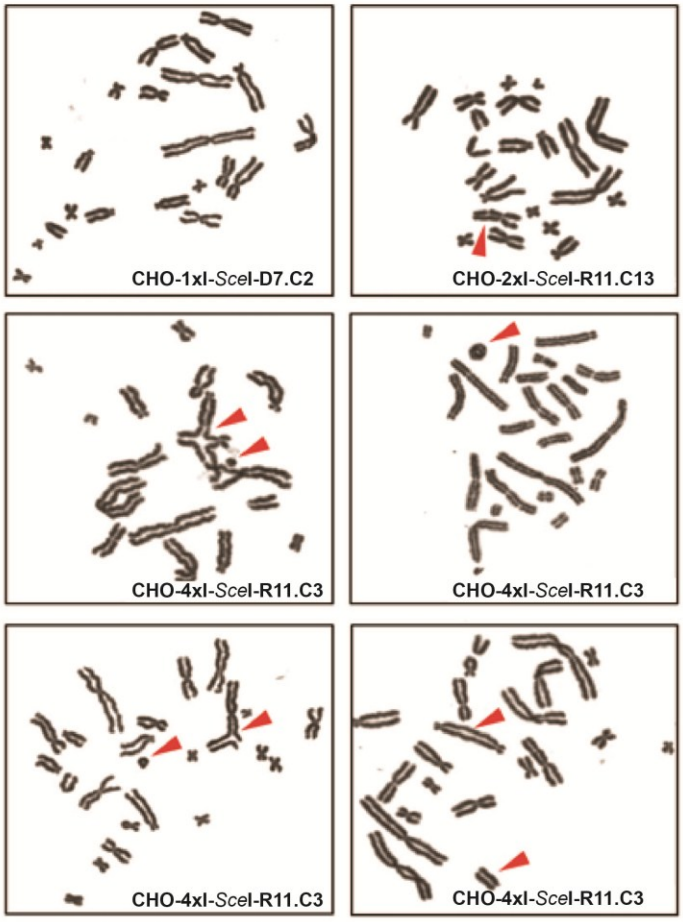

Fig. 25: Representative metaphase spreads of the cell lines CHO1xI*Sce*I-D7.C2, CHO2xI*Sce*I-R11.C13 and CHO-4xI*Sce*I-R11.C3 24h after transfection with pCMV3xnlsI-*Sce*I. Red arrows indicate chromatid breaks and chromosomal aberrations like dicentrics and rings.

As illustrated in Fig. 25, clustered DSBs generated in CHO-4xI*Sce*I-11R.C3 cells lead to chromatid breaks, dicentrics and rings. In contrast simple DSBs generated in CHO-1xI*Sce*I-7D.C2 cells only rare chromatid breaks.

Since a good correlation exists between chromosome aberration formation and cell killing, this observation provides an explanation for the increased killing of clustered DSBs measured above. Analysis at metaphase allows detection of irreversible chromosome aberrations that frequently cause cell death. To also detect reparable chromosome aberrations, we performed G2 premature chromosome condensation (G2-PCC). This method allows also the analysis of more cells, as typically only few cells reach metaphase after the treatment employed here.

5.2.3. G2-PCC breaks and exchanges are elevated in cells with clustered as compared to simple DSBs

Calyculin A induced G2 premature chromosome condensation was performed to study chromosome aberrations in the form of chromatid breaks and exchanges in interphase cells. The Serine/Threonine Phosphatase inhibitor calyculin A inhibits the activity of protein phosphatases PP1 and PP2 thus causing a very rapid condensation of chromosomes in G2 phase cells (in CHO cells within 5-10min). In this way analysis of chromosome aberrations is possible at interphase and cells do not need to progress to mitosis.

The clones CHO-1xI*Sce*I-D7.C2 and CHO-2xI*Sce*I-R11.C13 and CHO-4xI*Sce*I-R11.C3 were transfected with I-*Sce*I expressing plasmid (6 x 10^6 cells with 6 µg plasmid) and incubated at 37 °C for 8 h and 24 h. 100 nM calyculin A was added for 30 min before collection at these times. Cells with condensed chromosomes were detected with a metaphase finder (Meta-Systems) and analyzed with the Ikaros software (MetaSystems). For every time point 100 cells with condensed chromosomes were scored.

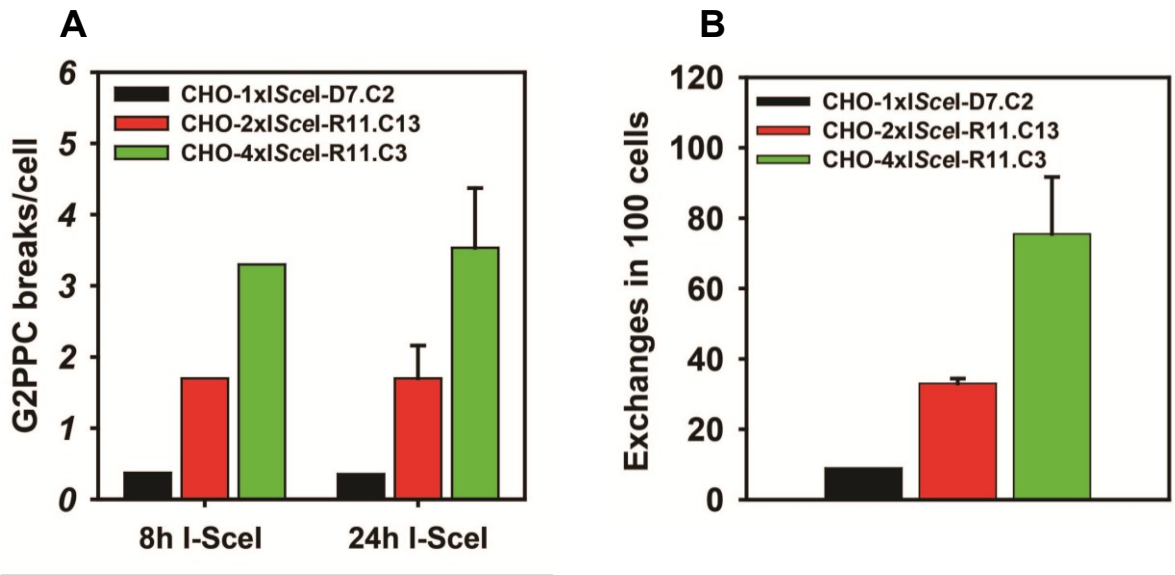

Fig. 26A: G2-PCC breaks per cell in CHO-1xI*Sce*l-D7.C2, CHO-2xI*Sce*l-R11.C13 and CHO-4xI*Sce*l-R11.C3 cells 8 h and 24 h after pCMV3xnlsI-*Sce*I transfection. Graphs represent data after background subtraction measured in non-transfected cells that have approx. 1.2 G2PCC breaks/cell. **B: Chromosome exchanges in CHO-1xI*Sce*l-D7.C2, CHO-2xI-*Sce*l-R11.C13 and CHO-4xI*Sce*l-R11.C3 cells 24h after pCMV3xnlsI-*Sce*I transfection.** For each experiment 100 metaphases were analysed. No exchanges could be detected in nontransfected controls.

G2-PCC breaks (Fig. 26A) and exchanges (Fig. 26B) were scored separately. The high number of G2-PCC breaks and chromosomal exchanges measured by G2-PCC, strengthens the above observations that clustered DSBs have a higher killing potential than simple DSBs. Whereas the clustering with two I-*Sce*I sites shows only a slight increase in G2-PCC breaks and exchanges (approx 1.8 G2-PCC/breaks per cell and 30 exchanges in 100 cells), the number of G2-PCC breaks for a higher degree of clustering is clearly elevated (approx. 3.5 G2-PCC breaks/cell and 75 exchanges in 100 cells). We conclude that clustered DSBs are toxic to the cells because they have a high risk for chromosomal aberrations formation.

5.3. Analysis of DNA damage signaling elicited by simple and clustered DSBs

We followed DSB-generated signaling to detect possible differences in signaling characteristics for different levels of DSB complexity. As a first step, we present γ-H2AX foci formation at chromatin. Subsequently foci formations by MDC1 and 53BP1 proteins downstream in the signaling cascade were analyzed. The latter proteins are recruited and are not inherently part of the chromatin like H2AX, therefore they can be observed by live cell imaging to analyze subcellular localization and dynamics in real time over a period of 24 h.

5.3.1. Theoretical foci-maximum upon DSB induction by I-*Sce*I

As the number of I-*Sce*I-construct integrations represents the number of possible DSBs that can be induced by I-*Sce*I, the theoretical maximum of foci for the cell lines used in the experiments was calculated. For this purpose, the percentage of cells in the different phases of the cell cycle, as measured by flow cytometry at different time points after pCMV3xnlsI-*Sce*I transfection, was taken into consideration (Fig. 27). The following formula was applied in the calculation:

1 x (% G1-cells : 100) + 1.5 x (% S-cells : 100) + 2 x (% G2-cells : 100) x number of integrations

The theoretical maximum calculated in this ways for each cell line is indicated as grey shading in the stacked bar graphs (Fig. 29) or as a dotted line in the graph (Fig. 31 and 34).

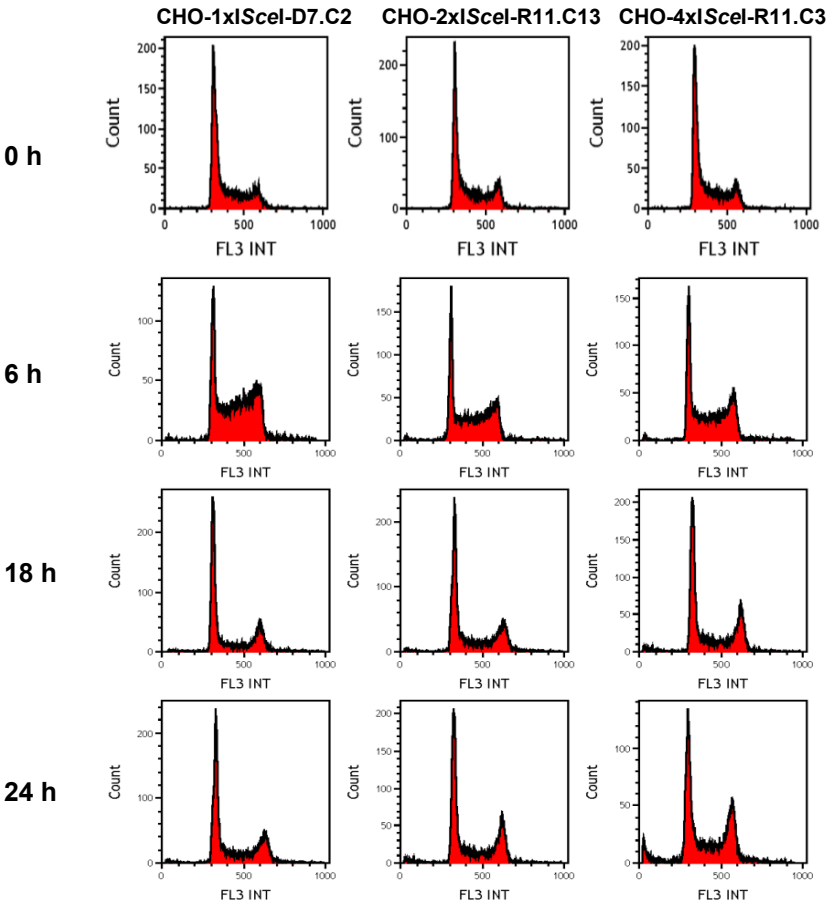

Fig. 27: Flow cytometry analysis of PI stained DNA of I-*Sce*I transfected CHO-1xI*Sce*I-D7.C2, CHO-2xI*Sce*I-R11.C13 and CHO-4xI*Sce*I-R11.C3 cells. Cells were measured 6 h, 18 h and 24 h after transfection.

5.3.2. I-*Sce*I induced DSBs trigger γ-H2AX foci formation at DSB sites

One of the earliest cellular responses to a DSB is the phosphorylation of H2AX at Ser 139 to generate γ-H2AX (Kinner, Wu et al. 2008). As demonstrated in the introduction it occurs through PIKK mediated phosphorylation that triggers a chain of events facilitating eventual repair. After 1Gy X-ray irradiation approx. 27 γ-H2AX foci are induced in the clones CHO-1xI*Sce*I-D7.C2and CHO-4xI*Sce*I-R11.C31h, as measured by immunostaining (Fig. 28). This number corresponds to the expected number of γ-H2AX foci in exponentially growing cells after irradiation with 1 Gy X-rays.

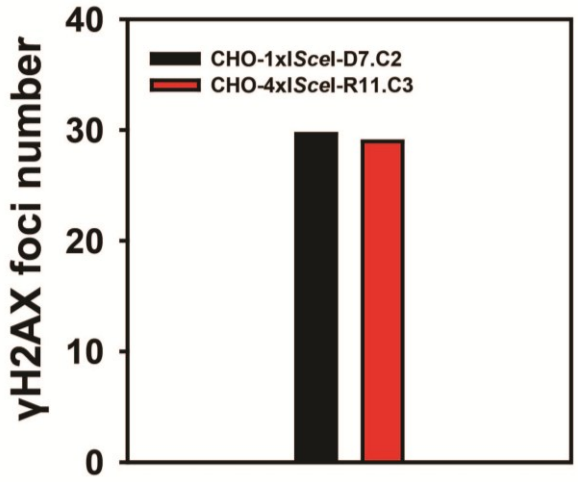

Fig. 28: γ-H2AXfoci in CHO-1xI*Sce*I-D7.C2 and CHO-4xI*Sce*I-R11.C3 cells 0.5 h after 1Gy X-ray irradiation. Cells were fixed and immunostained for γ-H2AX 1 h after irradiation. Foci were scored in exponentially growing cells. This experiment was performed in collaboration with V. Nikolov.

To examine whether the degree of DSB clustering affects the degree of signaling emanating from DSBs, we investigated the accumulation of γ-H2AX at I-*Sce*I induced DSBs. γ-H2AX foci were detected in fixed cells 6 h after transfection with a plasmid expressing I-*Sce*I in CHO-1xI*Sce*I-D7.C2, CHO-2xI*Sce*I-R11.C13 and CHO-4xI*Sce*I-R11.C3 cells (Fig. 29).

The foci number measured is close to the theoretical maximum that can be induced in the individual clones according to the number of transposon mediated I-*Sce*I-construct integrations and to the cell cycle phase measured by flow cytometry (see 1.4). This result suggests that practically all I-*Sce*I induced DSBs are recognized by the DDR apparatus.

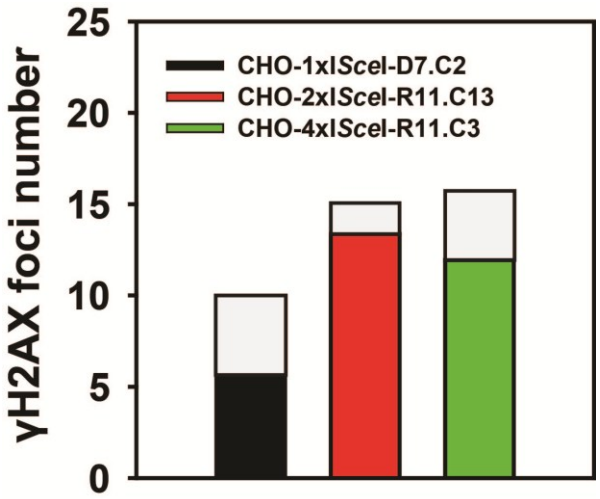

Fig. 29: γH2AX foci in CHO-1xI-*Sce*I-D7.C2, CHO-2xI-*Sce*I-R11.C13 and CHO-4xI-*Sce*I-R11.C3 cells 12 h after pCMV3xnlsI-*Sce*I transfection. Cells were fixed and immunostained for γ-H2AX 12 h after transfection. The light grey shaded extensions of each bar show the theoretical maximum of foci that can be reached for each cell line according to the number of I-*Sce*I construct integrations and the cell cycle distribution measured by flow cytometry (See Fig. 27). This experiment was performed in collaboration with V. Nikolov.

5.3.3. I-*Sce*I induced DSBs trigger MDC1 foci formation

MDC1 plays a key role in the assembly of radiation-induced foci and is one of the earliest factors accumulating at DSB sites. MDC1 foci formation depends on the presence of γ-H2AX, as it directly binds to the C-terminal end of γ-H2AX. Kinetics of MDC1 foci were followed by live cell imaging for 24 hours.

For all experiments 10^6 cells were plated two days prior to transfection aiming at approx. 70% confluence. After trypsinization and nucleofection, cells were incubated in Leibovitz Medium supplemented with 10% FBS and were allowed to adhere for 6 h in special live cell microscopy chambers.

After the incubation period, chambers were placed under a Leica confocal microscope at 37 °C and 10-16 fields were defined and tracked every 15 min for a period of 24 h. For each of the indicated time points, 50 cells were analyzed utilizing the Imaris image analysis software. MDC1 foci formation was followed after 1 Gy X-ray irradiation as well

as after DSB induction by I-*Sce*I of CHO clones harboring I-*Sce*I constructs of different complexity and different numbers of integrations.

24 h before irradiation all three clones were transfected with the MDC1-GFP expressing plasmid. The live cell measurement was performed 0.5 h after irradiation. Approx. 22 MDC1-foci were measured for all three clones after 0.5 h that went down to approx. 14 foci after 4 h (Fig. 30).

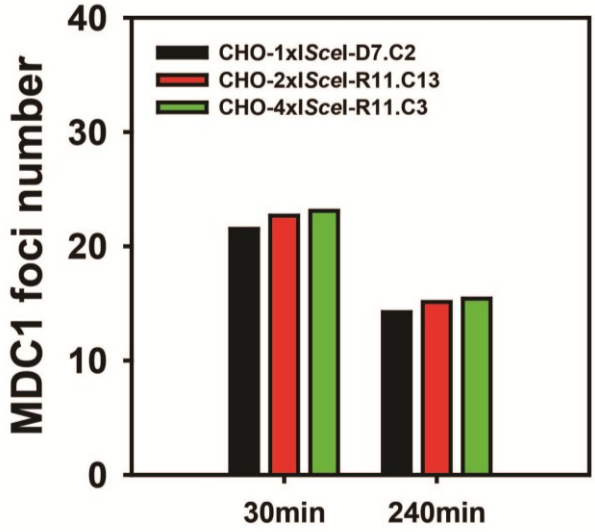

Fig. 30: GFP-MDC1 foci detected by live cell imaging in CHO-1xI*Sce*I-D7.C2, CHO-2xI*Sce*I-R11.C13 and CHO-4xI*Sce*I-R11.C3 cells 30 min and 240 min after 1 Gy X-ray irradiation. This experiment was performed in collaboration with V. Nikolov.

To measure MDC1 foci formation after DSB induction by I-*Sce*I, individual clones were cotransfected with the GFP tagged MDC1 expression construct together with the I-*Sce*I expression construct pCMV3xnlsI-*Sce*I (2 x 10^6 cells were transfected with 2 µg plasmid). The break in the x Axis of the graphs indicates that the analysis of foci formation started 6 h after transfection.

The numbers of MDC1 foci at the early time points are similar to the number of foci obtained by analysing γ-H2AX and approaches the theoretical maxima for all cell lines with simple and clustered DSBs (Fig. 31B-D). The number of foci decreases only slightly, approx. 1 focus for simple DSBs (Fig. 31B) and approx. 5 foci for clustered DSBs (Fig. 31C and D), as a function of time.

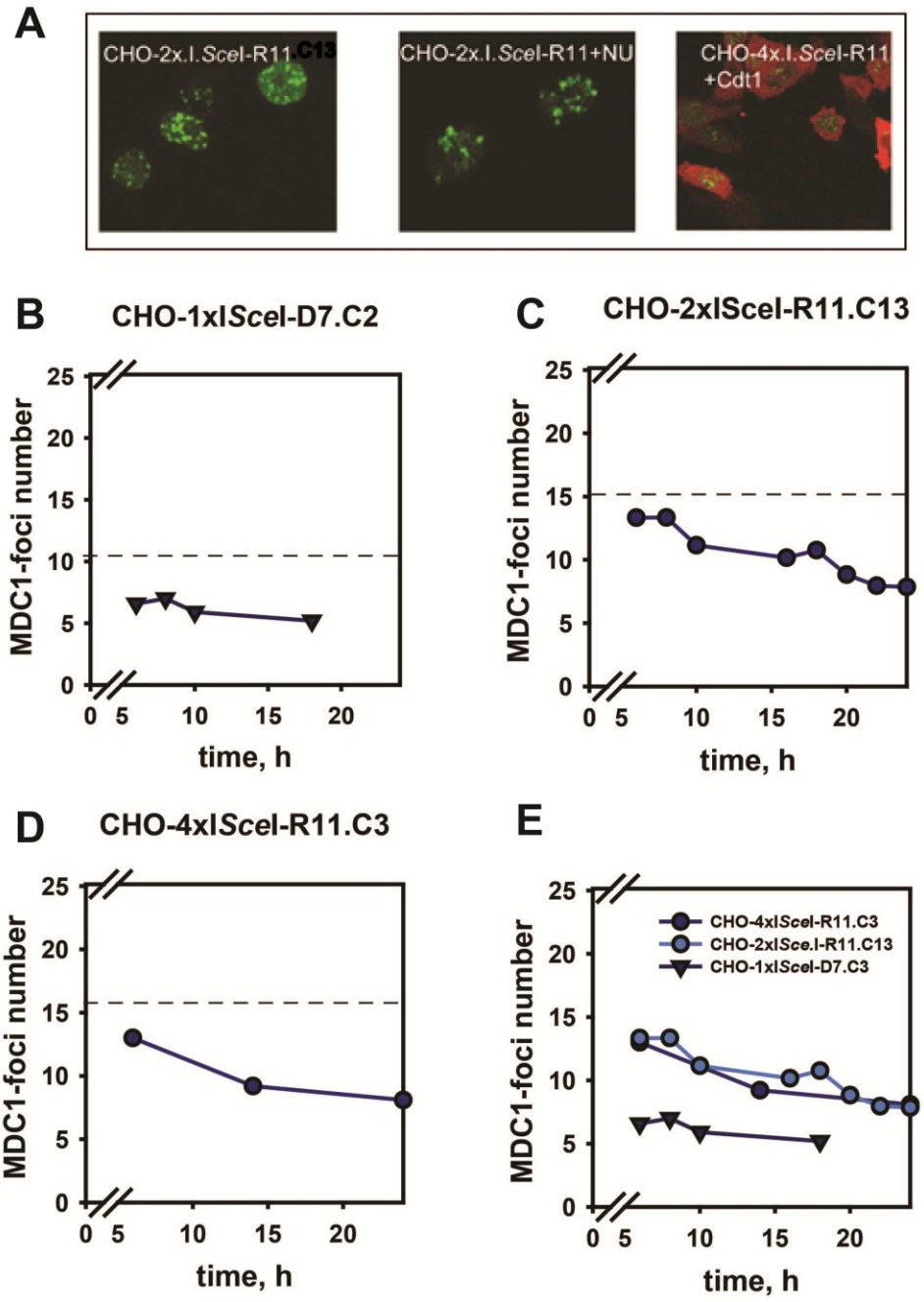

Fig. 31: Representative images and graphs showing GFP-MDC1 foci in pCMV3xnlsI-SceI and GFP-MDC1 cotransfected cells. A: Representative images of MDC1 foci in CHO-2xI*Sce*I-R11.C13 cells 6 h after transfection. The CHO-4xI*Sce*I-R11.C3 cells are cotransfected with an I-*Sce*I expressing plasmid tagged with M-Cherry. The even distribution of M-Cherry shows that I-*Sce*I is expressed and is distributed throughout cell. **B:** Foci were followed for 6-24 h after transfection in CHO-1xI*Sce*I-7D.C2. **C:** CHO-2xI*Sce*I-R11.C13 and **D:** CHO-4xI*Sce*I-R11.C3. **E:** Results of all clones are (B-D) plotted together to allow direct comparison. The theoretical maximum for each cell line is indicated with dotted lines. All data are plotted after background subtraction of foci numbers obtained after transfection of only MDC1-GFP (approx. 1-2 foci). These experiments were carried out in collaboration with V. Nikolov.

5.3.4. Marked differences in 53BP1 foci formation at simple and clustered DSBs

53 binding Protein1 (53BP1) is recruited at a late step of the multistep signaling cascade initiated at DSBs. It accumulates at DNA double strand breaks (DSBs) over a 1 Mbp region. 53BP1 foci formation is dependent on PIKK- (ATM/ATR/DNA-PKcs) induced phosphorylation of histone H2AX and can thus be utilized as a marker for DSBs. It has been experimentally determined that in cells exposed to ionizing radiation, the maximum foci number is reached 30 min after irradiation and that foci numbers return to baseline levels after 12-14 h (Schultz, Chehab *et al.* 2000). Human 53BP1 comprises two N-terminal BRCT repeats that bind p53, a tandem Tudor domain, a GAR methylation stretch, two dynein light chain (LC8) binding sites, and numerous PIK kinases and cyclin-dependent (CDK) phosphorylation sites.

The same clones used for MDC1 analysis were transfected with EGFP tagged 53BP1 for live cell imaging experiments under the same conditions as described for MDC1-GFP. The transfection efficiency after nucleofection, as measured using a pmax-GFP plasmid and FACS, ranged from 90-98%. Analysis of the same cells using live cell microscopy gives a transfection efficiency of 80% with optimized conditions (value calculated by dividing GFP-53BP1 positive cells by the total cell number obtained from the DIC image). The difference probably reflects the lower sensitivity of live microscopy as compared to FACS. The background foci level detected in cells only transfected with 53BP1-EGFP ranged between 0 and 2. As a control, CHO cells without I-*Sce*I integrations were transfected with the I-*Sce*I expressing plasmid (Fig. 32).

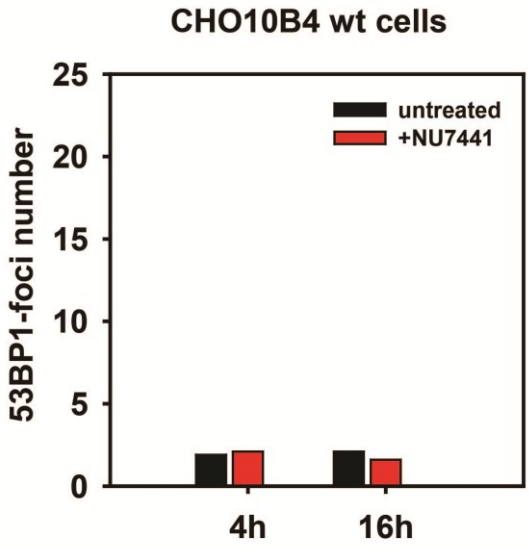

Fig. 32: 53BP1 foci analysis of CHO cells by live cell imaging 4 and 16 h after co-transfection of plasmids expressing EGFP-53BP1 and pCMV3xnlsI-*Sce*I. Shown is the total number of foci detected and corresponds to what we define as background. Quantitatively similar results were obtained with CHO cells transfected only with EGFP-53BP1.

Furthermore wt cells and the clone with CHO-4xI*Sce*I-R11.C3 were exposed to 0.5 Gy and foci kinetics were followed for up to 5 h (Fig. 33). The dose of 0.5 Gy was selected to induce about 10 DSBs in (G1) or 20 DSBs in (G2) that approximates the maximum number of I-*Sce*I-construct integrations.

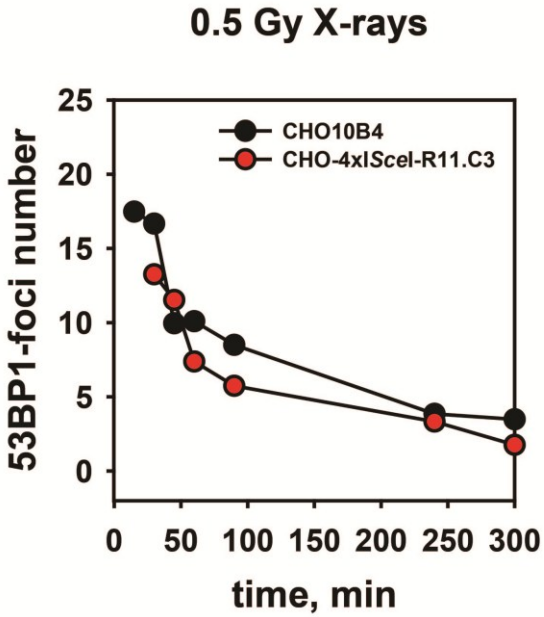

Fig. 33: 53BP1 foci analysis in wt CHO and CHO-4xI*Sce*I-R11.C3 cells measured by live cell imaging from 15 min to 5 h after exposure to 0.5 Gy X-rays. Cells were transfected with the EGFP-53BP1 plasmid 24 h before irradiation

The number of foci measured after I-*Sce*I mediated DSB induction in clones modeling different degrees of DSB complexity is shown in Fig. 34. Notably, 53BP1 foci are barely detectable on single I-*Sce*I sites; develop at approx. 50% the expected level with 2xI-*Sce*I sites and at nearly 100% level with 4xI-*Sce*I sites. This is the first evidence that the complexity of the DSB affects the development of the associated signaling.

.

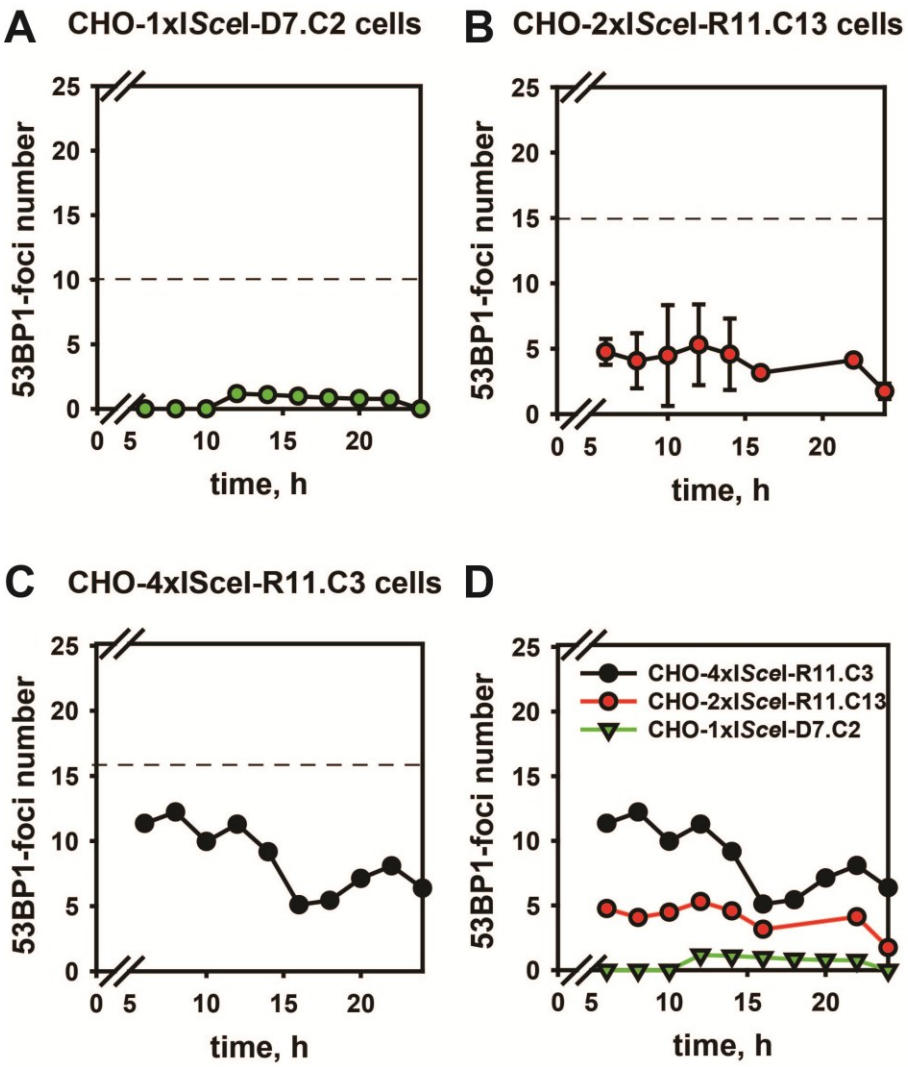

Fig. 34: 53BP1 foci analysis 6-24 hours after cotransfection of CHO-1xI*Sce*I-D7.C2, CHO-2xI*Sce*I-R11.C13 and CHO-4xI*Sce*I-R11.C3 cells with an EGFP-53BP1 and an I-*Sce*I expressing plasmid. The dotted lines indicate the theoretical maximum of I-*Sce*I induced DSBs for the different clones calculated according to cell cycle distribution measured by flow cytometry (see fig. 27).

There are two possible scenarios that may explain the persistence of the foci even after 24 h. First, the growth conditions in Leibovitz media in the 37 °C chamber may not be optimal for cell growth. This may cause some delay in repair. Second, the repeated I-*Sce*I cutting may maintain the signaling at the sites. If this scenario is the case, it is likely that the reduction in the number of 53BP1 foci seen after 12 h reflects loss of the I-*Sce*I site as the enzyme level does not decrease even after 72 h, shown by western blot (Fig. 35).

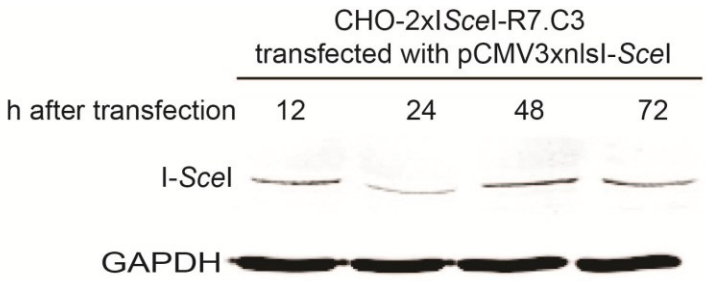

Fig. 35: Western blot results showing expression level of I-*Sce*I in whole cell extracts of I-*Sce*I transfected cells after 12, 24, 48 and 72 h.

This would indicate that different overall responses apply to IR and I-*Sce*I induced DSBs. It is also interesting that the number of 53BP1 foci scored in the clone with the single I-*Sce*I site increases after 12 h. This may suggest that complications associated with repeat-cutting in a subset of the potential cutting sites leads to signaling. Experiments are currently being performed to address these questions.

5.3.5. The number of 53BP1 foci is increased in G2 cells

In order to differentiate cells according to their cell cycle stages, we cotransfected the cells additionally to the I-*Sce*I plasmid with the cell cycle fluorescent reporter vector Cdt1. Expression of the Cdt1 reporter plasmid allows the monitoring of the cell cycle phase in real time. The levels of cell cycle regulating proteins fluctuate throughout the cell cycle with a high expression level of Cdt1 in the G1 phase that decreases during the S phase. Cdt1 is tagged with KO that allows follow up of its expression by live cell

imaging and thus the approximate characterization of the cell cycle phase for each individual cell.

In order to measure 53BP1 foci distribution in different cell cycle phases we cotransfected cells with KO-tagged Cdt1, GFP-tagged 53BP1 and I-*Sce*I expressing plasmid. Fig. 36 shows foci kinetics according to cell cycle phase in CHO-1xI*Sce*I-7R.C2 cells and CHO-2xI*Sce*I-11R.C13. The results show a general increase, by approx. a factor of two, in the number of 53BP1 foci in G2 cells as compared to G1 cells for I-*Sce*I transfected clones – particularly for the initial time points. At later times the foci number in G2-phase cells decreases to the level of G1-phase cells.

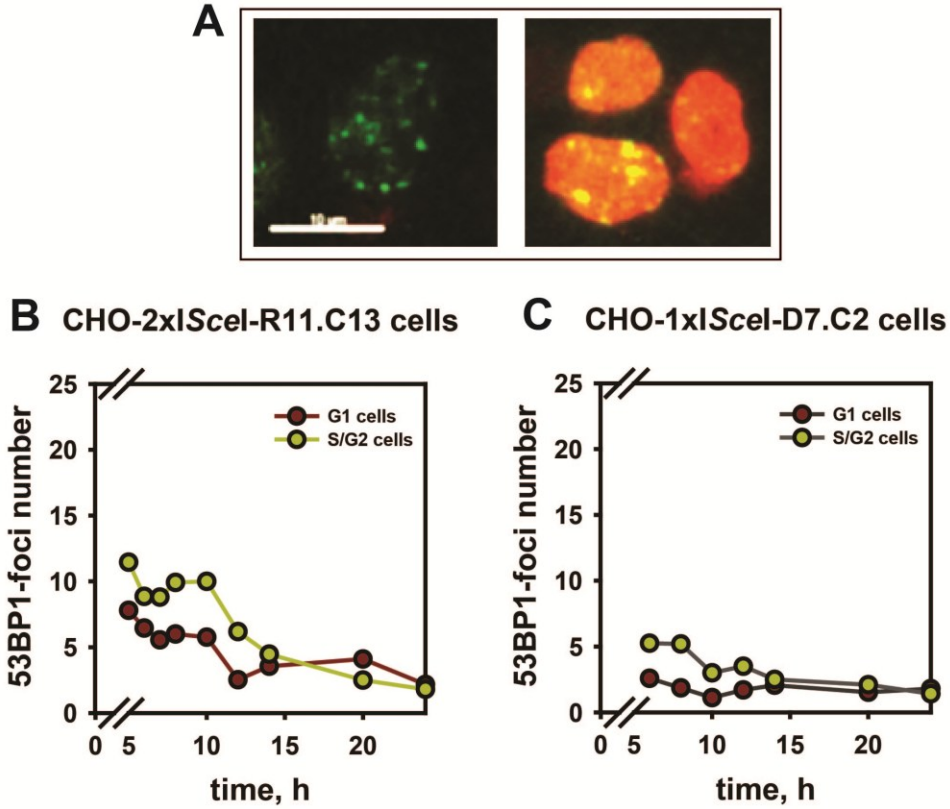

Fig. 36: Representative Images of CHO-2xI*Sce*I-R11.C3 cells in different cell cycle phases and graphs showing cell cycle distribution of CHO-2xI*Sce*I-R11.C3 and CHO-1xI*Sce*I-D7.C2 obtained by live cell imaging. A: Cells were co-transfected with KO2-Cdt1, 53BP1-GFP and pCMV3xnlsI-*Sce*I. G1 cells expressing Cdt1 and 53BP1 are yellow whereas S and G2 do not express KO2 tagged Cdt1 and are therefore green**.** 53BP1 foci were scored separately for G1 and G2 in CHO-2xI*Sce*I-R11.C3 cells **(B)** and in CHO-1xI*Sce*I-D7.C2 cells **(C)**. 100 cells were analyzed for each time point. This experiment was performed in cooperation with V. Nikolov.

5.4. Increasing the complexity of DSBs by various means compromises repair

To further investigate the effect of DSB complexity on signaling, the following two approaches were followed: Oxidative damage was induced by H_2O_2 in addition to I-*Sce*I induced DSBs to increase the damage complexity at DSB ends. In a further approach the D-NHEJ pathway was inhibited after DSB induction to leave the DSB ends open for longer time, thus increasing the probability of inappropriate end processing and misrepair events.

5.4.1. Increasing the complexity of I-*Sce*I DSBs by treatment with H_2O_2

As illustrated in the Introduction, RE induced DSBs are T1-DSBs, i.e. they can be removed by simple ligation. Radiation induced DSBs on the other hand are more complex and belong to the T2-6 types. To generate information on the possible effect of this form of complexity for the detection and signaling from a DSB, we introduced oxidative damage in cells harboring I-*Sce*I constructs, arguing that this will also reach the DSBs and will increase their complexity. To generate oxidative damage, cells were treated with H_2O_2 after DSB induction by I-*Sce*I.

A concentration of 25 µM that does not significantly increase the number of 53BP1 background foci was chosen for these experiments. H_2O_2 causes a marked increase in the number of 53BP1 foci in CHO-1xI*Sce*I-D7.C2 and CHO-2xI*Sce*I-R11.C13 cells when added immediately after I-*Sce*I transfection and measured after 6 h (Fig. 37). These results indicate that increasing the complexity at DSB ends also increases the 53BP1 foci formation to the theoretical maximum for the individual clones. For the higher complexity DSBs in CHO-4xI*Sce*I-R11.C3 cells, the addition of H_2O_2 did not increase the foci number as the theoretical maximum is reached already without additional treatment.

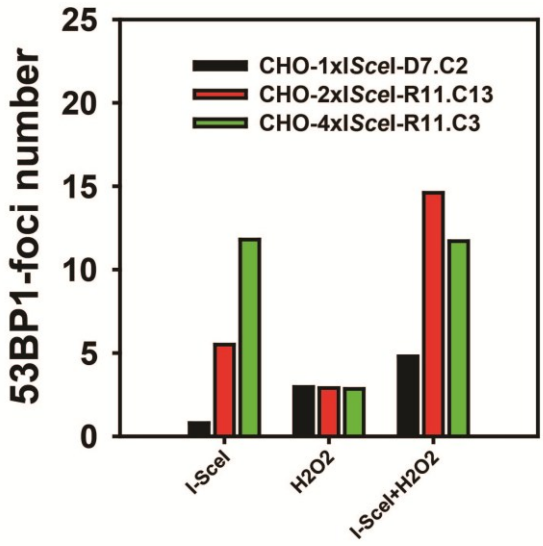

Fig. 37: 53BP1 foci in I-*Sce*I transfected CHO-1xI*Sce*I-D7.C2, CHO-2xI*Sce*I-R11.C13 and CHO-1xI*Sce*I-R11.C3 cells after treatment with H_2O_2, without additional treatment and EGFP-53BP1 transfected cells treated with H_2O_2. 25 µm H_2O_2 was added immediately after transfection. Results were obtained 6 h after transfection. This experiment was performed in collaboration with V. Nikolov.

5.4.2. Increasing the complexity of I-*Sce*I induced DSB ends by compromising D-NHEJ using small molecule inhibitors, or D-NHEJ defective mutants

The D-NHEJ inhibitor NU7441 that inhibits DNA-PKcs was applied to the cells at a concentration of 2.5 µM immediately after cotransfection of pCMV3xnlsI-SceI with EGFP-53BP1. For these experiments the CHO-2xI*Sce*I-R11.C13 and CHO-4xI*Sce*I-R11.C3 were employed, as well as CHO-1xI*Sce*I-D7.C2. A clear difference in 53BP1 foci number with and without NU7441 treatment can be observed for the clones CHO-2xI*Sce*I-R11.C13 and CHO-1xI*Sce*I-D7.C2. Interestingly the number of 53BP1 foci does not differ in NU7441 treated CHO-4xI*Sce*I-R11.C3 from untreated cells (Fig. 38 and 40).

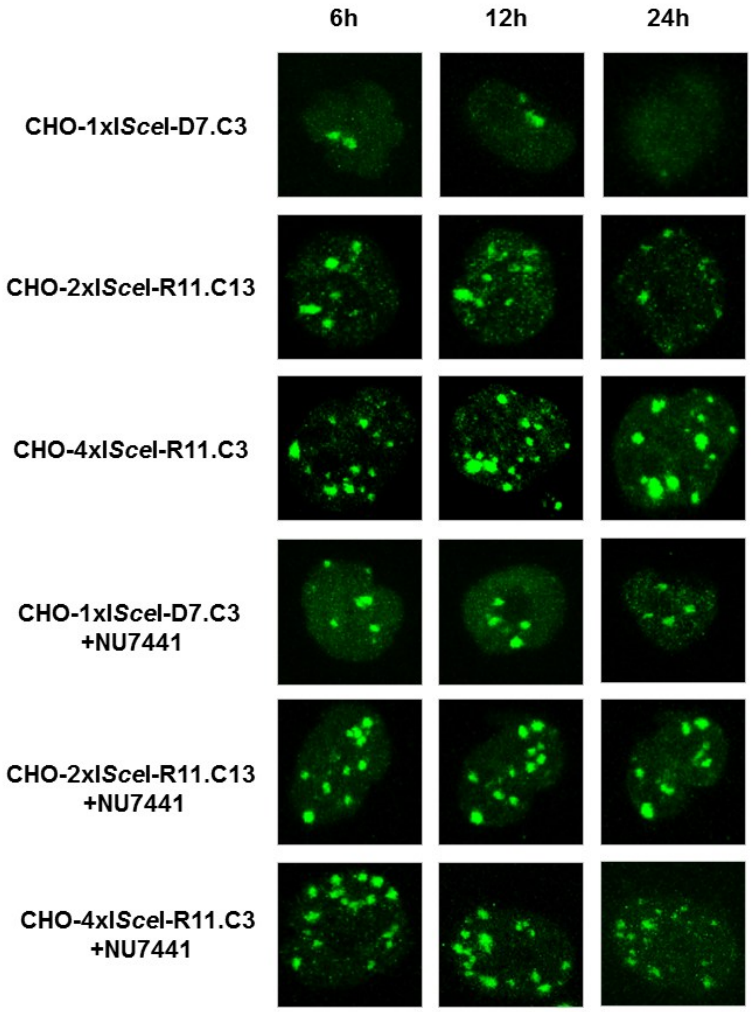

Fig.38: Representative images of pCMV3xnlsI-*Sce*I and 53BP1-GFP cotransfected cells measured by live cell imaging. CHO-1xI.*Sce*I-D7.C2, CHO-2xI.*Sce*I-R11.C13 and CHO-4xI.*Sce*I-R11.C3 cells are shown 6 h, 12 h and 24 h after transfection. Cells are shown without additional treatment and with addition of the NU7441 inhibitor.

To calculate the theoretical maximum of 53BP1 foci for NU7441 treated cells, the same calculations were performed as described in 5.3.1 based on the flow cytometry measurement from Fig. 39.

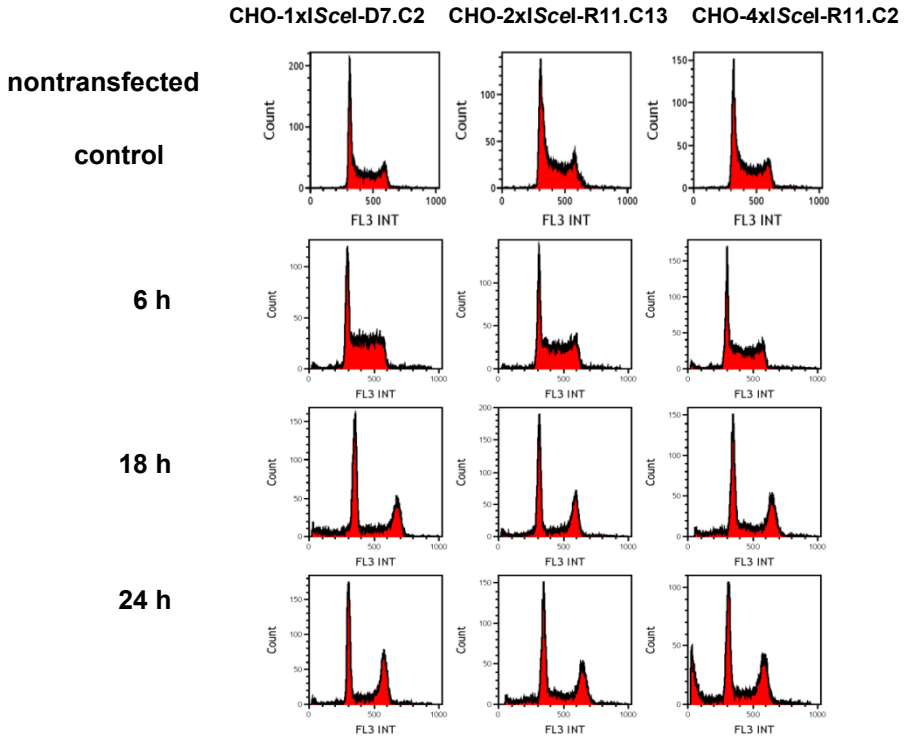

Fig. 39: Flow Cytometry Analysis of PI stained DNA of I-*Sce*I transfected CHO-1xI*Sce*I-D7.C2, CHO-2xI*Sce*I-R11.C13 and CHO-4xI*Sce*I-R11.C2 cells with the addition of the NU7441 Inhibitor. Cells were measured 6 h, 18 h and 24 h after transfection in the presence of NU7441.

Notably, treatment with NU7441 uniformly increased the number of 53BP1 foci detected to the theoretical maximum except in the case of 4xI-*Sce*I where no significant difference can be detected between NU7441 treated and untreated cells (Fig. 40). This result indicates that in the case of highly clustered DSBs, 53BP1 signaling is always required, as without the D-NHEJ inhibitor already the theoretical maximum of foci number is reached.

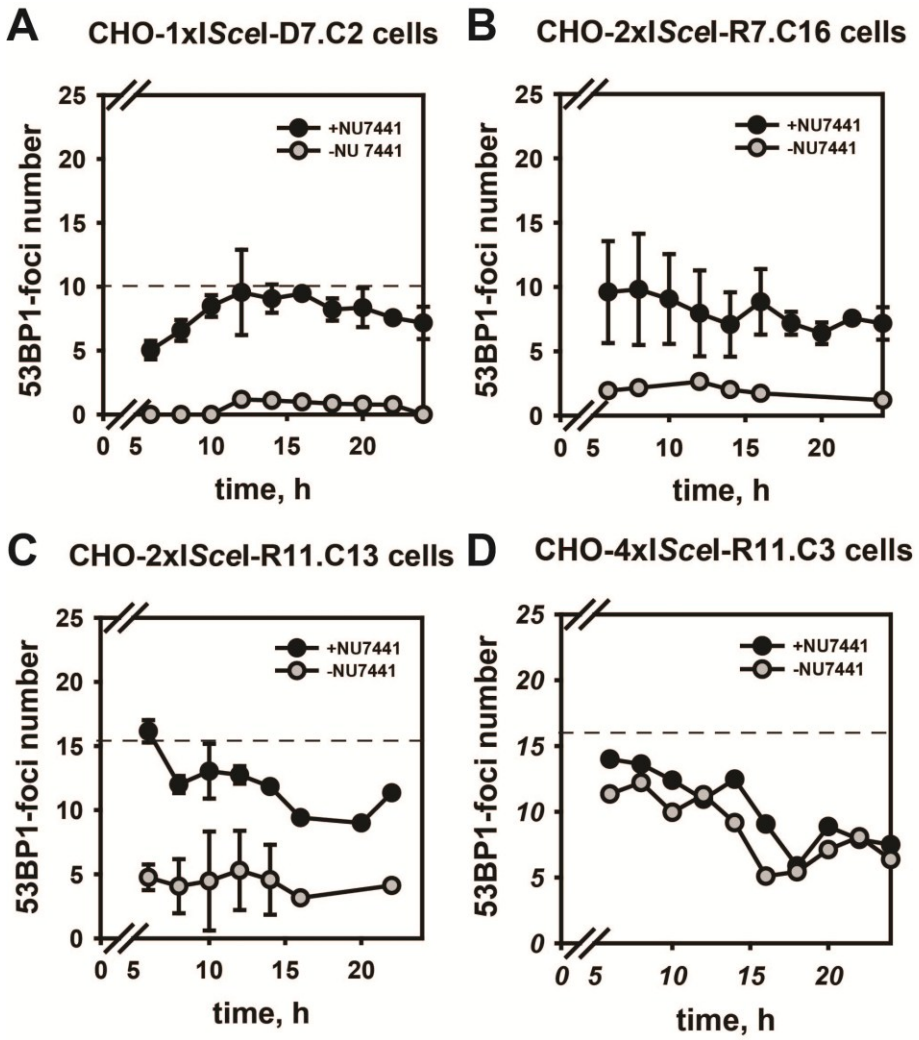

Fig. 40: Analysis of 53BP1 foci kinetics through live cell imaging in CHO clones with the indicated integrations of I-*Sce*I constructs in the presence of NU7441 to inhibit DNA-PKcs. Foci scoring started 6 h after transfection. Dotted lines indicate theoretical maximum of foci-number according to cell cycle distribution measured by flow cytometry (Fig. 39). For illustration purposes the I-*Sce*I transfected cells without NU7441 treatment shown in Fig. 27 are indicated in grey.

To extend the above observations, different NHEJ mutant clones with I-*Sce*I integrations mimicking clustered DSBs were analyzed in a similar set of experiments. Live cell imaging experiments were carried out with the NHEJ mutants XR-C1-3 (defective in DNA-PKcs) (Fig.41 C) and Xrs6 (defective in Ku80) (Fig. 42).

The experimental protocols employed were as described for CHO cells. The number of foci plotted is calculated after background subtraction obtained with the same cells after transfection with the 53BP1 expression vector alone. The clones selected for these experiments are XRC13-2xI*Sce*I-R11.C5 and XRS6-2xI*Sce*I-R11.C4. In order to follow 53BP1 foci kinetics in D-NHEJ deficient cells after irradiation, XRC13-2xI*Sce*I-R11.C5 cells were irradiated with 1 Gy X-rays 24 h post EGFP-53BP1 transfection. The measurement was performed 15 min after irradiation. Starting with 30 foci, after 12 h still approx. 15 foci are present indicating slow repair compared to CHO wt cells, where after 5 h the foci levels decrease to background (Fig. 41 A). The analysis of foci formation after DSBs induction by I-*Sce*I clearly reveal that in a D-NHEJ deficient background, foci form in nearly 100% of the expected I-*Sce*I sites (Fig. 41C). Furthermore a G2 block could be observed by flow cytometry 12 h after transfection (Fig. 41D).

53BP1 has an inhibitory effect on DSB resection and has the ability to tether distally formed DSBs in close proximity (Chapman, Taylor et al. 2012). This could explain the requirement of 53BP1 signaling at clustered or complex DSB ends to hinder end resection that could lead to repair failures.

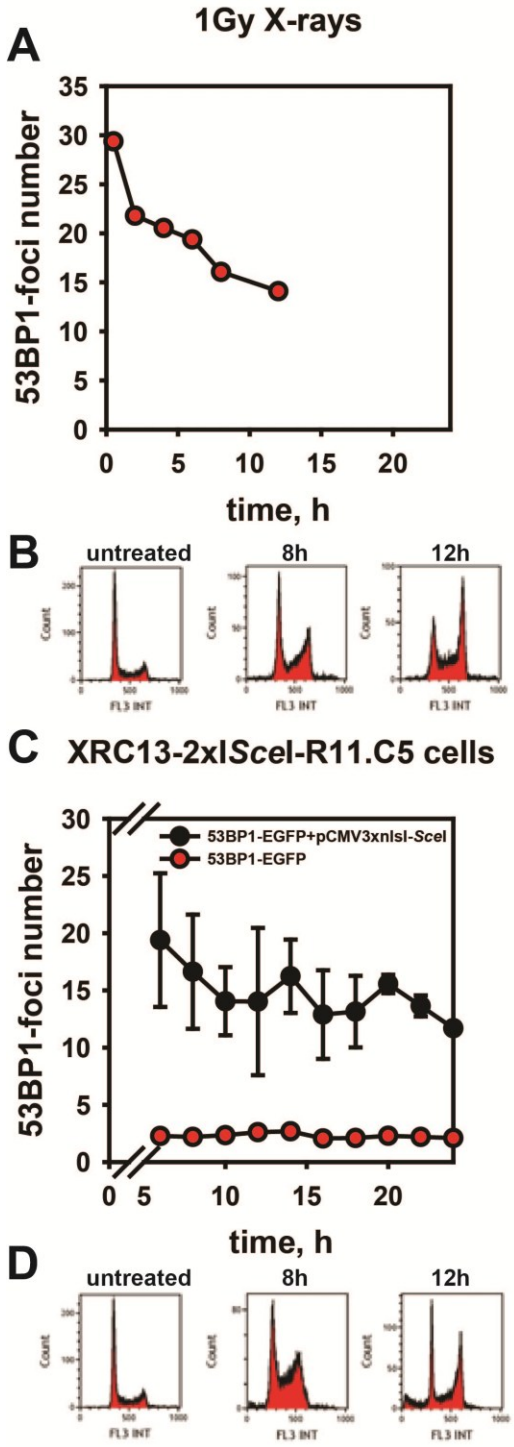

Fig. 41: XRC13-2xI*Sce*I-R11.C5 cells were analyzed for 53BP1 foci formation after I-*Sce*I transfection and after exposure to 1 Gy X-rays. A: Irradiated cells (irradiation 6 h after transfection with 53BP1-EGFP) are measured from 0.5-14 h after irradiation. **B:** The flow cytometry analysis of PI stained DNA is shown under the graph for 8 h and 12 h after IR and the unirradiated control. **C:** Accumulation of 53BP1 foci is measured by live cell imaging from 6 to 24 h after transfection of pCMV3xnlsI-SceI. (Vertical bars represent ± SD). The Experiments were repeated eight times with different types of controls and confirmed repeatedly by V. Nikolov. **D:** The flow cytometry analysis of PI stained DNA 8 h and 12 h after transfection and the nontransfected control are shown.

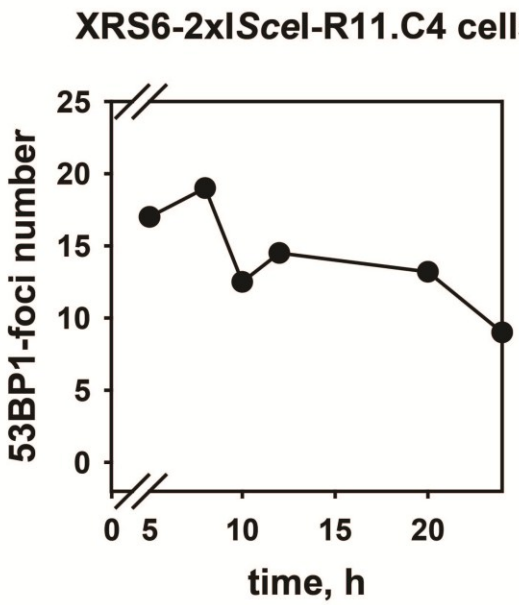

Fig. 42: 53BP1 foci measured by live cell imaging of XRS6-2xI*Sce*I-R11.C4 clones after pCMV3xnlsI-SceI co-transfection with 53BP1-EGFP. Foci were scored 5-24 h after transfection and 50 cells were counted for each time point. The experiment was performed two times.

5.4.3. Incidence of G2-PCC breaks and exchanges after increasing complexity at DSB sites

To analyze the incidence of repair failures upon increasing the complexity at DSB ends, G2-PCC was performed in D-NHEJ compromised cells. (Fig. 43 and 44) The results show that G2-PCC breaks and exchanges are increased after NU7441 treatment of I-*Sce*I transfected CHO-1xI*Sce*I-D7.C2 and CHO-2xI*Sce*I-R11.C13 cells. In contrast, the number of G2-PCC breaks and exchanges does not increase in the case of highly clustered DSBs (CHO-4xI*Sce*I-R11.C3) after NU7441 treatment, indicating that the maximum frequency (according to the number of integrations) of misrepair events is generated in this cell line even when the repair pathways are not compromised.

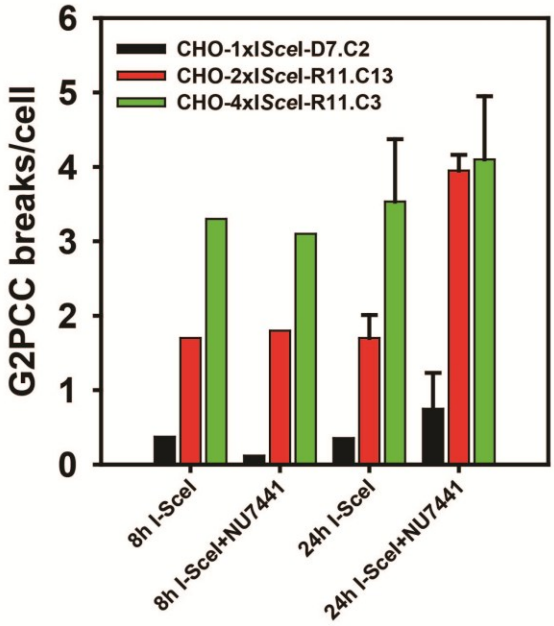

Fig. 43: G2-PCC breaks per cell in CHO-1x*Sce*I-D7.C2-, CHO-2xI*Sce*I-R11.C13-, and CHO-4xI*Sce*I-R11.C3 cells, 8 h and 24 h after pCMV3xnlsI-*Sce*I transfection, untreated (taken from Fig. 17) and treated with NU7441. Graphs represent data after background subtraction (from nontransfected cells and is approx. 1.2 G2-PCC breaks/cell with and without NU7441 treatment).

The number of G2-PCC breaks in NU7441 treated CHO-2xI*Sce*I-R11.C13 cells corresponds approx. to the number of G2-PCC breaks observed in the XRC13-2xISceI-R11.C5 cells with a D-NHEJ deficient background (Fig. 44). This result suggests that misrepair events occur if HR associated end-resection is carried out but HRR is inhibited, thus directing DSB processing to B-NHEJ.

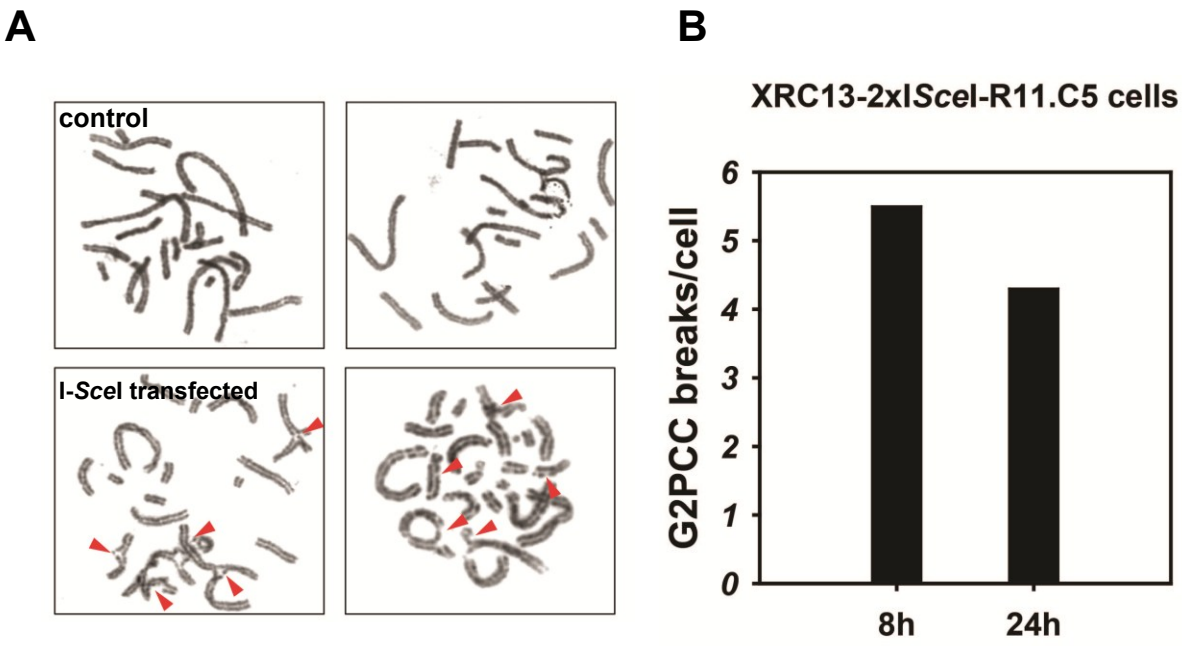

Fig. 44: G2-PCC Graph of XRC13-2xI*Sce*I-R11.C5 (B) with representative chromosome spreads from cells transfected with pCMV3xnlsI-*Sce*I and nontransfected controls (A).

Interestingly the number of exchanges in CHO-4xI*Sce*I-11R.C3 cells decrease approx. 50% after inhibiting PARP with PJ34 (Fig. 45). The two-site clones do not show any reduction in the exchange number and in the single-site clone the exchanges are reduced from 9 to 5 out of 100 cells.

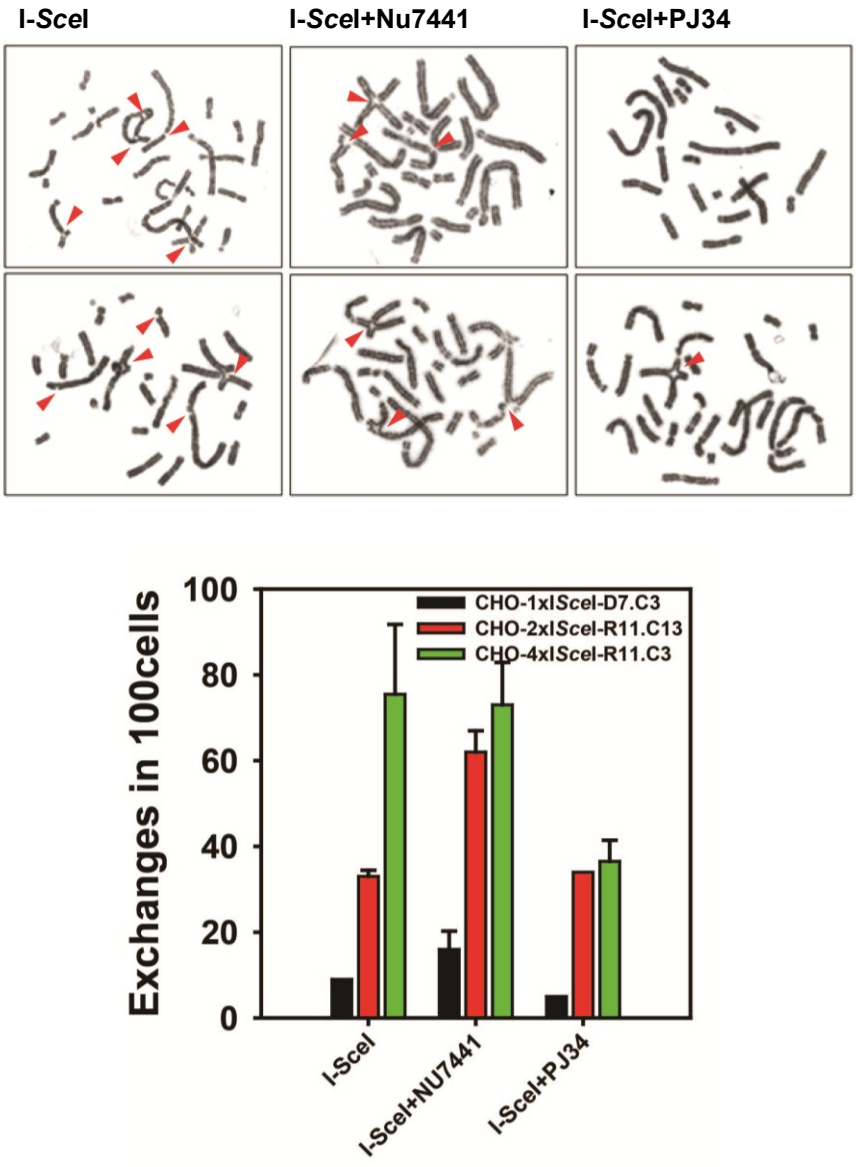

Fig. 45 A: Graph showing total number of exchanges out of 100 pCMV3xnlsI-*Sce*I transfected, CHO-1xI*Sce*I-D7.C2, CHO-2xI*Sce*I-R11.C13 and CHO-4xISceI-R11.C3 cells (with representative images of chromosome spreads of CHO-4xI*Sce*I-R11.C3 cells) and cells with additional NU7441 or PJ34 treatment with representative images. No exchanges could be detected in the nontransfected controls with NU7441 and PJ34 treatment.

5.5. An inducible I-*Sce*I system overcomes some limitations of the transient I-*Sce*I transfection

For the induction of DSBs in the above experiments, the I-*Sce*I expressing plasmid pCMV3xnlsI-SceI was co-transfected with the 53BP1 expressing plasmid. This system allows little control for the induction of DSBs, the cells are stressed by the electroporation and expression of I-*Sce*I that takes at least 2 h. We generated an inducible I-*Sce*I activation system to overcome some of the limitations associated with this approach. This system gives the possibility to analyze early foci kinetics. After stable integration in CHO-2xI-*Sce*I-R6.C10-cells with the NEIE plasmid, a cell line is generated where the localization of I-*Sce*I can be easily regulated. This is because the plasmid expresses a fusion I-*Sce*I protein containing the mutant human estrogen receptor ligand-binding domain that allows 4HT regulated translocation of I-*Sce*I from the cytoplasm where it normally resides to the nucleus. Fig. 46A shows the domain composition of the regulated I-*Sce*I, whereas Fig. 46C shows a western blot demonstrating the expected translocation of I-SceI from the cytoplasm into the nucleus upon addition of 4HT.

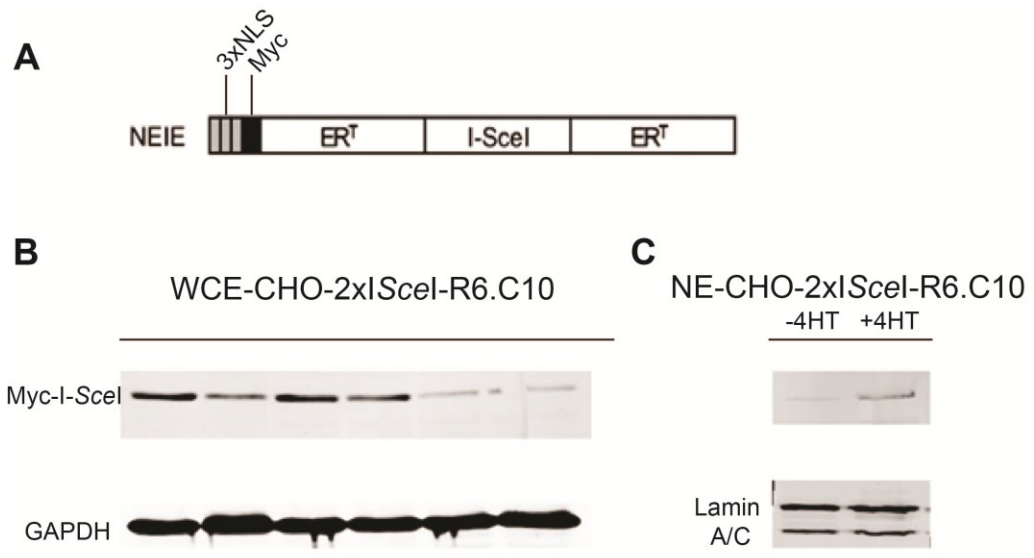

Fig. 46: Characteristics of an I-*Sce*I inducible system. A: Representative scheme of the stably integrated I-*Sce*I-expressing construct. The NEIE plasmid expresses from a pCMV promoter an I-*Sce*I chimera with an N-terminal triple-Myc tag, a nuclear localization signal and the mutant human estrogen receptor ligand-binding domain. It carries puromycin as selection marker. (Description of the nomenclature of **NEIE:** N: NLS, E: modified estrogen receptor, I: I-*Sce*I) **B: Western blot with whole cell extracts of clones that were stably transfected with the NEIE plasmid and grown in phenol red free media.** Six puromycin resistant clones were tested for Myc tagged I-*Sce*I expression. The expression level varies between the different clones. The clone with the highest expression level (lane 3) was chosen for further testing of I-*Sce*I expression and regulation, shown in C. **C: Nuclear extract of the clone from lane 3 (B) was prepared for western blotting, to test for I-*Sce*I translocation from the cytoplasm to the nucleus.** Lane 1 represents the level of Myc tagged I-*Sce*I in the nucleus without 4HT induction, indicating that I-*Sce*I is mainly localized in the cytoplasm. Upon addition of 4HT (1 µM) (lane 2) I-*Sce*I translocates into the nucleus where it digests the integrated I-*Sce*I recognition sites (Clones were generated in phenol red free media and stripped serum.)

To validate the system, live cell experiments were carried out with the cell line CHO-2xISceI-R6.C10 transfected with EGFP-53BP1. Measurement was started immediately after 4HT induced I-SceI translocation in NU7441 treated and untreated cells (Fig. 47). Foci formation can be detected approx. 1.5 h after addition of 4HT. Further experiments are needed to refine and validate this system.

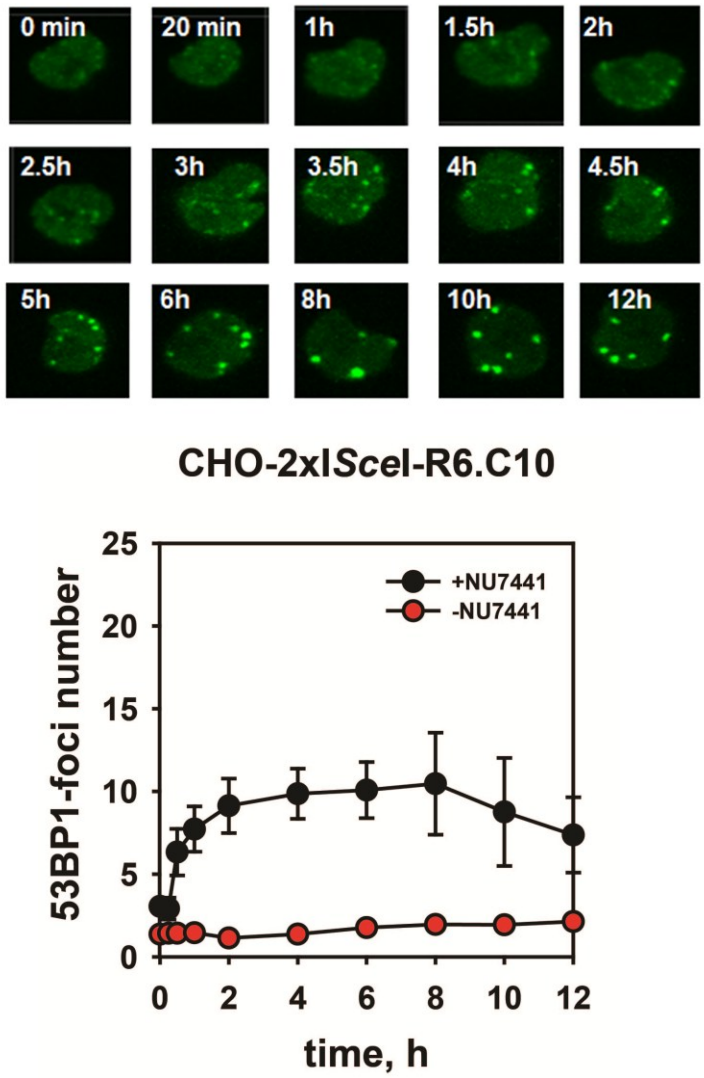

Fig. 47: Live cell imaging of CHO-2x*ISce*I-R6.C10 that expresses constitutively a regulable form of I-*Sce*I RE. Nuclear translocation of I-*Sce*I upon addition of 4HT leads to the formation of DSBs that are detectable as 53BP1 foci only in the presence of NU7441. **A:** Typical images obtained at the indicated times after addition of 4HT and NU7441 treatment. **B:** The graph shows the induction kinetics of 53BP1 after 4HT treatment with and without NU7441.

6. Discussion

6.1. Generation and characterization of model systems for simple (T1-) and clustered (T6-) DSBs

In an attempt to elucidate the type of lesion dominating the adverse effects of IR we established I-*Sce*I based model systems in wt, NHEJ and HR deficient CHO cells. One of the major advantages of these systems is that DSBs are exclusively induced in contrast to the plethora of lesion types induced by IR. In addition to the control over the type of lesion the spacing between consecutive DSBs can also be defined. The distances were engineered to resemble the winding around either one or two nucleosomes plus the linker regions in order to elucidate the probability for repair accidents caused by the simultaneous cleavage of two or more linker regions that may lead to chromatin destabilization. Additionally, as a control a model system for simple lesions was also generated.

In contrast to numerous I-*Sce*I based reporter systems that are mostly integrated at a single genomic locus, we applied the transposon technology to generate clones with a high number of integrations at random genomic sites thus achieving integration numbers that correspond to the number of DSBs induced after approx. 0.5 Gy X-rays. Hypothesizing that clustering of DSBs is a key source for repair accidents caused by IR, simple (T1-DSBs) and clustered DSBs (T6-DSBs) were induced upon I-*Sce*I transfection to analyze their biological consequences.

The features of the CHO-4xI*Sce*I cells also make them a potential candidate as a model system for chromothripsis, an event that is not triggered by IR but can spontaneously arise during cancer development. Chromothripsis describes the formation of tens to hundreds of locally clustered DNA rearrangements interspersed with widespread losses of sequence fragments through a single, cataclysmic event. Rearrangements can occur by chromosome shattering and rejoining of pieces by end-joining DNA repair pathways,

or by aberrant DNA replication-based mechanisms (Forment, Kaidi et al. 2012; Korbel and Campbell 2013).

Similar to chromothripsis, in the 4xI*Sce*I cells a high number of clustered DSBs are induced in a single event leading to genomic rearrangement. However, further investigations are required to examine similarities between chromothripsis and the 4xI-*Sce*I based system.

6.2. Clustered DSBs have a higher killing potential compared to simple DSBs

The reproductive cell death was measured by loss of colony forming ability for simple and clustered DSBs with different degrees of clustering. A clear killing effect was seen for T6-DSBs compared to T1-DSBs with a correlation between the increase in clustering and the decrease in the colony forming ability. The increase in clustering also leads to a higher probability for the local disruption of chromatin as more nucleosomes are involved and a larger fragment can get lost from the chromatin context. As an additional control for simple lesions the *Asi*SI-ER-U2OS cells were used, generating DSBs upon 4HT induction separated by at least 1 Mb. As the *Asi*SI sites are inherent in the human genome the theoretical maximum of breaks that can be induced is around 1750 in G1 cells. Still the killing effect is similar to the killing observed after only 11 four-DSB-clusters, underlining the high killing potential of clustered DSBs compared to simple DSBs.

6.3. The probability for misrepair of clustered DSBs is clearly elevated compared to simple-DSBs

In order to address the questions how the cellular repair machinery deals with simple and complex DSBs and which DSB type is the cause for misrepair and thus for lethal events, we measured chromatid breaks and inter chromosomal chromatid exchanges using the G2-PCC technique. According to the models of aberration formation, chromosome exchanges result from the interaction of two or more breaks in close

spatial and temporal proximity, where the wrong chromosome ends are joined (Savage 1998; Loucas, Durante et al. 2013), whereas chromatid breaks are caused by the lack of repair.

The results show that the yields of G2-PCC breaks as well as exchanges are clearly increased in clones with complex DSBs (CHO-2xI.*Sce*I-R11.C13 and CHO-4xI.*Sce*I-R11.C3) compared to the clone with simple DSBs (CHO-1xI.*Sce*I-D7.C2) (Fig. 26A and B). These observations imply that complex DSBs lead to repair accidents and therefore could be the main cause for lethal events leading to the high killing observed in survival experiments.

It has to be pointed out that repair failures are clearly increased in CHO-4xI.*Sce*I-R11.C3-cells compared to CHO-2xI.*Sce*I-R11.C13-cells. G2-PCC breaks as well as exchanges are increased at least two-fold. These results suggest that not only the DSB type, (T1-DSB or T-6DSB) determines cellular consequences but also the degree of DSB clustering of T6-DSBs, with a correlation between increased repair accidents and increased DSB clustering.

In cells harboring the 2xI-*Sce*I constructs the following two DSB-induction scenarios are probable; either both I-*Sce*I sites are cleaved simultaneously, or the sites are cleaved one after another and most likely repaired faithfully. The simultaneous cleavage of both sites possibly leads to the loss of a fragment comprising a single nucleosome and results in a deletion of >200 bp or sometimes in the rejoining with wrong ends. For the cells harboring 4xI-*Sce*I site constructs, there are various possibilities for DSB induction; i.e. only two or three sites out of the four possible sites may be cleaved simultaneously in various combinations. The most likely scenario is that the whole intervening fragment of 446 bp between the outer sites gets lost after simultaneous cleavage of all four sites. The simultaneous cleavage of all four sites probably leads to chromatin loss comprising two nucleosomes, as the intervening two DSBs destabilize the DNA in addition to the two outer I-*Sce*I-sites. The remaining DSB ends are then probably misrejoined with higher probability than in the case of 2xI-*Sce*I DSBs as seen by the high number of exchanges for CHO-4xI.*Sce*I-R11.C3-cells (approx. 80 in 100 metaphases, Fig. 26)

compared to the CHO-2xI.SceI-R11.C13-cells that have approx. half the number of exchanges (approx. 35 in 100 metaphases).

It remains to investigate whether the distance between the two I-*Sce*I sites or the increased number of I-*Sce*I sites compared to the two-DSB construct leads to the high frequency of misrepair. This question can be addressed by generating clones with the 500 and 1000 bp spacer I-*Sce*I constructs illustrated in Fig. 11B and measuring exchanges after DSB induction. However, both scenarios may lead to the loss of DNA fragments and destabilize the chromatin structure.

Also the analysis of metaphase chromosomes is in accordance with the G2-PCC data and shows the most severe repair outcomes, i.e. the highest number of chromosome aberrations, for CHO-4xI.*Sce*I-R11.C3 clones. Lethal asymmetric chromosome aberrations like dicentrics, rings and their associated acentric fragments are formed frequently, whereas in CHO-2xI.*Sce*I-R11.C13 cells chromatid breaks are abundant and in CHO-1xI.*Sce*I-D7.C2 cells only very few chromatid breaks could be observed.

In human cells approx. 2.8 dicentricsper 100 cells are formed after 0.5 Gy irradiation (Bauchinger and Gotz 1979). Taking the number of chromosomes in CHO cells into consideration, the frequency of dicentrics in CHO-4xI.*Sce*I-R11.C3 cells after induction of clustered DSBs is clearly elevated. Nevertheless, further quantitative analysis is required to validate this observation. In conclusion, T6-DSBs are clearly more deleterious for the cells than T1-DSBs, and the degree of T6-DSB clustering evidently also plays an important role.

Pioneering research in elucidating restriction enzyme induced chromosomal aberrations in mammalian cells was performed by P. Bryant, G. Obe and W. Morgan (Bryant 1984). They applied (various) PvuII and BamHI for restriction; these enzymes recognize numerous sites in the human genome and in this way cause a high degree of fragmentation, i.e. BamHI leads to 5 kb fragments when cleaving naked human DNA. Site specific endonucleases are widely-used up to date to investigate the formation of translocations after DSB induction, as the precise mechanisms that mediate translocation formation are poorly understood. They are essential events not only after

IR induced DSB misrepair but also in the malignant transformation of several tumor types (Coquelle, Rozier et al. 2002; Weinstock, Elliott et al. 2006; Brunet, Simsek et al. 2009). The results presented in this thesis confirm the formation of chromosomal aberrations by stable chromosomally integrated I-*Sce*I sites at multiple genomic locations. The analysis of translocation frequencies in our I-*Sce*I model-systems by whole genome sequencing or fluorescence in situ hybridization (FISH) would reveal further important information about the formation of translocations in simple compared to clustered DSBs.

6.4. I-*Sce*I-induced simple- and clustered DSBs activate the DDR

To investigate the recruitment of DDR signaling proteins to simple and clustered DSB damage sites, immunostaining of γ-H2AX and live cell imaging of MDC1 and 53BP1 were performed. Foci formation for γ-H2AX and MDC1 was triggered for all I-*Sce*I sites independently of complexity indicating that the DDR signaling cascade is activated for all types of DSBs induced. These results are important as they validate the I-*Sce*I model system as a reliable approach to investigate DDR signaling from simple and complex lesions.

In contrast to radiation induced DSBs, the I-*Sce*I-generated DSBs are not induced simultaneously. In this case, DSB induction is a long process of cutting and religation until a mutation event occurs or chromatin destabilization takes place and the recognition site becomes altered. The simplest form of repairing an I-*Sce*I induced DSB would be by religation, in this way reconstructing the I-*Sce*I restriction site and making it available for renewed cleavage.

In the case of DSB repair involving end resection the I-*Sce*I site would be lost. The MDC1 foci kinetics for all types of DSBs (T1- and T6-DSBs) reach the theoretical maximum 6 h after transfection and slightly decline thereafter. This observation could be an indication for repeated cycles of cleavage and ligation, which would complicate analysis of DSB repair kinetics using this model system. Also, for firm conclusions concerning MDC1 foci kinetics the long term growth conditions utilized in live cell

imaging need to be investigated in greater detail. Furthermore the I-*Sce*I-trex (Bennardo, Cheng et al. 2008), a fusion protein that has in addition to I-*Sce*I cleavage a 3` to 5`exonucleolytic activity, can be used to hinder reconstitution of I-*Sce*I sites after the initial cleavage.

6.5. 53BP1 recruitment differs between simple and complex DSBs

In contrast to γ-H2AX and MDC1 that are present in all types of lesions, our results show that 53BP1 recruitment to DSB sites depends on the type of lesion. 53BP1 foci formation was followed by live cell imaging for 24 h after co-transfection with the 53BP1-GFP and I-*Sce*I expressing plasmids. Whereas for CHO-4xI*Sce*I.R11.C3 the theoretical maximum of 53BP1-foci was reached after 6 h, only about half of the theoretical maximum was reached for CHO-2xI*Sce*I.R11.C13 and the number of 53BP1- foci for CHO-1xI*Sce*I.D7.C2 corresponded to the background foci levels.

53BP1-foci formation is γ-H2AX and H4K20 dimethylation dependent and spans a 1 Mb region surrounding the DSB. 53BP1 is involved in long range intrachromosomal V(D)J recombination and CSR (Difilippantonio, Gapud et al. 2008), as well as in the fusion between dysfunctional telomeres (Dimitrova, Chen et al. 2008). Therefore it is considered that 53BP1 serves as a synapsis factor to mediate long range joining of distant DNA breaks. Recently it has been discovered that 53BP1 plays a role in pathway selection by blocking 5` end resection with the help of Rif1 (Bothmer, Robbiani et al. 2010; Bunting, Callén et al. 2010; Zimmermann, Lottersberger et al. 2013).

A possible explanation for the difference in 53BP1 recruitment triggered by simple and clustered DSBs could be the role of 53BP1 to promote genomic stability by regulating the metabolism of DNA ends. The protection of DNA ends from end resection favors D-NHEJ and prevents B-NHEJ and HR that require extensive end processing (Bothmer, Robbiani et al. 2010). Therefore it is reasonable to protect DNA ends of complex DSBs that are prone to cause chromatin destabilization and mediate fast repair by D-NHEJ.

A further explanation could be a correlation between chromatin remodeling and lesion complexity, where complex DSBs induce a modification of the chromatin structure that

is required for 53BP1 recruitment, whereas simple DSBs are immediately religated. Chromatin architecture in the region surrounding the DSB has a critical impact on the ability of cells to mount an effective DNA damage response. DSBs promote the formation of open, relaxed chromatin domains which are spatially confined to the area surrounding the break. For simple T1-DSBs with compatible ends, it is likely that chromatin remodeling around the DSB is limited and fast and does not reach the 53BP1 recruitment step. To investigate this hypothesis it would be important to analyze foci formation of upstream proteins in the signaling cascade, like RNF8 and RNF168.

The connection between lesion complexity and 53BP1 recruitment is also underlined by the results obtained with different NHEJ mutant cell lines and the application of the NU7441 inhibitor to inhibit DNA-PKcs. In this case, 53BP1 foci form according to the theoretical maximum numbers for all cell lines including CHO-1xI*Sce*I-D7.C2. Compromising D-NHEJ leads to an increase in complexity at DSB ends, as the ends probably remain open for a longer time period.

A further modification of DSB ends was achieved by the addition of H_2O_2 that converts T1-DSBs to T3-DSBs. The increase of complexity at the DSB ends here also leads to an increase in 53BP1 signaling. A conclusion can be drawn that a synergistic effect exists between 53BP1 foci formation and aspects of DSB repair.

6.6. The number of 53BP1 foci is doubled in G2 cells (contribution of HR)

It will be important for future experiments to investigate the performance of HR in the developed model systems. The I-*Sce*I constructs are stably integrated at random loci in the genome of CHO cells, therefore upon I-*Sce*I mediated DSB induction most probably a DSB will be induced by I-*Sce*I in the homologous sequence as well. This hypothesis is supported by the doubling of 53BP1 foci number in G2- compared to G1-cells observed by live cell imaging after co-transfection with a Cdt1 construct identifying G1 cells.

During HR the resected 3` ssDNA invades an intact homologous duplex, driving the pairing of homologous sequences and strand exchange. In a scenario where the

homologous sequence is not intact due to a DSB at the same location, HR will be compromised. In this case the cells become reliant on D-NHEJ or B-NHEJ that do not require an intact chromatin as a template for repair, but have the propensity to direct joining across the break site which may produce complex chromosomal rearrangements that promote genomic instability and cell death (Iliakis, Wu et al. 2007)

6.7. Inhibiting PARP reduces the number of exchanges for T6-DSBs - A hint to the contribution of B-NHEJ for the repair of clustered lesions

To elucidate the contribution of NHEJ and B-NHEJ to the repair of simple compared to clustered DSBs, pathway-specific proteins were inhibited and the formations of exchanges were analyzed.

Inhibition of DNA-PKcs, a protein involved in the early steps of NHEJ leads to an increase in exchanges and G2-PCC-breaks for CHO-1xI*Sce*I-D7.C2 and CHO-2xI*Sce*I-R11.C13 cells not only after inhibition with NU7441 but also in the DNA-PKcs deficient cell line XRC13-2xI*Sce*I-R11.C5. These results clearly indicate the important role for D-NHEJ in the repair of T1-DSBs and also the 2xI*Sce*I-T6-DSB. In contrast, the theoretical maximum of breaks and exchanges for CHO-4xI*Sce*I-R11.C3-cells is already reached in NHEJ proficient cells. Two conclusions can be drawn from this observation. First, NHEJ cannot efficiently deal with highly clustered breaks leading to a high frequency of G2-PCC-breaks, misrejoining and asymmetric chromosomal aberrations. Second, it is likely that repair of highly clustered lesions is therefore directed to B-NHEJ.

The involvement of B-NHEJ is also underlined by the decrease in the formation of exchanges after PARP inhibition, where exchanges are reduced by around 50% after treatment with the PARP inhibitor PJ34. B-NHEJ is considered to be the main source for chromosomal translocations (Iliakis, Wang et al. 2004; Iliakis, Wu et al. 2007; Lieber 2010; Gostissa, Alt et al. 2011). Therefore the inhibition of PARP clearly reduces the incidence of chromosomal aberration formation (Boboila, Jankovic et al. 2010; Simsek, Brunet et al. 2011; Wray, Williamson et al. 2013).

7. Summary and outlook

A huge set of clones with different numbers of transposon mediated I-*Sce*I construct integrations, characterized by Southern blot, have been generated in CHO wt, NHEJ and HR deficient CHO cells for the use in various experiments as a model system mimicking the effects of IR. Biological consequences of simple and clustered DSBs in CHO wt and NHEJ deficient cells have been tested with different approaches, clearly proving the toxic effect of clustered DSBs.

In future experiments it would be interesting to measure translocation events induced by clustered DSBs compared to simple DSBs. Translocations could be analyzed by fluorescence in situ hybridization (FISH) or by whole genome sequence analysis. Furthermore the genomic locations of the integrated constructs could be revealed by whole genome sequencing. To determine whether the integrations are located at transcribed or non-transcribed regions is of particular interest. Hi-C analysis (Lieberman-Aiden, van Berkum et al. 2009) would shed light on the three dimensional architecture of the genomes and the spatial proximity of the integrated constructs. It could be investigated whether the spatial proximity in the three-dimensional structure leads to more translocations for simple and clustered lesions than spatially distant integrations.

Live cell imaging experiments showed differences in 53BP1 signaling characteristics between simple and clustered breaks. This result could be strengthened by increasing lesion complexity in clones with simple DSBs by the addition of H_2O_2 and by using repair compromised mutant cell lines. In order to further investigate the functional consequences of complexity dependent 53BP1 signaling, ubiquitylation and signaling by RNF8 and RNF168 should be examined. End resection should also be analyzed by immunostaining of the ssDNA binding protein RPA.

Further approaches with NHEJ (XR-C1-3 and Xrs6) and HR (irs1SF) deficient cells harboring the maximum number of integrations should be performed to evaluate the involvement of the different repair pathways. Especially the performance of HR in these

cell lines should be analyzed as I-*Sce*I induced DSBs are also present in the homologous strand that could pose problems during homology search for the HR-machinery.

An inducible I-*Sce*I system was generated that overcomes some limitations of the transient I-*Sce*I transfection. Still, after the induced translocation of the I-*Sce*I protein to the nucleus, the duration for cleavage cannot be controlled as the protein is expressed for at least 72 h. The stable genomic integration of a construct with a ligand dependent protein destabilization domain as an additional control for an I-*Sce*I inducible system would be helpful to control the time period of DSB induction as the removal of the ligand would stop further cleavage by inducing the degradation of the I-*Sce*I protein. Using this approach could help to elucidate the contribution of the different repair pathways as DSBs could be induced in specific cell cycle phases.

8. References

Audebert, M., B. Salles, et al. (2004). "Involvement of Poly(ADP-ribose) Polymerase-1 and XRCC1/DNA Ligase III in an Alternative Route for DNA Double-strand Breaks Rejoining." Journal of Biological Chemistry 279: 55117-55126.

Bancaud, A., C. Lavelle, et al. (2012). "A fractal model for nuclear organization: current evidence and biological implications." Nucleic Acids Research 40(18): 8783-8792.

Bauchinger, M. and G. Gotz (1979). "Distribution of radiation induced lesions in human chromosomes and dose-effect relation analysed with G-banding." Radiation and Environmental Biophysics 16: 355-366.

Bekker-Jensen, S. and N. Mailand (2010). "Assembly and function of DNA double-strand break repair foci in mammalian cells." DNA Repair 9(12): 1219-1228.

Belfort, M. and R. J. Roberts (1997). "Homing endonucleases: keeping the house in order." Nucleic Acids Research 25(17): 3379-3388.

Bennardo, N., A. Cheng, et al. (2008). "Alternative-NHEJ Is a Mechanistically Distinct Pathway of Mammalian Chromosome Break Repair." PLoS Genetics 4(6): e1000110.

Bindra, R. S., A. G. Goglia, et al. (2013). "Development of an assay to measure mutagenic non-homologous end-joining repair activity in mammalian cells." Nucleic Acids Research in press.

Boboila, C., F. W. Alt, et al. (2012). Chapter One - Classical and Alternative End-Joining Pathways for Repair of Lymphocyte-Specific and General DNA Double-Strand Breaks. Advances in Immunology. W. A. Frederick, Academic Press. Volume 116: 1-49.

Boboila, C., M. Jankovic, et al. (2010). "Alternative end-joining catalyzes robust IgH locus deletions and translocations in the combined absence of ligase 4 and Ku70." Proceedings of the National Academy of Sciences of the United States of America 107(7): 3034-3039.

Bohgaki, T., M. Bohgaki, et al. (2010). "DNA double-strand break signaling and human disorders." Genome Integrity 1: 15.

Bothmer, A., D. F. Robbiani, et al. (2010). "53BP1 regulates DNA resection and the choice between classical and alternative end joining during class switch recombination." Journal of Experimental Medicine 207(4): 855-865.

Brunet, E., D. Simsek, et al. (2009). "Chromosomal translocations induced at specified loci in human stem cells." Proceedings of the National Academy of Sciences of the United States of America 106(26): 10620-10625.

Bryant, P. E. (1984). "Enzymatic restriction of mammalian cell DNA using Pvu II and Bam H1: evidence for the double-strand break origin of chromosomal aberrations." International Journal of Radiation Biology 46: 57-65.

Bryant, P. E. and P. J. Johnston (1993). "Restriction-endonuclease-induced DNA double-strand breaks and chromosomal aberrations in mammalian cells." Mutation Research 299: 289-296.

Bunting, S. F., E. Callén, et al. (2010). "53BP1 Inhibits Homologous Recombination in Brca1-Deficient Cells by Blocking Resection of DNA Breaks." Cell 141: 243-254.

Bzymek, M., N. H. Thayer, et al. (2010). "Double Holliday junctions are intermediates of DNA break repair." Nature 464(7290): 937-941.

Carson, C. T., R. A. Schwartz, et al. (2003). "The Mre11 complex is required for ATM activation and the G_2/M checkpoint." EMBO Journal 22: 6610-6620.

Chapman, J. R., Martin R. G. Taylor, et al. (2012). "Playing the End Game: DNA Double-Strand Break Repair Pathway Choice." Molecular Cell 47(4): 497-510.

Chappell, C., L. A. Hanakahi, et al. (2002). "Involvement of human polynucleotide kinase in double-strand break repair by non-homologous end joining." EMBO Journal 21: 2827-2832.

Chevalier, B. S. and B. L. Stoddard (2001). "Homing endonucleases: structural and functional insight into the catalysts of intron/intein mobility." Nucleic Acids Research 29(18): 3757-3774.

Ciccia, A. and S. J. Elledge (2010). "The DNA Damage Response: Making It Safe to Play with Knives." Molecular Cell 40(2): 179-204.

Coquelle, A., L. Rozier, et al. (2002). "Induction of multiple double-strand breaks within an hsr by meganuclease I-SceI expression or fragile site activation leads to formation of double minutes and other chromosomal rearrangements." Oncogene 21: 7671-7679.

Dekker, J. (2008). "Mapping in Vivo Chromatin Interactions in Yeast Suggests an Extended Chromatin Fiber with Regional Variation in Compaction." Journal of Biological Chemistry 283(50): 34532-34540.

Di Noia, J. M. and M. S. Neuberger (2007). "Molecular Mechanisms of Antibody Somatic Hypermutation." Annual Review of Biochemistry 76(1): 1-22.

Difilippantonio, S., E. Gapud, et al. (2008). "53BP1 facilitates long-range DNA end-joining during V(D)J recombination." Nature 456: 529-533.

Dimitrova, N., Y.-C. M. Chen, et al. (2008). "53BP1 promotes non-homologous end joining of telomeres by increasing chromatin mobility." Nature 456: 524-528.

Dudley, D. D., J. Chaudhuri, et al. (2005). "Mechanism and Control of V(D)J Recombination versus Class Switch Recombination: Similarities and Differences." Advances in Immunology 86: 43-112.

Durante, M. and J. S. Loeffler (2010). "Charged particles in radiation oncology." Nature Reviews. Clinical Oncology 7(1): 37-43.

Eltsov, M., K. M. MacLellan, et al. (2008). "Analysis of cryo-electron microscopy images does not support the existence of 30-nm chromatin fibers in mitotic chromosomes in situ." Proceedings of the National Academy of Sciences 105(50): 19732-19737.

Fernandez-Capetillo, O., H.-T. Chen, et al. (2002). "DNA damage-induced G_2-M checkpoint activation by histone H2Ax and 53BP1." Nature Cell Biology 4: 993-997.

Finnie, N. J., T. M. Gottlieb, et al. (1995). "DNA-dependent protein kinase activity is absent in xrs-6 cells: implications for site-specific recombination and DNA double-strand break repair." Proceedings of the National Academy of Sciences of the United States of America 92: 320-324.

Forment, J. V., A. Kaidi, et al. (2012). "Chromothripsis and cancer: causes and consequences of chromosome shattering." Nature Reviews. Cancer 12(10): 663-670.

Friedland, W., M. Dingfelder, et al. (2005). "Calculated DNA double-strand break and fragmentation yields after irradiation with He ions." Radiation Physics and Chemistry 72(2–3): 279-286.

Friedland, W., P. Jacob, et al. (2003). "Simulation of DNA Damage after Proton Irradiation." Radiation Research 159(3): 401-410.

Friedland, W., P. Jacob, et al. (1998). "Monte Carlo Simulation of the Production of Short DNA Fragments by Low-Linear Energy Transfer Radiation Using Higher-Order DNA Models." Radiation Research 150: 170-182.

Friedrich, T., U. Scholz, et al. (2011). "Calculation of the biological effects of ion beams based on the microscopic spatial damage distribution pattern." International Journal of Radiation Biology 88(1-2): 103-107.

Fussner, E., M. Strauss, et al. (2012). "Open and closed domains in the mouse genome are configured as 10-nm chromatin fibres." EMBO Reports 13(11): 992-996.

Georgakilas, A. G. (2008). "Processing of DNA damage clusters in human cells: current status of knowledge." Molecular BioSystems 4(1): 30-35.

Georgakilas, A. G., P. O'Neill, et al. (2012). "Induction and Repair of Clustered DNA Lesions: What do we know so far?" Radiation Research in press.

Goodhead, D. T. (1994). "Initial events in the cellular effects of ionizing radiations: clustered damage in DNA." International Journal of Radiation Biology 65(1): 7-17.

Goodhead, D. T. (1995). "Molecular and cell models of biological effects of heavy ion radiation." Radiation and Environmental Biophysics 34: 67-72.

Goodhead, D. T. and H. Nikjoo (1989). "Track structure analysis of ultrasoft X-rays compared to high- and low-LET radiations." International Journal of Radiation Biology 55(4): 513-529.

Goodhead, D. T., J. Thacker, et al. (1993). "Effects of radiations of different qualities on cells: molecular mechanisms of damage and repair." International Journal of Radiation Biology 63(5): 543-556.

Gostissa, M., F. W. Alt, et al. (2011). "Mechanisms that Promote and Suppress Chromosomal Translocations in Lymphocytes." Annual Review of Immunology 29(1): 319-350.

Gruen, M., K. Chang, et al. (2002). "An in vivo selection system for homing endonuclease activity." Nucleic Acids Research 30(7): e29.

Gulston, M., C. de Lara, et al. (2004). "Processing of clustered DNA damage generates additional double-strand breaks in mammalian cells post-irradiation." Nucleic Acids Research 32(4): 1602-1609.

Hada, M. and B. M. Sutherland (2006). "Spectrum of Complex DNA Damages Depends on the Incident Radiation." Radiation Research 165: 223-230.

Hall, E. J. and A. J. Giaccia (2006). Radiobiology for the Radiologist. Philadelphia, Baltimore, New York, London, Buenos Aires, Hong Kong, Sydney, Tokyo, Lippincott Williams & Wilkins.

Hartlerode, A., S. Odate, et al. (2011). "Cell Cycle-Dependent Induction of Homologous Recombination by a Tightly Regulated I-SceI Fusion Protein." PLoS ONE 6(3): e16501.

Heyer, W.-D., K. T. Ehmsen, et al. (2010). "Regulation of Homologous Recombination in Eukaryotes." Annual Review of Genetics 44: 113-139.

Holley, W. R. and A. Chatterjee (1996). "Clusters of DNA damage induced by ionizing radiation: Formation of short DNA fragments. 1. Theoretical modeling." Radiation Research 145: 188-199.

Honma, M., M. Sakuraba, et al. (2007). "Non-homologous end-joining for repairing I-SceI-induced DNA double strand breaks in human cells." DNA Repair 6(6): 781-788.

Huen, M. S. Y., R. Grant, et al. (2007). "RNF8 transduces the DNA-damage signal via histone ubiquitylation and checkpoint protein assembly." Cell 131: 901-914.

Iacovoni, J. S., P. Caron, et al. (2010). "High-resolution profiling of gH2AX around DNA double strand breaks in the mammalian genome." EMBO Journal 29(8): 1446-1457.

Iliakis, G., H. Wang, et al. (2004). "Mechanisms of DNA double strand break repair and chromosome aberration formation." Cytogenetic and Genome Research 104: 14-20.

Iliakis, G., W. Wu, et al. (2007). Backup Pathways of Nonhomologous End Joining May Have a Dominant Role in the Formation of Chromosome Aberrations. Chromosomal Alterations. G. Obe, Vijayalaxmi. Berlin, Heidelberg, New York, Springer Verlag: 67-85.

Ivics, Z., P. B. Hackett, et al. (1997). "Molecular Recontruction of Sleeping Beauty, a Tc1-like Transposon from Fish, and Its Transposition in Human Cells." Cell 91: 501-510.

Ivics, Z. and Z. Izsvak (2004). "Transposable Elements for Transgenesis and Insertional Mutagenesis in Vertebrates." Methods in Molecular Biology 260: 255-276.

Izsvak, Z. and Z. Ivics (2004). "Sleeping Beauty Transposition: Biology and Applications for Molecular Therapy." Molecular Therapy 9: 147-156.

Izsvak, Z., E. E. Stüwe, et al. (2004). "Healing the Wounds Inflicted by Sleeping Beauty Transposition by Double-Strand Break Repair in Mammalian Somatic Cells." Molecular Cell 13: 279-290.

Jackson, S. P. and J. Bartek (2009). "The DNA-damage response in human biology and disease." Nature 461(7267): 1071-1078.

Jasin, M. (1996). "Genetic manipulation of genomes with rare-cutting endonucleases." Trends in Genetics 12: 224-228.

Jones, N. J., R. Cox, et al. (1988). "Six complementation groups for ionising-radiation sensitivity in Chinese hamster cells." Mutation Research 193: 139-144.

Kinner, A., W. Wu, et al. (2008). "g-H2AX in recognition and signaling of DNA double-strand breaks in the context of chromatin." Nucleic Acids Research 36(17): 5678-5694.

Korbel, Jan O. and Peter J. Campbell (2013). "Criteria for Inference of Chromothripsis in Cancer Genomes." Cell 152(6): 1226-1236.

Lieber, M. R. (2010). "The Mechanism of Double-Strand DNA Break Repair by the Nonhomologous DNA End-Joining Pathway." Annual Review of Biochemistry 79: 1.1-1.31.

Lieber, M. R. (2010). "NHEJ and its backup pathways in chromosomal translocations." Nature Structural & Molecular Biology 17(4): 393-395.

Lieberman-Aiden, E., N. L. van Berkum, et al. (2009). "Comprehensive Mapping of Long-Range Interactions Reveals Folding Principles of the Human Genome." Science 326(5950): 289-293.

Loucas, B. D., M. Durante, et al. (2013). "Chromosome Damage in Human Cells by γ Rays, α Particles and Heavy Ions: Track Interactions in Basic Dose-Response Relationships." Radiation Research 179(1): 9-20.

Luijsterburg, M. S. and H. van Attikum (2012). "Close encounters of the RNF8th kind: when chromatin meets DNA repair." Current Opinion in Cell Biology 24(3): 439-447.

Lukas, C., F. Melander, et al. (2004). "Mdc1 couples DNA double-strand break recognition by Nbs1 with its H2AX-dependent chromatin retention." EMBO Journal 23: 2674-2683.

Mailand, N., S. Bekker-Jensen, et al. (2007). "RNF8 ubiquitylates histones at DNA double-strand breaks and promotes assembly of repair proteins." Cell 131: 887-900.

Mansour, W. Y., T. Rhein, et al. (2010). "The alternative end-joining pathway for repair of DNA double-strand breaks requires PARP1 but is not dependent upon microhomologies." Nucleic Acids Research 38(18): 6065-6077.

McVey, M. and S. E. Lee (2008). "MMEJ repair of double-strand breaks (director's cut): deleted sequences and alternative endings." Trends in Genetics 24(11): 529-538.

Mirny, L. (2011). "The fractal globule as a model of chromatin architecture in the cell." Chromosome Research 19(1): 37-51.

Mladenov, E. and G. Iliakis (2011). "Induction and Repair of DNA Double Strand Breaks: The Increasing Spectrum of Non-homologous End Joining Pathways." Mutation Research/Fundamental and Molecular Mechanisms of Mutagenesis 711: 61-72.

Molenaar, J. J., J. Koster, et al. (2012). "Sequencing of neuroblastoma identifies chromothripsis and defects in neuritogenesis genes." Nature 483(7391): 589-593.

Nikjoo, H., P. O. O'Neill, et al. (1999). "Quantitative modelling of DNA damage using Monte Carlo track structure method." Radiation and Environmental Biophysics 38: 31-38.

Nishino, Y., M. Eltsov, et al. (2012). "Human mitotic chromosomes consist predominantly of irregularly folded nucleosome fibres without a 30-nm chromatin structure." EMBO Journal 31(7): 1644-1653.

Obe, G. and A. T. Natarajan (1985). "Chromosomal aberrations induced by the restriction endonuclease Alu I in Chinese hamster ovary cells: Influence of duration of treatment and potentiation by cytosine arabinoside." Mutation Research 152: 205-210.

Olive, P. L. (1998). "The Role of DNA Single- and Double-Strand Breaks in Cell Killing by Ionizing Radiation." Radiation Research 150 (Suppl.): S42-S51.

Pang, D., T. A. Winters, et al. (2011). "Radiation-generated Short DNA Fragments May Perturb Non-homologous End-joining and Induce Genomic Instability." Journal of Radiation Research 52: 309-319.

Paretzke, H. G. (1987). Radiation track structure theory. Kinetics of Nonhomogeneous Processes. G. R. Freeman, John Wiley & Sons, Inc.: 89-170.

Pfeiffer, P., E. Feldmann, et al. (2005). "Analysis of double-strand break repair by non-homologous DNA end joining in cell-free extracts from mammalian cells." Methods in Molecular Biology 291: 351-371.

Pierce, A. J., R. D. Johnson, et al. (1999). "XRCC3 promotes homology-directed repair of DNA damage in mammalian cells." Genes & Development 13: 2633-2638.

Ponomarev, A. L. and F. A. Cucinotta (2006). "Chromatin loops are responsible for higher counts of small DNA fragments induced by high-LET radiation, while chromosomal domains do not affect the fragment sizes." International Journal of Radiation Biology 82(4): 293-305.

Rass, E., A. Grabarz, et al. (2009). "Role of Mre11 in chromosomal nonhomologous end joining in mammalian cells." Nature Structural & Molecular Biology 16(8): 819-825.

Rogakou, E. P., D. R. Pilch, et al. (1998). "DNA double-stranded breaks induce histone H2AX phosphorylation on serine 139." Journal of Biological Chemistry 273: 5858-5868.

Rosidi, B., M. Wang, et al. (2008). "Histone H1 functions as a stimulatory factor in backup pathways of NHEJ." Nucleic Acids Research 36(5): 1610-1623.

Rydberg, B. (1996). "Clusters of DNA damage induced by ionizing radiation: Formation of short DNA fragments. 11. Experimental detection." Radiation Research 145: 200-209.

Saha, J. (2010). "Development of Defined Biological Models for Complex Radiation-Induced DNA Lesions Using Homing Endonucleases and Transposon Technology: Feasibility and Initial Characterization." Ph.D. thesis.

Sallmyr, A., A. E. Tomkinson, et al. (2008). "Up-regulation of WRN and DNA ligase IIIa in chronic myeloid leukemia: consequences for the repair of DNA double-strand breaks." Blood 112(4): 1413-1423.

San Filippo, J., P. Sung, et al. (2008). "Mechanism of Eukaryotic Homologous Recombination." Annual Review of Biochemistry 77: 229-257.

Sanchez, Y., C. Wong, et al. (1997). "Conservation of the Chk1 checkpoint pathway in mammals: Linkage of DNA damage to Cdk regulation through Cdc25." Science 277: 1497-1501.

Savage, J. R. K. (1998). "A brief survey of aberration origin theories." Mutation Research 404: 139-147.

Schipler, A. and G. Iliakis (2013). "DNA double-strand-break complexity levels and their possible contributions to the probability for error-prone processing and repair pathway choice." Nucleic Acids Research Epub ahead of print.

Schultz, L. B., N. H. Chehab, et al. (2000). "p53 binding protein 1 (53BP1) is an early participant in the cellular response to DNA double-strand breaks." Journal of Cell Biology 151: 1381-1390.

Shiloh, Y. (2003). "ATM and related protein kinases: Safeguarding genome integrity." Nature Reviews. Cancer 3: 155-168.

Simsek, D., E. Brunet, et al. (2011). "DNA Ligase III Promotes Alternative Nonhomologous End-Joining during Chromosomal Translocation Formation." PLoS Genetics 7(6): e1002080.

Singh, S. K., T. Bednar, et al. (2012). "Inhibition of B-NHEJ in Plateau-Phase Cells Is Not a Direct Consequence of Suppressed Growth Factor Signaling." International Journal of Radiation Oncology Biology Physics 84(2): e237-e243.

Singh, S. K., M. Wang, et al. (2011). "Post-irradiation chemical processing of DNA damage generates double-strand breaks in cells already engaged in repair." Nucleic Acids Research 39(19): 8416-8429.

Singh, S. K., W. Wu, et al. (2011). "Widespread Dependence of Backup NHEJ on Growth State: Ramifications for the Use of DNA-PK Inhibitors." International Journal of Radiation Oncology Biology Physics 79(2): 540-548.

Stephens, P. J., C. D. Greenman, et al. (2011). "Massive Genomic Rearrangement Acquired in a Single Catastrophic Event during Cancer Development." Cell 144: 27-40.

Stucki, M., J. A. Clapperton, et al. (2005). "MDC1 directly binds phosphorylated histone H2AX to regulate cellular responses to DNA double-strand breaks." Cell 123: 1213-1226.

Thurman, R. E., E. Rynes, et al. (2012). "The accessible chromatin landscape of the human genome." Nature 489(7414): 75-82.

Tsai, C. J., S. A. Kim, et al. (2007). "Cernunnos/XLF promotes the ligation of mismatched and noncohesive DNA ends." Proceedings of the National Academy of Sciences of the United States of America 104(19): 7851-7856.

van Attikum, H. and S. M. Gasser (2009). "Crosstalk between histone modifications during the DNA damage response." Trends in Cell Biology 19(5): 207-217.

van Berkum, N. L. and J. Dekker (2009). "Determining Spatial Chromatin Organization of Large Genomic Regions Using 5C Technology." Methods in Molecular Biology 567: 189-213.

van Gent, D. C. and M. van der Burg (2007). "Non-homologous end-joining, a sticky affair." Oncogene 26(56): 7731-7740.

Vigdal, T. J., C. D. Kaufman, et al. (2002). "Common Physical Properties of DNA Affecting Target Site Selection of Sleeping Beauty and other Tc1/mariner Transposable Elements." Journal of Molecular Biology 323(3): 441-452.

Walker, J. R., R. A. Corpina, et al. (2001). "Structure of the Ku heterodimer bound to DNA and its implications for double-strand break repair." Nature 412: 607-614.

Wang, H., B. Rosidi, et al. (2005). "DNA Ligase III as a Candidate Component of Backup Pathways of Nonhomologous End Joining." Cancer Research 65(10): 4020-4030.

Wang, M., W. Wu, et al. (2006). "PARP-1 and Ku compete for repair of DNA double strand breaks by distinct NHEJ pathways." Nucleic Acids Research 34(21): 6170-6182.

Ward, J. F. (1985). "Biochemistry of DNA lesions." Radiation Research 104: S103-S111.

Ward, J. F. (1990). "The yield of DNA double-strand breaks produced intracellularly by ionizing radiation: a review." International Journal of Radiation Biology 57: 1141-1150.

Weinstock, D. M., B. Elliott, et al. (2006). "A model of oncogenic rearrangements: differences between chromosomal translocation mechanisms and simple double-strand break repair." Blood 107(2): 777-780.

Weterings, E. and D. J. Chen (2007). "DNA-dependent protein kinase in nonhomologous end joining: a lock with multiple keys?" Journal of Cell Biology 179(2): 183-186.

Weterings, E. and D. J. Chen (2008). "The endless tale of non-homologous end-joining." Cell Research 18(1): 114-124.

Windhofer, F., W. Wu, et al. (2007). "Marked dependence on growth state of backup pathways of NHEJ." International Journal of Radiation Oncology Biology Physics 68(5): 1462-1470.

Wray, J., E. A. Williamson, et al. (2013). "PARP1 is required for chromosomal translocations." Blood in press.

Wu, W., M. Wang, et al. (2008). "Enhanced Use of Backup Pathways of NHEJ in G_2 in Chinese Hamster Mutant Cells with Defects in the Classical Pathway of NHEJ." Radiation Research 170: 512-520.

Zimmermann, M., F. Lottersberger, et al. (2013). "53BP1 Regulates DSB Repair Using Rif1 to Control 5′ End Resection." Science 339(6120): 700-704.

Curriculum vitae

Der Lebenslauf ist in der veröffentlichten Version aus Gründen des Datenschutzes nicht enthalten.